TWO-PHOTON ABSORPTION IN CRUCIFORM AND DIPOLAR CHROMOPHORES: EXCITONIC INTERACTIONS AND RESPONSE TO METAL IONS

A Dissertation
Presented to
The Academic Faculty

by

Nisan Naftali Siegel

In Partial Fulfillment
of the Requirements for the Degree
PhD in the
School of Chemistry and Biochemistry

Georgia Institute of Technology
August 2010

TWO-PHOTON ABSORPTION IN CRUCIFORM AND DIPOLAR CHROMOPHORES: EXCITONIC INTERACTIONS AND RESPONSE TO METAL IONS

Approved by:

Dr. Joseph W. Perry, Advisor
School of Chemistry and Biochemistry
Georgia Institute of Technology

Dr. Thomas Orlando
School of Chemistry and Biochemistry
Georgia Institute of Technology

Dr. Robert L. Whetten
School of Chemistry and Biochemistry
Georgia Institute of Technology

Dr. Laren M. Tolbert
School of Chemistry and Biochemistry
Georgia Institute of Technology

Dr. Rick Trebino
School of Physics
Georgia Institute of Technology

Date Approved: May 27, 2010

This thesis is dedicated to my family, especially:

my wife Andrea,

my daughter Clara,

and

my great grandfather Rabbi Nissen Telushkin,
who always wanted a scientist in the family.

ACKNOWLEDGEMENTS

The completion of a doctorate does not happen as a result of the efforts of only one person. There are many people whose help, advice and support have enabled me to reach this point.

My calculus professor in college, Professor Susan Lewis, helped me learn to appreciate and enjoy the mathematics that describe the world around us; without her truly expert and concerned teaching I would not be here.

After college, I worked with Dr. Louis Stuhl, Dr. Mark Spitler, Dr. Anne Ehret, and Dr. Amy Grant at ChemMotif, Incorporated. Their friendship and mentorship along with my experiences at ChemMotif showed me the rewards of working daily in a laboratory to produce both good science and practically useful products, and heavily influenced my choice of graduate field of study.

Here at Georgia Tech, I have had the privilege of working with many gifted and concerned professors, research scientists, postdocs and graduate students. As a spectroscopist I have relied on synthetic chemists to provide me with material to study. In the group of Professor Uwe Bunz, Dr. James Wilson and Dr. Anthony Zucchero made the cruciform compounds on which so much of this thesis is focused. In the group of Professor Christoph Fahrni, Dr. Sumalekshmy Sarojini-Amma, Dr. Manjusha Verma, Dr. Karl Huettinger and Yonggang Wu provided me with the dipolar zinc-sensing dyes discussed in Chapter 5. In the group of Professor Seth Marder, Chun Huang made several compounds that provided interesting and rewarding diversions from the rest of my work. I thank them all for the time they spent working on the synthesis and characterization of

the compounds, and for their discussions with me. Without them, too, this would not be possible.

The research group in which the PhD research is performed is the most important group of people to a graduate student, and I feel privileged to have belonged to the group of Professor Joseph Perry. Above all, I wish to thank Dr. Mariacristina Rumi, from whom I learned what it takes to be a good spectroscopist. The countless hours of teaching and discussion that she spent with me, both in the lab and in the office and seminar room, have been invaluable. Dr. Joel Hales has always been available to help with laboratory questions or to help me figure out what questions are and are not worth pursuing; his advice and help when it came time to look for postdoctoral work were also most helpful. Working with Matteo Cozzuol and Dr. Matthew Sartin was always a pleasure; what I did not learn from Cristina about the practical details of lasers and electronics I learned form them. The fellow students with whom I began in the group, Vincent Chen, Dr. Sarah Chi, Dr. Philseok Kim, Dr. Wojciech Haske and Dr. Michal Malicki became valued friends over the years. Along with the students who joined the group since then, Nathan Jarnagin, Ariel Marshall and Anselmo Kim, they provided friendship and ears to listen to many practice talks and presentations along the way, and I thank them all.

I would like to thank my advisor, Professor Joseph Perry, for his support through my time in graduate school. The time he has spent with me has taught me how to properly formulate, address and report on significant scientific questions; the three tasks central to scientific inquiry. I also thank my thesis committee for their time and assistance with my thesis, and the Georgia Tech School of Chemistry and Biochemistry for providing an excellent environment in which to learn.

Last, but certainly not least, I thank my family, particularly my wife Andrea and my daughter Clara, for all of the love, support, and joy they have brought to my life, and for providing me the inspiration to keep going even when it felt difficult.

TABLE OF CONTENTS

LIST OF TABLES

LIST OF FIGURES

Page

LIST OF SYMBOLS AND ABBREVIATIONS

δ	Two-photon absorption cross-section
ε	Molar exctinction coefficient
$\lambda_{max}^{(1)}$	One-photon absorption peak wavelength
$\lambda_{max}^{(2)}$	Two-photon absorption peak wavelength
1PA	One-photon absorption
2PA	Two-photon absorption
2PEF	Two-photon excited fluorescence
2PLSM	Two-photon laser scanning microscopy
A	Electron acceptor group
D	Electron donor group
CT	Charge-transfer
FC	Franck-Condon
GM	Goppert-Mayer; unit of 2PA cross-section; 10^{-50} cm^4 s $photon^{-1}$ $molecule^{-1}$
NIR	Near-infrared
NLO	Nonlinear optics, nonlinear optical
UV	Ultraviolet

SUMMARY

Structure-property relationships for two-photon absorption (2PA) in branched organic chromophores is a topic of current interest, as is the design of chromophores with advantageous properties for two-photon laser scanning microscopy (2PLSM). The main goals of this dissertation were to study and explain the one-photon absorption (1PA) and 2PA properties of cruciform chromophores based on 1,4-distyryl-2,5-bis(phenylethynyl)benzene with varying electron donor (D) and acceptor (A) groups, and to characterize the 2PLSM-relevant response of some of these chromophores and a set of dipolar chromophores to binding with zinc ions. The compounds were studied by 1PA, fluorescence and 2PA spectroscopy. A ππ* exciton model was developed to explain the spectral properties of the 1,4-distyryl-2,5-bis(phenylethynyl)benzene cruciform with no D or A groups or with four identical D groups at the termini of the linear arms of the chromophore. This model indicated that there is some coupling and mixing of the lowest excited states *e* of the linear arms, leading to splitting of the 1PA spectrum of the cruciform. There was little coupling or mixing of the higher excited states *e*′ accessed in 2PA, leading to a two-band 2PA spectrum for the chromophore, in contrast to cruciform compounds in the literature with identical conjugated arms, which have one visible 2PA band. For cruciforms with D groups on the styryl arm and A character on the terminal phenyls of the phenylethynyl arms (D/A cruciforms), the ππ* exciton model was complemented with a charge-transfer (CT) exciton model describing interactions of charge-transfer pathways between the D and A groups. This model explained the

broadness of the 1PA band of D/A cruciforms as well as the two 2PA bands observed for these chromophores.

The fluorescence and 2PA spectral responses to binding of Zn^{2+} ions to the D or A groups of some cruciform compounds were also assessed, to provide insight into the design of new analyte-sensing cruciforms for 2PLSM that take advantage of enhancement or reduction of D/A character upon analyte binding. It was found that canceling charge donation from the D groups in differing D/A cruciforms resulted in fluorescence and 2PA spectra nearly indistinguishable from each other, suggesting that turn-off of D groups is not an optimal modality of 2PLSM analyte sensing in cruciforms. Binding Zn^{2+} to A groups was shown to result in an increase in the D/A character of the cruciform, with fluorescence peak energies that changed depending on the location of the A group. It is suggested that the use of non-binding donors and analyte-binding A groups in differing patterns on the arms could be a valuable design motif to achieve 2PLSM sensor compounds based on this cruciform structure.

The 2PA spectra of a set of dipolar Zn^{2+} sensing dyes designed for ratiometric imaging in 2PLSM were also studied. These dyes had moderate 2PA strength, with redshifts of fluorescence 2PA spectra on Zn^{2+} binding. The isosbestic point of 2PA of most chromophores was within the range of 2PLSM excitation sources commonly used, rendering these dyes good candidates for use in ratiometric sensing in 2PLSM.

CHAPTER 1: INTRODUCTION AND BACKGROUND

1.1 Introduction to nonlinear optics

Since the development of the laser, the response of matter to intense light has been the subject of much study. At the extremely high optical electric field intensities that can be produced by focused laser light, many phenomena and material properties are observed that are not readily observable under normal conditions. These are non-linear optical (NLO) properties, which can be expressed as the higher-order terms in a power series expansion for the polarization induced in matter by an incident electric field: [1,2]

$$P_I = \chi^{(1)}E + \chi^{(2)}E^2 + \chi^{(3)}E^3 + \ldots \qquad (1.1)$$

In this expression the susceptibility coefficients $\chi^{(n)}$ are complex and frequency dependent and the terms E^2 and E^3 represent product of fields that can be of arbitrary frequency and and polarization. Accordingly, the susceptibilities are tensors of order n + 1 and the products in Eq. 1 are n-fold products of the tensor and the field vectors that yield the polarization vector. The $\chi^{(1)}$ coefficient is the first-order or linear susceptibility, while the $\chi^{(2)}$ and $\chi^{(3)}$ coefficients are the second- and third-order susceptibilities (that are macroscopic parameters related to the molecular first and second hyperpolarizabilities), which describe the quadratic and cubic induced polarizations. The effects of the induced polarization components involving $\chi^{(2)}$ and $\chi^{(3)}$ are generally much smaller than those associated with $\chi^{(1)}$ at relatively small field strengths. However, at high field strengths the

higher-order polarization properties of the material may come to dominate the overall response of the material to the light field. It should be noted that the electric field product in the higher-order terms (e.g. $E_a*E_b*E_c$) can give rise to a wide range of NLO effects. While there are many different NLO properties, this dissertation will focus on a particular NLO property, two-photon absorption, which, as described below can be quantified by a molecular parameter that is proportional to the imaginary part of $\chi^{(3)}$.

1.2 Two-photon absorption

Described theoretically by Maria Göppert-Mayer in 1931,[3] and first observed in the laboratory in 1961,[4] two-photon absorption (2PA) is a topic of interest for many applications, including fluorescence microscopy,[5-12] lithographic micro- and nano-fabrication with high three-dimensional resolution,[13-22] optical power limiting,[23-31] and dynamic range compression in optical signal processing.[32] Much research has been devoted to organic and polymeric materials that exhibit 2PA.[33-37] On a conceptual basis, 2PA occurs when a chromophore absorbs two photons simultaneously* instead of one, as in the case of linear or one-photon absorption (1PA). Each of the photons has approximately half the energy of the photon that would be absorbed in 1PA, although electronic structure and symmetry of the chromophore dictate the energies and selection rules for the 1PA and 2PA transitions. For chromophores that obey Kasha's rule,[38] there

* It should be noted that sequential absorption of two photons (e.g. by excited state absorption) can also be termed 2PA; the research described herein uses the term 2PA to refer exclusively to simultaneous absorption of two photons.

is relaxation to the lowest energy singlet state following 2PA, followed by radiative or nonradiative decay to the ground state or may undergo other processes such as intersystem crossing or photochemical reactions. Since 2PA requires two photons to be effectively in the same place at the same time, the likelihood of two photons being absorber at the same time depends on the square of the intensity of the excitation light. Thus, $N^{(2)}$, the number density of chromophores per unit time that undergo 2PA can be expressed as:

$$N^{(2)} = \frac{1}{2}\delta(\omega)N_g\left(\frac{I}{\hbar\omega}\right)^2 \tag{1.2}$$

where $\delta(\omega)$ is the 2PA cross-section of the chromophore at the excitation frequency (typically expressed in GM units, corresponding to 1×10^{-50} cm^4 s, N_g is the number density of chromophores in the ground state, I is the intensity of the excitation beam, and $\hbar\omega$ is the photon energy of the excitation beam. Since $I \propto E^2 \propto z^{-2}$, where z is the distance away from the focus in the direction of beam propagation, it follows that $N^{(2)} \propto z^{-4}$. Thus the probability of 2PA is highest at the focus of a laser beam, and drops off rapidly away from the focus of the beam, resulting in only a small volume within the sample being excited. This is illustrated in Figure 1.1; a solution of dye excited by 1PA shows fluorescence over the whole interaction path length of the focused excitation beam with the sample, while the same dye only emits fluorescence near the focus of an excitation beam using 2PA. The inherent three-dimensional spatial confinement of 2PA induced processes is what makes 2PA so attractive for use in microscopy and microfabrication.

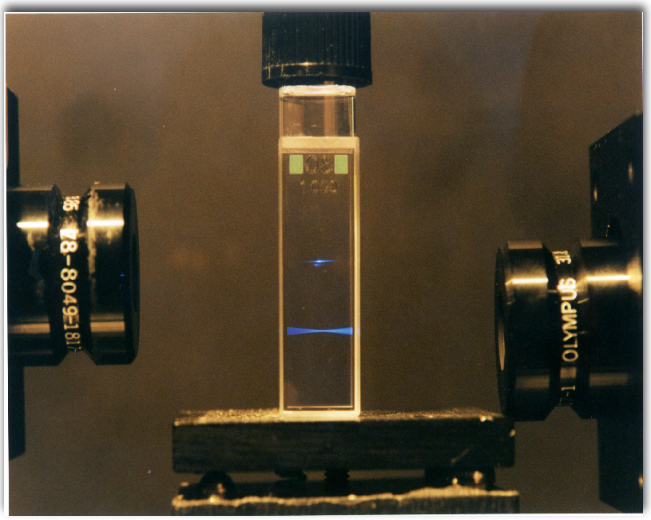

Figure 1.1. A comparison of two-photon excited (top) and one-photon excited (bottom) fluorescence in the same chromophore solution. Photo courtesy of Dr. Wim Wenseleers.

1.2.1 Theoretical description of 2PA

A Taylor series analogous to equation 1.1 describes the response of the molecular dipole moment to an applied electric field:[1]

$$\mu_i(E) = \mu_0 + \sum_j \alpha_{ij} E_j + \frac{1}{2}\sum_{jk} \beta_{ijk} E_j E_k + \frac{1}{6}\sum_{jkl} \gamma_{ijkl} E_j E_k E_l + \ldots \qquad (1.3)$$

where μ_i is the projection of $\vec{\mu}$ on the Cartesian axis i, μ_0 is the permanent dipole, α_{ij} is the linear polarizability of the molecule, and β_{ijk} and γ_{ijkl} are the first and second-order hyperpolarizabilities, respectively. Two-photon absorption is related to γ_{ijkl} by the following expression:[1,39-41]

$$\delta = \frac{4\pi\hbar\omega^2}{n^2c^2} f^4 \,\mathrm{Im}[\gamma(-\omega;\omega\omega-\omega)] \tag{1.4}$$

where δ is the 2PA cross section, n is the refractive index of the medium, c is the speed of light, and f is the local field factor. The dependence of $\gamma_{ijkl}(-\omega;\ \omega,\ \omega,-\omega)$ on molecular characteristics is given by the sum-over-states equation: [41]

$$\begin{aligned}\gamma_{ijkl}(-\omega;\omega,\omega,-\omega) &= \frac{1}{6\hbar^3} P(i,j,k,l;-\omega;\omega,\omega,-\omega) \\ &\times \left[\begin{aligned} &\sum_{m\neq 0}\sum_{n\neq 0}\sum_{p\neq 0} \frac{\langle 0|\mu_i|m\rangle\langle m|\bar{\mu}_j|n\rangle\langle n|\bar{\mu}_k|p\rangle\langle p|\bar{\mu}_l|0\rangle}{(\omega_{m0}-\omega-i\Gamma_{m0})(\omega_{n0}-2\omega-i\Gamma_{n0})(\omega_{p0}-\omega-i\Gamma_{p0})} \\ &-\sum_{m\neq 0}\sum_{n\neq 0} \frac{\langle 0|\mu_i|m\rangle\langle m|\mu_j|0\rangle\langle 0|\mu_k|n\rangle\langle n|\mu_l|0\rangle}{(\omega_{m0}-\omega-i\Gamma_{m0})(\omega_{n0}-\omega-i\Gamma_{n0})(\omega_{n0}+\omega-i\Gamma_{n0})} \end{aligned} \right]\end{aligned} \tag{1.5}$$

where $P(i,j,k,l;\ -\omega;\ \omega,\ \omega,-\ \omega)$ is a permutation operator that accounts for all possible combinations of incident electrical fields and all possible projections of molecular coordinate i on the Cartesian dimensions j, k, and l. $|0\rangle$ is the ground state of the molecule, and $|m\rangle$, $|n\rangle$ and $|p\rangle$ are excited states. $\langle 0|\mu_i|m\rangle$ and $\langle m|\bar{\mu}_i|n\rangle$ are the components μ^i_{0m} and μ^i_{mn} of the transition dipole moments between $|0\rangle$ and $|m\rangle$ and between $|m\rangle$ and $|n\rangle$ along molecular axis i, and $\langle n|\bar{\mu}_i|n\rangle$ is the component of the static dipole moment difference $\mu^i_{nn} = \Delta\mu^i_{0n}$ along molecular axis i. The energy of excited state $|m\rangle$ with respect to the ground state is represented by $\hbar\omega_{m0}$, and the damping terms of the form Γ_{m0} are the homogeneous widths of the transition between the states indicated in the subscripts. If it is assumed that only one intermediate real excited state e and only one final real excited state e' dominate the response of the molecule, equation 1.5 can be rewritten as:[42]

$$\gamma_{xxxx}(-\omega;\omega,\omega,-\omega) \propto \left[\begin{array}{l} \dfrac{M_{ge}^2 \Delta\mu_{ge}^2}{(E_{ge} - \hbar\omega - i\Gamma_{ge})^2 (E_{ge} - 2\hbar\omega - i\Gamma_{ge})} \\ + \dfrac{M_{ge}^2 M_{ee'}^2}{(E_{ge} - \hbar\omega - i\Gamma_{ge})^2 (E_{ge'} - 2\hbar\omega - i\Gamma_{ge'})} \\ - \dfrac{M_{ge}^4}{(E_{ge} - \hbar\omega - i\Gamma_{ge})^2 (E_{ge} + \hbar\omega - i\Gamma_{ge})} \end{array} \right] \tag{1.6}$$

for a linear molecule with the long axis along the *x* direction, where M_{ge} represents the transition dipole moment between states *g* and *e* and $\Delta\mu_{ge}$ is the difference in dipole moments between states *g* and *e*. The first term on the right side of equation 1.6 describes a two-photon resonant transition between the ground and first excited states of a chromophore, and is called the dipolar or D term, as it only has a non-zero value when there is a change in dipole moment between states *g* and *e*. The second term is called the two-photon or T term, as it includes contributions from two different virtual transitions, between *g* and *e* and *e* and *e*′. The last term is the negative or N term, which only contributes at a one-photon resonance and is not taken into consideration for 2PA processes that are far from a one-photon resonance.

Figure 1.2 is a pictorial representation of 2PA. The first photon incident on the chromophore creates an intermediate "virtual" state, *v*, which then undergoes further excitation from the second photon to promote the chromophore to a real excited state of the chromophore. Figure 1.2(a) shows the states involved in 1PA and 2PA transitions in a centrosymmetric chromophore belonging to point group C_{2v} (as do the centrosymmetric chromophores described in Chapters 3 and 5 of the current work) while Figure 1.2(b) shows the states involved in the 1PA and 2PA transitions of a non-centrosymmetric chromophore. For centrosymmetric chromophores, 2PA is allowed between states with the same parity, while there is no such restriction for non-centrosymmetric

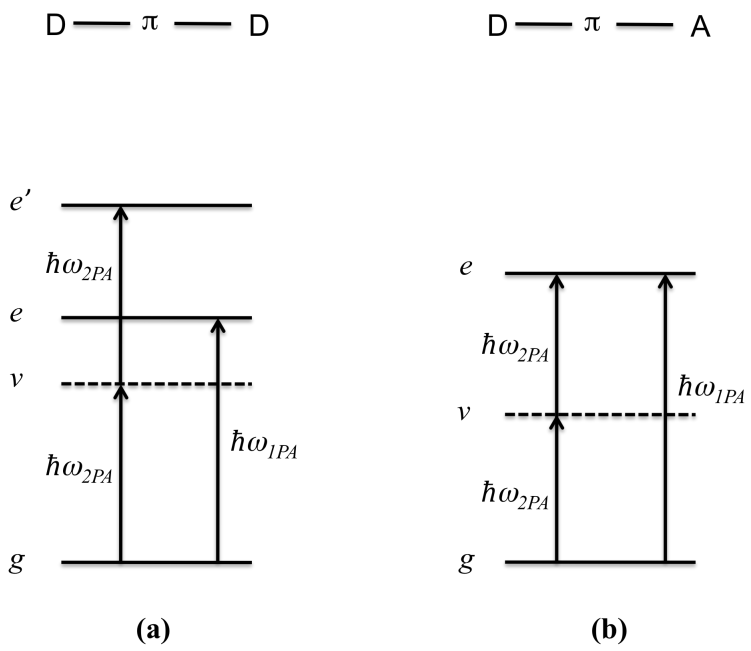

Figure 1.2: Schematic of the energy levels involved in the two-photon absorption process in **(a)** centrosymmetric and **(b)** non-centrosymmetric chromophores. Letters D and A symbolize electron donor and acceptor groups.

chromophores. In the former case, the ground state, *g*, has A_g symmetry, while the lowest allowed state for 1PA, *e*, has B_u symmetry. The higher-lying excited state *e′* has A_g symmetry, and 2PA to *e′* is symmetry allowed. In the latter case, 2PA transitions to the lowest 1PA state are allowed , and Figure 1.2(b) shows 2PA to the 1PA excited state.

1.2.2 Structure-property relationships of 2PA in organic chromophores

The first research into 2PA in organic chromophores was performed on small molecules and commonly used dyes and was used primarily as a complementary spectroscopic tool to elucidate electronic structure and symmetry.[36] With the advent of 2PA-based applications such as two-photon microscopy and microfabrication, much new

research was devoted to identifying molecular structures that possessed strong 2PA coefficients. By making the assumption that the damping width Γ_{ge} in equation 1.6 is very small in comparison to the energy detuning term E_{ge} - $\hbar\omega$ in the denominator, the T and D terms at the two-photon resonance can be simplified to eq. 1.7 and 1.8, respectively. In particular, for centrosymmetric chromophores, for which $\Delta\mu_{ge} = 0$, only the T term of equation 1.6 is significant and equation 1.6 may be reduced to the following relationship for the peak two-photon resonance of the higher lying excited state e' (i.e. $E_{ge'} = 2\hbar\omega$), also known as the three-state model:[33,42]

$$\delta_{g\to e'} \propto \frac{M_{ge}^2 M_{ee'}^2}{(E_{ge} - \hbar\omega)^2 \Gamma_{ge'}} \tag{1.7}$$

For dipolar chromophores at the peak two-photon resonance of the lowest excited state ($E_{ge} = 2\hbar\omega$), the D term is non-zero and equation 1.6 simplifies to:[42]

$$\delta_{g\to e} \propto \frac{M_{ge}^2 \Delta\mu_{ge}^2}{(\frac{1}{2}E_{ge})^2 \Gamma_{ge}} \tag{1.8}$$

which is commonly known as the two-state model. The relationships shown in equation 1.7 and 1.8 implied that utilizing linear molecular structures would enable attainment of large δ by maximizing the transition dipole moments along the axis of the molecule while decreasing E_{ge}. One direct route toward maximizing M_{ge} and minimizing E_{ge} is to increase the conjugation length of the chromophore. Equation 1.7 also implies that one way of maximizing δ_{max} is to bring the energy of the 2PA excitation photon close to the energy of state e.

In 1998 two groups reported large peak 2PA values in linear organic molecules with structures that were designed based on these principles. Albota et al.[33] for

quadrupolar chromophores and Reinhardt et al.[34] for dipolar chromophores both showed experimentally that increasing conjugation length led to significant increases in δ. However, Reinhardt's data assumes consistent shape and peak position of the 2PA band in chromophores of different lengths, and are also affected by excited state absorption, and so are not useful for evaluating the effects of altering molecular parameters on absolute δ_{max}. Albota et al. also showed that for quadrupolar chromophores, increases in transition moment $M_{ee'}$ may be achieved by substituting electron-donating and withdrawing groups at the terminal positions of the chromopohore.[33] Table 1.1 lists a selection of centrosymmetric and dipolar chromophores in which the general increase of δ_{max} and red-shift of the peak of the 2PA band, $\lambda_{max}^{(2)}$, with increased conjugation length and donor/acceptor substitution can readily be observed.

1.3 Literature survey of 2PA in branched chromophores

With the molecular structure-property relationships for two-photon absorption in linear chromophores well understood, the use of branched molecules has been pursued as a means of achieving higher δ_{max}. The coupling of multiple chromophores into a single unit is a common motif in the design of multi-dimensionally conjugated chromophores due to the potential for obtaining enhancement of 2PA properties beyond what is achievable with linear compounds, as demonstrated by Beljonne et al.[42] Three multidimensional branched structures that have been studied for their 2PA and other properties are octupolar compounds,[42-52] dendrimers[41,53-60] and cruciform compounds.[61-83]

Table 1.1. Two-photon absorption characteristics of selected linear chromophores.

	Structure	$\lambda_{max}^{(2)}$ (nm)	δ_{max} (GM)	Reference
A	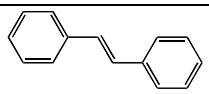	488	18	84
B	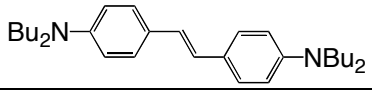	600	210	33,40
C	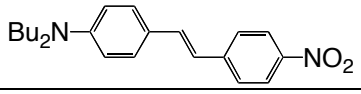	972	170	85
D	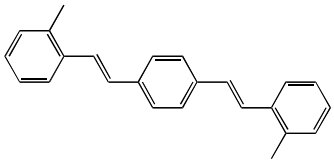	568	70.1	86,87
E	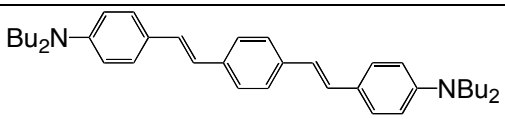	730	995	33,40
F	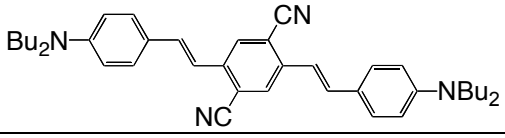	830	1750	88
G	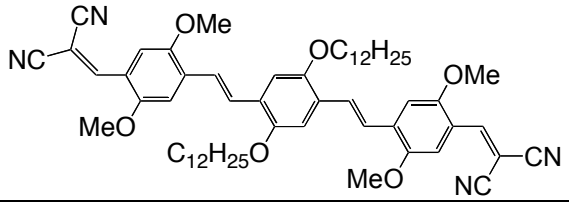	825 (940)	480 (620)	33
H	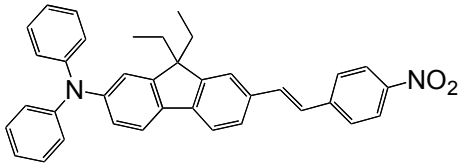	864	1300	89
I	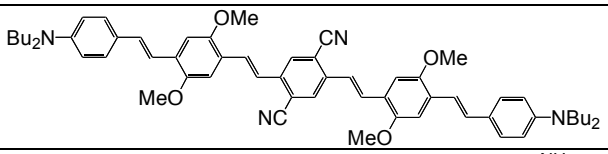	970	5300	90
J	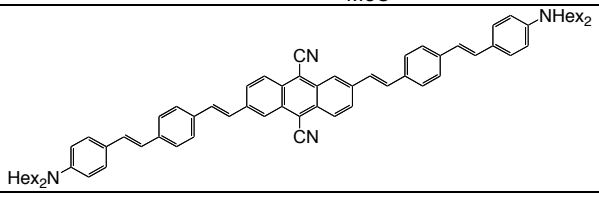	980	5530	91

K	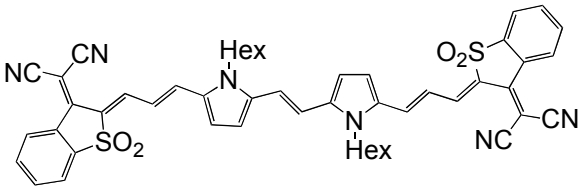	1240	5900	[92]

Parenthetical values are for secondary 2PA peaks.

1.3.1 Octupolar structures

In the octupolar structure (Figure 1.3), three arms share a core group such as a triphenylamine or benzene ring. Typically, these arms are similar in structure to linear chromophores, and a key question with respect to octupolar chromophores is whether the 2PA response of the octupolar chromophore is enhanced, i.e. greater than the sum of its linear arms. Beljonne et al.[42] showed in a combined theoretical and experimental study of crystal violet (amongst other octupolar dyes) that δ_{max}/unit was increased approximately threefold by its inclusion in the octupolar dye when there was significant "crosstalk" between the arms. Beljonne et al.'s calculations also indicated that when the inter-arm coupling is weak, there is no enhancement of δ_{max}/unit. Terenziani et al.[51,52] reported similar observations when comparing octupolar chromophores based on 1,3,5-substituted phenyl cores and triphenylamine cores. In cases where the arms of each of a pair of differing octupolar chromophores with either phenyl or triphenylamine cores had similar dipole moments to those of the arms of the other octupolar chromophore, the phenyl-cored compounds showed little deviation from additive behavior due to the lack of inter-arm interaction beyond simple electrostatic coupling. The triphenylamine-cored compounds, however, showed not only an enhancement of δ_{max}/unit, but also the

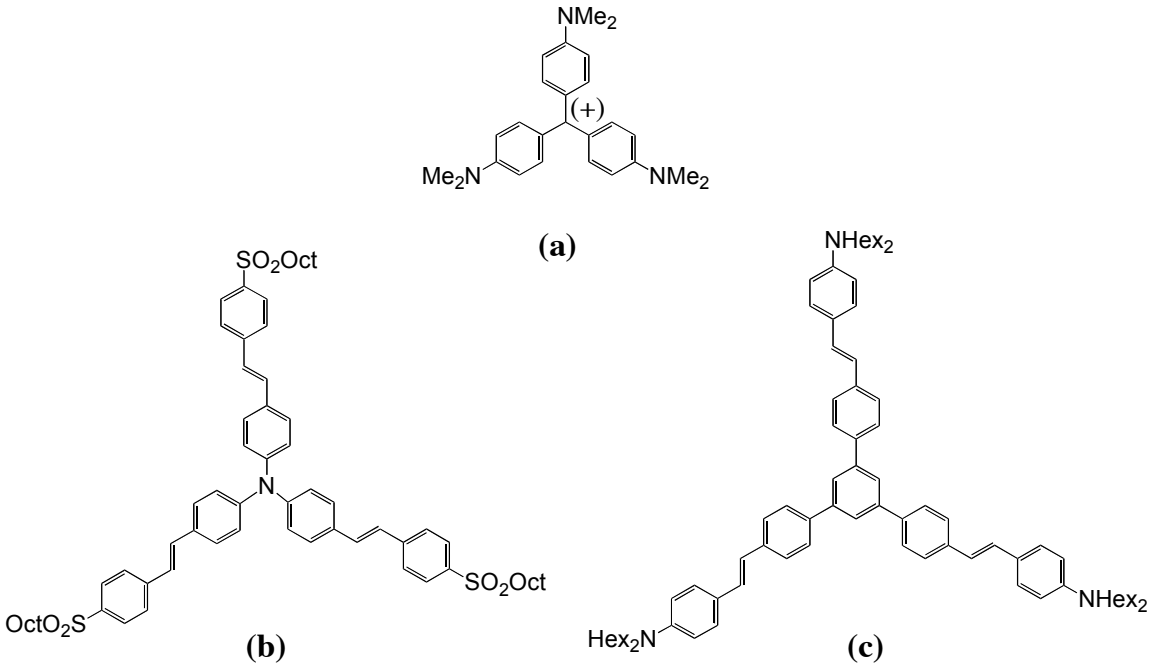

Figure 1.3. Octupolar chromophores with **(a)** carbocation, **(b)** triphenylamine and **(c)** 1,3,5-substituted benzene cores.

appearance of a new 2PA band blue-shifted from the main 2PA peak, which resulted from coherent interactions of the units. Yoo et al.[93] also observed an enhancement of 1.6 in δ_{max}/branch in a system of quadrupolar chromophores sharing a triphenylamine core.

1.3.2 Dendrimers

Another method of creating branched chromophores is through the dendrimeric architecture, in which chromophores are attached at one end to a central group, and their opposite ends serve as branching points for further chromophores. Dendrimers are of particular interest as they offer the possibility of grouping significantly more than the three chromophores of an octupolar compound together in a relatively small space.

Drobizhev et al.[54-56] have reported superlinear dependence of δ_{max} on dendrimer generation for dendrimers based on the bis(diphenylamino)stilbene chromophore, although the superlinear increase was found to saturate by the third or fourth generation of the dendrimer. The saturation of enhancement is ascribed to reductions in electronic coupling resulting from the out-of-plane arrangement forced on the dendrimer branches by steric interaction of closely spaced chromophores. Ramakrishna et al.[60] also observed superlinear dependence of δ_{max} on dendrimer generation for an oligothiophene dendrimer. However, the mechanism of enhancement may be different from that of the dendrimers studied by Drobizhev et al., as the oligothiophene dendrimer not only contained coupled discrete chromophores, but was characterized by a more extended conjugation length.

1.3.3 Cruciforms

Chromophores based on 1,2,4,5-substituted phenyl rings are commonly referred to as cruciform chromophores (see Table 1.2) and have been the subject of recent study for their general properties.[61-83] They may be viewed as pairs of 1,4-bis-substituted benzene chromophores coupled through the central phenyl and they have been experimentally observed to display subadditive 2PA strength in the case where all arms are donor-substituted.[72,73] According to an exciton model developed[72] to describe the interactions of the units, the 2PA strength of the cruciforms in these compounds depends on the angle between the transition dipoles of the units and the excited state coupling between the units. There is significant electronic interaction of the units, but no enhancement of δ_{max}. The question remains over the effects of coupling linear chromophores with different conjugated pathways. Recent research[64,66,67] has shown that

Table 1.2 Selected cruciform compounds reported in the literature and their key two-photon absorption characteristics.

Compound	$\lambda_{max}^{(2)}$ (nm)	δ_{max} (GM)	Reference
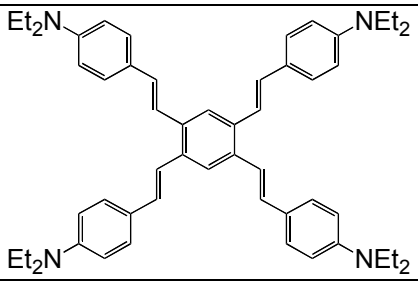	700	1100	72,73
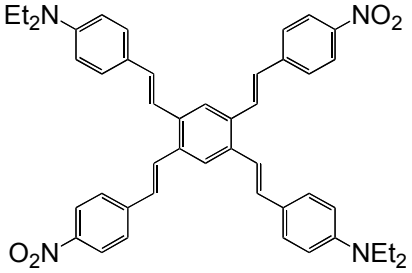	</= 710 (830)	>/=350 (250)	72,73
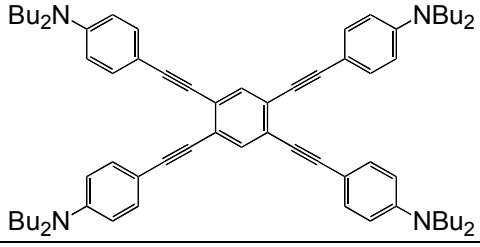	710	520	75,76
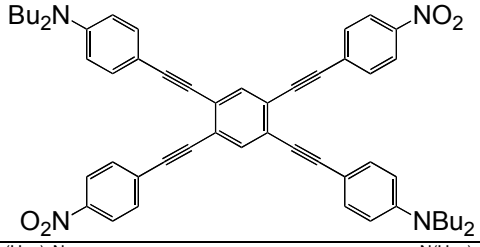	550 (750)	600 (240)	75,76
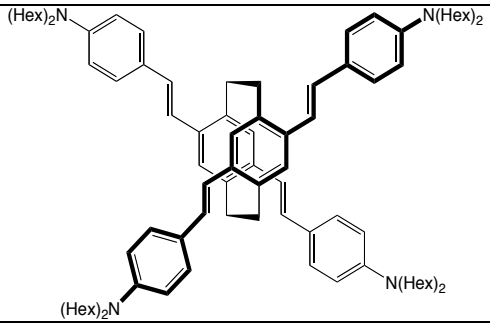	720	1410	94

the use of differing conjugation pathways (such as vinyl and ethynyl linkers) in different arms of the same cruciform chromophore leads to spatially distinct HOMOs and LUMOs, with significant effects on the linear spectroscopic properties of the compounds. However, the two-photon absorption properties of cruciform chromophores with non-degenerate conjugated linkers have not been investigated. Using this alternate method for controlling the energetic coupling of the arms in addition to using D/A substitution could provide better understanding of the nature of inter-arm coupling in cruciform chromophores, and could open up new design strategies for creating chromophores optimized for particular applications.

It should be noted that branched chromophores have also been developed in which two independent linear units are physically coupled by a paracyclophane linker on their central phenyl groups (see Table 1.2), bearing some resemblance to cruciform chromophores. These compounds did not have enhanced δ_{max} over their independent arms,[94] although several of them did have unusually high $\eta\delta_{max}$ (where η is the fluorescence quantum yield) in water of 294 and 359 GM, the largest figures for $\eta\delta_{max}$ of small organic molecules in water to date.[95]

1.4 Chromophores for two-photon microscopy

One of the most widely applied techniques utilizing 2PA is Two-Photon Laser Scanning Microscopy (2PLSM), in which a focused near-infrared laser beam is scanned

across and through a sample and it induces two-photon excitation in a fluorescent label. As the excitation is effective confined in a small region around the focus of the beam, the distribution of the resulting fluorescent light represents a map of the sample imaged, in three dimensions and at high resolution.[5,6,11,15,96,97] The advantages of 2PLSM over conventional and confocal microscopy with ultraviolet or visible excitation are manifold. Near-IR light of the wavelengths typically used for 2PA has a much longer penetration depth into biological tissue that does UV or visible light, allowing imaging of deeper structures and processes, and provides the additional advantage of lower cytotoxicity. Since its introduction in 1990, 2PLSM has been used in numerous biological and medical imaging applications to study cellular structure, function and transport. The many applications of 2PLSM would benefit for the development of new 2PA chromophores designed for various purposes. Ideally, dyes for 2PLSM should have:

- high two-photon excited fluorescence figures of merit, i.e. $\eta\delta$, where η is the quantum yield of fluorescence,
- δ_{max} that fall within the excitation range (~700 - ~1000 nm) used by most commercial 2PLSM apparatus,
- good solubility and photophysical properties in aqueous environments such as the cell, and
- for analyte-sensing dyes, significant shifts in absorption and emission bands upon analyte binding.

1.4.1 Conventional small molecule chromophores

Historically, most dyes used in 2PLSM have been commercially available dyes, many designed for use in confocal microscopy, which may display relatively high 2PA cross-sections, but which are not specifically designed or optimized for 2PA. Table 1.3 shows some of the dyes used in early applications of 2PLSM and their 2PA characteristics in the range of 700-1000 nm. The general characteristics that can be observed are relatively low $\eta\delta_{max}$ and relatively low-wavelength $\lambda_{max}^{(2)}$. The highest $\eta\delta_{max}$ shown in Table 1.3 is 196 GM for Rhodamine B in methanol, a relatively small value compared to chromophores optimized for 2PA, and one that would likely decrease further in aqueous environments, where the stabilization of intramolecular charge-transfer is expected to lead to a reductions in η and δ from their values in less polar environments.[95] Chromophores optimized for $\eta\delta_{max}$ in aqueous environments would offer significant advantages for 2PLSM, including further reduction of cytotoxicity of 2PLSM by use of lower dye concentrations and excitation powers, and could also enable the use of less expensive excitation sources,[10] and recent research has been devoted both to identifying native biological 2PA chromophores such as proteins and in designing new small molecule dyes for 2PLSM applications.

1.4.2 Proteins

When 2PLSM was introduced, there was immediate interest in using native biological chromophores as labels.[7,98,99] Xu et al.[7] investigated NADH and FMN, and found $\eta\delta_{max} < 1$ for both across the 2PLSM window of interest. Fluorescent proteins were quickly indentified as attractive potential 2PLSM chromophores, due to their innate biocompatibility and the ability to genetically program cells to express proteins in desired

Table 1.3. Examples of dyes used in early applications of two-photon microscopy.

Compound	$\lambda_{max}^{(2)}$ (nm)	$\eta\delta_{max}$ (GM)	Reference
Cascade Blue	800	<10	[100]
Lucifer Yellow	860	0.95	[100]
Bodipy	920	20	[100]
DAPI (not DNA conjugated)	700	0.16	[100]
Coumarin 307	800	15	[100]
Fluorescein	782 (920)	34.6 (23.7)	[100]
Rhodamine B	700 (840)	196 (147)	[100]
Indo-1 (with Ca^{2+})	680 675	5 2	[7]
Fura-2 (with Ca^{2+})	720 690	10 10	[7]

Data in last two rows are approximate values estimated from plots in cited reference. Parenthetical values are for secondary 2PA peaks.

locations or conditions,[101] and green fluorescent protein (GFP) was used in an early application of 2PLSM.[102] 2PA spectra of wild type and mutant green fluorescent protein were reported by Xu et al.[7] and showed $\eta\delta_{max}$ comparable to conventional dyes (see Table 1.4). In particular, the maximum 2PA strength observed was to the lowest excited state, offering a guideline for selecting appropriate fluorescent proteins for desired imaging applications based on the excitation wavelength to be used. However, the authors only reported on these proteins and only observed one 2PA band, which, they noted, restricted the number of other dyes that could be coexcited along with the protein. Recently, Drobizhev et al.[101,103] studied a comprehensive set of fluorescent proteins, particularly those with red-shifted absorption and fluorescence bands. They observed two 2PA bands, one near in energy to the 1PA band and one at roughly twice the energy of the 1PA band, allowing for a greater range of dyes that can be coexcited with the proteins

and broadening the potential 2PLSM applications of fluorescent proteins. As can be seen in Table 1.4, the figures of merit $\eta\delta$ for a number of these proteins were significantly higher than those of GFP, with some ranging over 100 GM for the high-energy 2PA transition and others at ~60 GM for the low-energy 2PA transition. In recent research, the high-energy 2PA band of a red fluorescent protein has been coexcited with the low-energy 2PA band of a blue fluorescent protein to produce two-color 2PLSM images with single-wavelength excitation.[104] However, even with the availability of proteins with strongly favorable 2PA properties, there is still need for novel small molecule organic chromophores for 2PLSM.

Table 1.4. Two-photon absorption properties of fluorescent proteins.

Compound	$\lambda_{max}^{(2)}$ (nm)	$\eta\delta_{max}$ (GM)	Reference
Green fluorescent protein, wild type	800	6	[7]
Green fluorescent protein, wild type	810 (550)	9.6 (21)	[103]
Green fluorescent protein, S65T mutant	920	8	[7]
Cyan fluorescent protein	860	δ=100	[103]
Red fluorescent protein monomer	1100	δ=30	[103]
mTangerine	698 (1055)	7.8 (3.3)	[101]
mBanana	674 (1070)	66 (42)	[101]
mOrange	640 (1080)	109 (37)	[101]
TagRFP	674 (1050	170 (39)	[101]
DsRed2	700 (1050)	69 (63)	[101]

Data in parentheses are for secondary 2PA peaks.

1.4.3 Chromophores for analyte sensing 2PLSM

One of the key applications of 2PLSM is in tracking the local concentrations of analytes such as metal ions or metabolic products in cells. This requires the use of dyes that display significant changes in spectral properties in the presence of analyte. As with other 2PLSM dyes, most sensing dyes characterized to date were designed with their 1PA properties in mind and are not optimized for 2PA;[7,10,11,100,105,106] most also have relatively low-wavelength 2PA peaks. A number of metal binding dyes, in fact, do not display different 2PA action spectra (that is, spectra of $\eta\delta$) at all when they are bound to a metal or as free ligands,[7] although most of the traditional dyes display blue shifts of spectral properties upon metal binding.[106] As with other 2PLSM dyes, desirable qualities for sensing dyes are long wavelength excitation, large 2PA cross-sections, and high quantum yields of fluorescence.

Several groups have recently developed chromophores specifically designed for 2PLSM sensing applications such as detection of metal and other analyte concentrations and local environmental conditions.[107-114] Pond et al.[107] developed a D-A-D chromophore based on compound **F** in Table 1.1 with mono-aza-crown-ether groups replacing one or both of the amine π-electron donor groups. In the absence of metal cations, all three compounds had very similar 2PA spectra, with $\lambda_{max}^{(2)}$ = 810 nm and δ_{max} on the order of 2000 GM, both of which quantities are suitable for 2PLSM use. The authors observed that upon binding of Mg^{2+} ions, the 2PA of both crown-ether substituted compounds was reduced significantly in the region of interest for 2PLSM. This was attributed to "turning-off" of the π-electron donors due to interactions of the aza-nitrogen electron lone pair with the Mg^{2+} ion. While the 2PA "turn-off" model of analyte sensing could be used for

2PLSM, a preferable model would be 2PA "turn-on," in which 2PA-induced fluorescence is enhanced by analyte binding.

1.5 Research objectives

The objectives of the work described in this thesis were to further the understanding of molecular structure-property relationships in chromophores designed for two-photon absorption, with specific attention to chromophores with multi-dimensional conjugation and to chromophores designed for the specific function as two-photon microscopy labels. The coupling of transitions in discrete components of a chromophore and the effects of the coupling on the 2PA strength of the chromophore over that of its components is the topic of Chapter 3, in which cruciform compounds composed of arms with non-degenerate conjugation and with varying patterns of electron donors and acceptors substituted at the termini of the arms were studied. The effects of the differing conjugated pathways and of the D/A substitution on the coupling between the arms and the resultant spectroscopic parameters were studied with linear and two-photon absorption spectroscopy. In Chapter 4, the 2PA response of some cruciforms to zinc ion binding is addressed. The D/A groups on some cruciform compounds are also subject to metal ion binding, and the combination of the cruciform structure and D/A sensing groups provide a potential route to designing new 2PLSM chromophores. With the advent of 2PLSM, the interest in chromophores optimized for both 2PA and

biological functionality is high. In Chapter 5, a general design for small-molecule dipolar dyes optimized for both ratiometric turn-on sensing of Zn^{2+} and two-photon absorption is examined experimentally to address these issues.

CHAPTER 2: MATERIALS AND METHODS

2.1 Materials

Cruciform chromophores **13**-**20** and linear model compounds **11** and **12** studied in this work were synthesized in the group of Professor Uwe Bunz at the Georgia Institute of Technology by Dr. James N. Wilson and Dr. Anthony J. Zucchero. The syntheses for compounds **13** and **19** were reported by Zucchero, et al.,[66] compounds **15**, **16**, **18** and **22** by Wilson et al.,[62] compound **17** by Wilson, et al.,[64] and **21** by Wilson et al.[65]

The syntheses of linear compounds **1** and **1B** used in Chapter 4 were reported in the literature.[40] Zinc trifluoromethanesulfonate and trifluoromethanesulfonic acid were obtained from Sigma-Aldrich.

Oxazole and thiazole chromophores were synthesized in the group of Professor Christoph Fahrni at Georgia Institute of Technology by Yonggang Wu (**YW2-068**), Dr. Sumalekshmy Sarojinni-Amma (**SL35**, **SL327**, **SL407**, **SL476** and **SL477**), Dr. Karl Huettinger (**SL477** attachment to peptide) and Dr. Manjusha Verma (**MV170**). Synthetic information for **SL35** was reported by Sumalekshmy, et al.[115] Solutions of the chromophores in Chapter 5 were prepared by members of the Fahrni group. Aqueous solutions contained PIPES (10 mM) and KCl (0.1 mM) buffer at a pH of 7.05. The source of Zn^{2+} was Zinc trifluoromethanesulfonate (Sigma-Aldrich).

All organic solvents used for spectroscopy including toluene, cyclohexane, ethanol,

methanol and dichloromethane were spectrophotometric grade (Aldrich) or comparable (Omnisolv, EMD) and were used as received, while aqueous solutions were made using deionized water. Commercially available compounds employed as reference materials for quantum yield and two-photon measurements were used as received, including fluorescein (Acros), 1,4-bis(2-methylstyryl)-benzene (Aldrich), and 9,10-bis(phenyl-ethynyl)anthracene (Aldrich). All were obtained in the highest purity available. Basic solutions of fluorescein were made using sodium hydroxide (Aldrich).

The solvent system used in Chapter 4 for the studies of zinc binding in cruciforms and model compounds was 95% dichloromethane and 5% toluene. Linear absorption and 2PA measurements were performed on solutions that were 10 μM in chromophore, with the exception of zinc-bound **14**, which was studied at a chromophore concentration of 5 μM. The concentration of zinc trifluoromethanesulfonate used to saturate the chromophore solutions was 52 μM. Due to relatively low solubility, fresh solutions of zinc trifluoromethanesulfonate in dichloromethane were prepared immediately before addition to chromophore solutions. Titrations of **15**, **22** and **1B** with trifluoromethanesulfonic acid in methanol were performed by the addition of 25 μl aliquots (measured using a pipettor) of 200 μM triflic acid solution to 2.5 ml of 10 μM chromophore solutions in methanol. Spectra were corrected for dilution by the titrant aliquots.

2.2 Linear Spectroscopic Measurements

2.2.1 UV/visible spectroscopic characterization

Linear absorption spectra were recorded on a Hewlett Packard 8453 diode array spectrophotometer. A blank spectrum of the solvent (pure deionized water in the case of NaOH or H_2SO_4 solutions) was used as a baseline correction for the chromophore solutions. Molar extinction coefficients (ε) were obtained from a linear regression analysis of solution absorbance as a function of chromophore concentration using the Beer-Lambert equation[116]

$$A(\lambda) = \varepsilon(\lambda)cl \qquad (2.1)$$

in which $A(\lambda)$ is the absorbance at wavelength λ, c is the chromophore concentration, and l is the optical path length of the sample in centimeters. Multiple dilutions of three independent stock solutions were used, spanning the concentration range between 1 x 10^{-7} M and 5 x 10^{-4} M. At higher concentrations, 0.1 cm cuvettes were used to extend the concentration range that could be studied, while 1 cm cuvettes were used for lower concentrations. Extending the concentration to 500 μM enabled the investigation of the possible aggregation of compounds at the concentrations as used in the two-photon absorption measurements.

2.2.2 Fluorescence spectroscopy and quantum yield determination

Fluorescence emission spectra were measured using a Spex Fluorolog-2 spectrofluorimeter. This instrument has two double-slit monochromators to independently adjust the power, peak wavelength and bandwidth/resolution of the excitation beam and collected fluorescence signals, enabling measurements of a wide

range of concentrations and fluorescence quantum yields. After passing through one double-slit monochromator, the excitation light is focused weakly through the sample solution to ensure a relatively uniform distribution of excited chromophores. The fluorescence emission is collected at a right angle to the propagation direction of the excitation beam and then passed through a second monochromator, which also has adjustable slits to control the fluorescence signal and the resolution of the measurement. The emitted light is then detected using a photomultiplier tube (Shimadzu R928) whose range is 200-850 nm. In order to avoid reabsorption effects, fluorescence spectra were taken of solutions with a peak absorbance of <0.05 in a 1 cm cuvette. Solutions for quantum yield measurements had an absorbance of <0.02 (in a 1 cm cuvette) at the excitation wavelength so that the excitation beam intensity would stay relatively constant as is passed through the sample. Solvent blank spectra and a correction factor were used to correct for the instrument response function and dark counts.

Fluorescence quantum yields (η) were measured using a reference-based method in which the fluorescence emission of a well-characterized reference compound is measured under the same excitation conditions as the unknown sample. The following relationship[117] was used to calculate the η of samples reported in this work:

$$\eta_u = \eta_r \frac{F_u A_r(\lambda_{exc}) n_u^2}{F_r A_u(\lambda_{exc}) n_r^2} \tag{2.2}$$

where $F = \int F(\lambda) d\lambda$ is the spectrally integrated fluorescence emission of a chromophore, $A(\lambda_{exc})$ is the absorption of a solution at the excitation wavelength, and n is the refractive index of the solvent used. The subscripts u and r refer to the unknown sample and reference solution, respectively. The measurements reported in this work were all made

with the same excitation wavelength for both unknown sample and reference. The references used for the quantum yield measurements in Chapter 3 were 1,4-bis(2-methylstyryl)-benzene in cyclohexane (η = 0.94)[118] for **11**-**13**, and 9,10-bis(phenyl-ethynyl)anthracene in cyclohexane (η = 1)[118] for **14**-**20**. In Chapter 4, 1,4-bis(2-methylstyryl)-benzene was used as the reference for **13**, **21** and **22** both in the absence and presence of zinc and for **1**, **14**, **15**, **17** and **19** in the presence of zinc. 9,10-bis(phenyl-ethynyl)anthracene was used for **1**, **14**, **15**, **17** and **19** in the absence of zinc and for **1B** both in the absence and presence of zinc. The quantum yield measurements for the chromophores in Chapter 5 were performed by members of the Fahrni group using quinine sulfate dihydrate in 1 N H_2SO_4 (η = 0.543)[119] except for MV170, for which the reference was fluorescein in pH 11 NaOH (η = 0.90).[119]

2.3 Determination of two-photon absorption spectra

The main spectroscopic techniques used to determine 2PA cross sections and spectra are nonlinear transmission (NLT), z-scan and two-photon excited fluorescence (2PEF). The first two methods measure the attenuation of an intense light beam through a concentrated sample. While the first two methods are commonly used, significant drawbacks include the need to use a very well-characterized laser beam including spatial and temporal pulse characteristics, the possibility of aggregation affecting the 2PA properties of the material at the relatively high concentrations needed, and, most importantly, the fact that they are not selective for 2PA; additional absorption processes

such as excited-state absorption contribute to the observed beam attenuation. As a result both methods are subject to significant overestimation of 2PA cross-sections, unless appropriate beam propagation treatments are used that account for additional absorption processes. 2PEF techniques avoid this disadvantage; since the fluorescence signal is directly proportional to the number of excited states created, additional absorption processes do not contribute to the measurement, provided that certain conditions (to be discussed below) are met. Additionally, when using a comparative measurement to calibrate the 2PEF of the sample to the 2PEF of a well-characterized reference, it is not as important to know the precise characteristics of the beam, as will be discussed below. However, a disadvantage of 2PEF methods is that the compounds under investigation must be fluorescent and preferably with at least a moderate quantum yield (> 5 - 10%) in order to allow measurements with high signal-to-noise ratio.

2.3.1 Theory of Two-Photon Excited Fluorescence excitation method

The 2PEF method measures a fluorescence signal proportional to the number of chromophores in the emissive excited states following absorption of two photons, which is directly related to N_{abs}, the number of photons absorbed by a sample of chromophore in the 2PA process:[100]

$$N_{abs}(t) = \delta \int_V C(\vec{r},t) I^2(\vec{r},t) dV \qquad (2.3)$$

In which δ is the two-photon absorption cross-section, C is the concentration of the chromophore, I is the intensity of the excitation, and V is the interaction volume of the sample under illumination. By using low excitation intensity conditions to effectively eliminate saturation and photobleaching of the chromophore, C may be considered a

constant. Additionally, the intensity may factored into separate terms for the temporal and spatial distributions of the excitation light, $I_0(t)$ and $S(r)$ respectively, resulting in equation 2.4:[100]

$$N_{abs}(t) = \delta C I_0^2(t) \int_V S^2(\vec{r}) dV \tag{2.4}$$

Taking into account the fluorescence quantum yield η, the overall collection efficiency ϕ of the measurement system, and the fact that two excitation photons are required to produce each fluorescent photon, the number of two-photon excited fluorescent photons detected per unit time is then:[100]

$$F(t) = \frac{1}{2} \eta \phi N_{abs}(t) \tag{2.5}$$

As a matter of practice the quantity measured in the laboratory is the time averaged fluorescence $\langle F(t) \rangle$, and thus equation 2.4 may be substituted into equation 2.5 to give:[100]

$$\langle F(t) \rangle = \frac{1}{2} \eta \phi \delta C \langle I_0^2(t) \rangle \int_V S^2(\vec{r}) dV \tag{2.6}$$

Since the signal obtained from detectors is generally proportional to $\langle I_0(t) \rangle$ and not $\langle I_0^2(t) \rangle$, we rewrite equation 2.6 to express the time averaged fluorescence as a function of the time averaged excitation intensity:[100]

$$\langle F(t) \rangle = \frac{1}{2} \eta \phi \delta C g^{(2)} \langle I_0(t) \rangle^2 \int_V S^2(\vec{r}) dV \tag{2.7}$$

where[100]

$$g^{(2)} = \frac{\langle I_0^2(t) \rangle}{\langle I_0(t) \rangle^2} \tag{2.8}$$

is the second-order temporal coherence parameter of the excitation light. It can be seen from equation 2.7 that four experimentally determined parameters generally must be

known in order to calculate the 2PA cross-section: the fluorescence quantum yield, the collection efficiency of the experimental apparatus, the second-order temporal coherence of the excitation light, and the spatial distribution of the excitation light. Typically, Kasha's rule[38] is assumed to hold for large organic molecules, and the fluorescence quantum yield measured under one-photon excitation is used for determination of the 2PA cross section using 2PEF. The photon collection efficiency is the fraction of photons detected to the total photons emitted by the sample and depends on solid angle of the collection optics, the transmission of the optics and monochromator leading to the detector, and the quantum efficiency of the detector. While absolute calibrations of the total collection efficiency can be performed, a more common method is to use a relative measurement technique in which the time-averaged 2PEF signal of the unknown sample is compared to the time-averaged 2PEF signal of a well-characterized reference compound measured under identical conditions. The 2PA cross section can then be calculated by solving equation 2.7 for δ and taking the ratio of the unknown sample δ to the reference compound δ:

$$\delta_u(\lambda) = \delta_r(\lambda)\frac{F_u \eta_r \phi_r C_r}{F_r \eta_u \phi_u C_u} \tag{2.9}$$

where F is the time averaged 2PEF signal detected. The exact form of ϕ depends on the detection system used; the ϕ used in this work will be described below.

2.3.2 Nanosecond two-photon excited fluorescence excitation experimental setup

The 2PA spectra reported in this work were determined using the reference-based two-photon excited fluorescence (2PEF) method.[100] The experimental setup is shown in Figure 2.1. The source of excitation light was a nanosecond pulsed optical parametric

oscillator (Quanta-Ray MOPO 730) that was pumped by the third harmonic (355 nm) of a Q-switched Nd:YAG laser (Quanta-Ray Pro-250) at a 10 Hz repetition rate with a pulse width of approximately 5 ns. The laser output of the MOPO is continuously tunable over the ranges of 430-700 nm (signal beam) and 720-2000 nm (idler beam). The output of the MOPO is steered using prisms to a zero-order achromatic half-wave plate and then through an uncoated Glan-laser polarizer. The angle of the half-wave plate may be altered to provide continuous control of the excitation intensity, as the polarizer is set to pass only vertically polarized light. Immediately after the polarizer is a filter block containing several long-pass filters with cutoffs at approximately 400 nm to block any remaining 355 nm pump light from the MOPO. The excitation beam is then split by a beam-splitter into two arms, designated as the sample arm and the reference arm. The unknown sample and reference compound are rotated through the sample arm at each excitation wavelength, while the reference arm contains another sample of the reference compound, to perform shot-to-shot normalization of fluctuations in the laser intensity over the course of the data collection. Thus, F_u and F_r are measured as normalized intensitites:

$$F_u = \frac{F_u(\text{sample arm})}{F_r(\text{reference arm})}$$
$$F_r = \frac{F_r(\text{sample arm})}{F_r(\text{reference arm})} \qquad (2.10)$$

In each arm a 50 cm focal length lens focuses the excitation beam into the 1 cm cuvette containing the sample; given this focal length and the diameter of the MOPO output

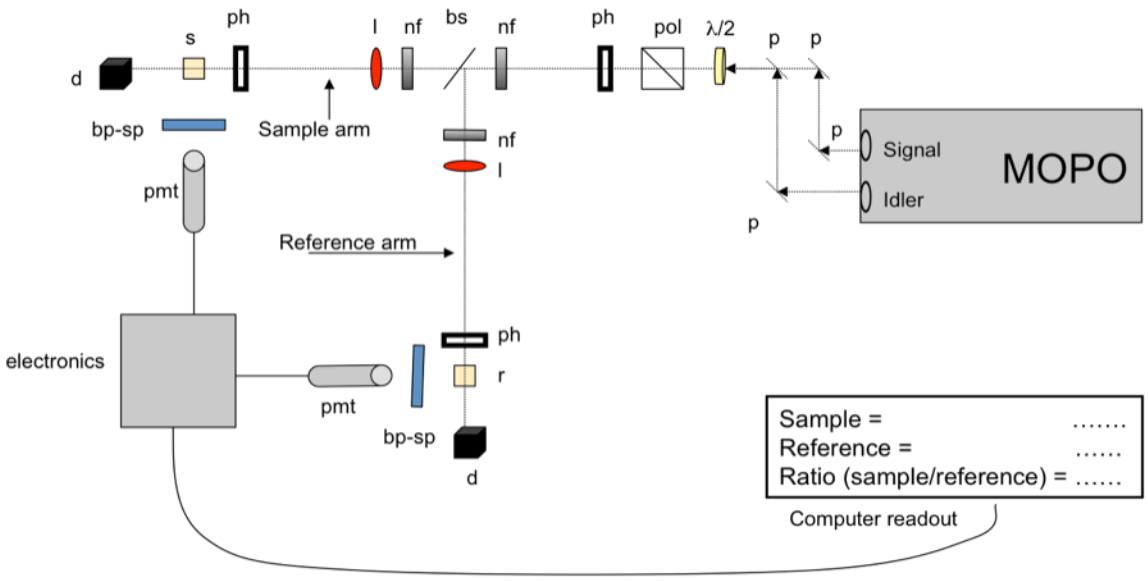

Figure 2.1. Experimental apparatus for nanosecond TPEF. The abbreviations are: P = prism; λ/2 = half-wave plate; pol = Glan-laser polarizer; ph = alignment pinhole aperture; nf = neutral density filter block; bs = beam splitter; l = lens; bp-sp = bandpass or shortpass filter block (also used for neutral density filters); s = measurement sample cuvette; r = measurement reference cuvette; d = beam dump; pmt = photomultiplier tube.

beams (approximately 0.5 cm) the excitation beam is approximately collimated through the sample. To eliminate reabsorption of the emitted light, the excitation beam is also passed through the cuvette as close as possible (~1 mm) to the window facing the collection lens. The fluorescent light is collected at a right angle to the propagation direction of the excitation beam by a biconvex lens and imaged onto a PMT (Hamamatsu R928) with a manufacturer supplied wavelength dependent response function. Immediately prior to the PMT, the collected light is passed through two bandpass filters to block stray or scattered excitation light; neutral density filters with well-characterized transmittance may also be used at this point to reduce the overall intensity of the collected light to within the linear operating range of the PMT. The signal from the PMT

is amplified (Melles-Griot model 13AMP007 supplying 400 V; gain of ~120-140) and sent to a boxcar integrator (Stanford Research Systems model PS325 with high voltage power supply). The gate width over which the 2PEF signal was integrated for these measurements was approximately 50 ns. The integrated 2PEF signal is then converted to a voltage, which is sent to a connector box (National Instruments model BNC 2120) and A/D converter (National Instruments model NIDAQ PCI-6025E). A Labview VI (virtual instrument) acquires the data from the A/D convertor and calculates the ratio of F_u to F_r. This ratio is averaged over two hundred shots of the laser and three independent acquisitions of 200 shots are taken. The average of these three acquisitions is then used with equation 2.9 for the calculation of δ_u.

For this experimental setup, ϕ depends on the refractive index n of the solvent used,[119] the fluorescence emission spectrum of the compound $f_{fluor}(\lambda)$, the wavelength-dependent response of the PMT $R_{PMT}(\lambda)$, and the transmittances $T_i(\lambda)$ of all filters placed before the PMT:

$$\phi = \frac{\int f_{fluor}(\lambda) \times R_{PMT}(\lambda) \times \prod_i T_i(\lambda) d\lambda}{n^2 \int f_{fluor}(\lambda) d\lambda} \qquad (2.11)$$

The intensity dependence of all solutions was checked for to confirm the quadratic dependence of 2PEF signal on excitation power (i.e. $1.85 \le n \le 2.15$ for $2\text{PEF} \propto I^n$). The 2PEF measurements of the cruciforms and model compounds discussed in Chapter 3 were made in toluene solution at chromophore concentrations of 50 - 100 μM. The cruciform and bis(styryl)benzene chromophores discussed in Chapter 4 were measured in 95% dichloromethane, 5% toluene at concentrations of 5 -10 μM in

chromophore and 0 or 53 μM in zinc trifluoromethanesulfonate, while the oxazole and thiazole chromophores discussed in Chapter 5 were measured in pH 7 buffered water, methanol or ethanol solution at concentrations of 25 - 100 μM. The primary reference compounds used were 1,4-bis(2-methylstyryl)benzene[86,87] in cyclohexane for the spectral region between 550 - 680 nm and fluorescein[100] in pH 11 NaOH for the spectral region between 690 - 1040 nm. The 2PA cross-section values of 1,4-bis(2-methylstyryl)benzene reported by Kennedy[86] were reduced in scale by a factor of 10 as described by Fisher.[87] Unless otherwise noted, the uncertainties in the measured cross sections are approximately ±15%.

CHAPTER 3: ONE- AND TWO-PHOTON SPECTROSCOPY OF CRUCIFORM CHROMOPHORES WITH PHENYLETHYNYL AND STYRYL ARMS: EFFECTS OF ELECTRON DONOR/ACCEPTOR SUBSTITUTION

3.1 Introduction

As discussed in Chapter 1, quadrupolar compounds such as **1** and **2** in Figure 3.1 have been widely developed as two-photon absorption (2PA) chromophores. Recently, 2PA structure-property relationships have been investigated for organic chromophores with conjugation extending in two or three dimensions. It has been reported that branched structures and other types of superstructures (in which the individual units are themselves 2PA chromophores) may display cooperative enhancement of 2PA due to electronic interactions between the individual units. Some fully conjugated superstructure systems for which cooperative enhancement of 2PA has been reported include porphyrin dimers linked through conjugated bridges,[120-123] porphyrins linked in a macromolecular ring motif[124,125] and porphyrin ladder polymers.[126,127] These structures have been reported to show increases ranging between a factor of 3 to a factor of ~60 in δ_{max}/chromophore unit with respect to the δ_{max} of the individual chromophores they are made from. This phenomenon that has been ascribed to resonant interactions between the units and to increases in the transition dipole moments between the states participating in the 2PA transition. In the case of branched chromophore structures such as octupolar[42-46,128,129] or

dendritic[53,54,57,58] structures, the question of enhancement is more complex. In general, for these structures, the effects of the branched structure on the 2PA properties of each individual unit is strongly dependent on the nature and extent of the inter-unit electronic coupling through the shared core.[130] Various types of coupling through conjugated linkers or through shared core groups have been reported to have negligible impact[52] or approximately 2- to 4-fold enhancement[42,54,55,131] or a slight reduction[44,132] of δ_{max}/chromophore unit, as well as broadening[48,50,131] and shifts[48,131] of the 2PA spectrum.

Cruciform chromophores such as compounds **3**-**6** in Figure 3.1 are another prototypical form of two-dimensional conjugated structure, which may be thought of as two linear chromophores coupled directly through a central ring. Two-photon absorption spectra have been reported for systems with arms extended via four double-bonded[72,73] or four triple-bonded[75,76] linkages. These recent studies have shown δ_{max} values of 1100 GM at 700 nm for an all-double bonded cruciform with four dialkylamine donor groups (compound **3**)[72,73] and 570 GM at approximately 700 nm for an all-triple bonded cruciform with four dialkylamine substituents (compound **5**).[75,76] In the case of **3**, it was found that there is no enhancement of the δ_{max}/chromophore unit or the integrated 2PA band per chromophore unit as compared with the corresponding linear compound **1**, although the 2PA band does show a slight blue shift and broadening.[72,73] Rumi et al.[72,73] applied Kasha's molecular exciton model[133] to gain insight into the one- and two-photon properties of cruciform compounds with four identical double-bonded arms such as **3**, treating the system as a pair of coupled linear quadrupolar chromophores such as **1**. This model predicted that δ_{max} for the case of a cruciform compound with degenerate arms is

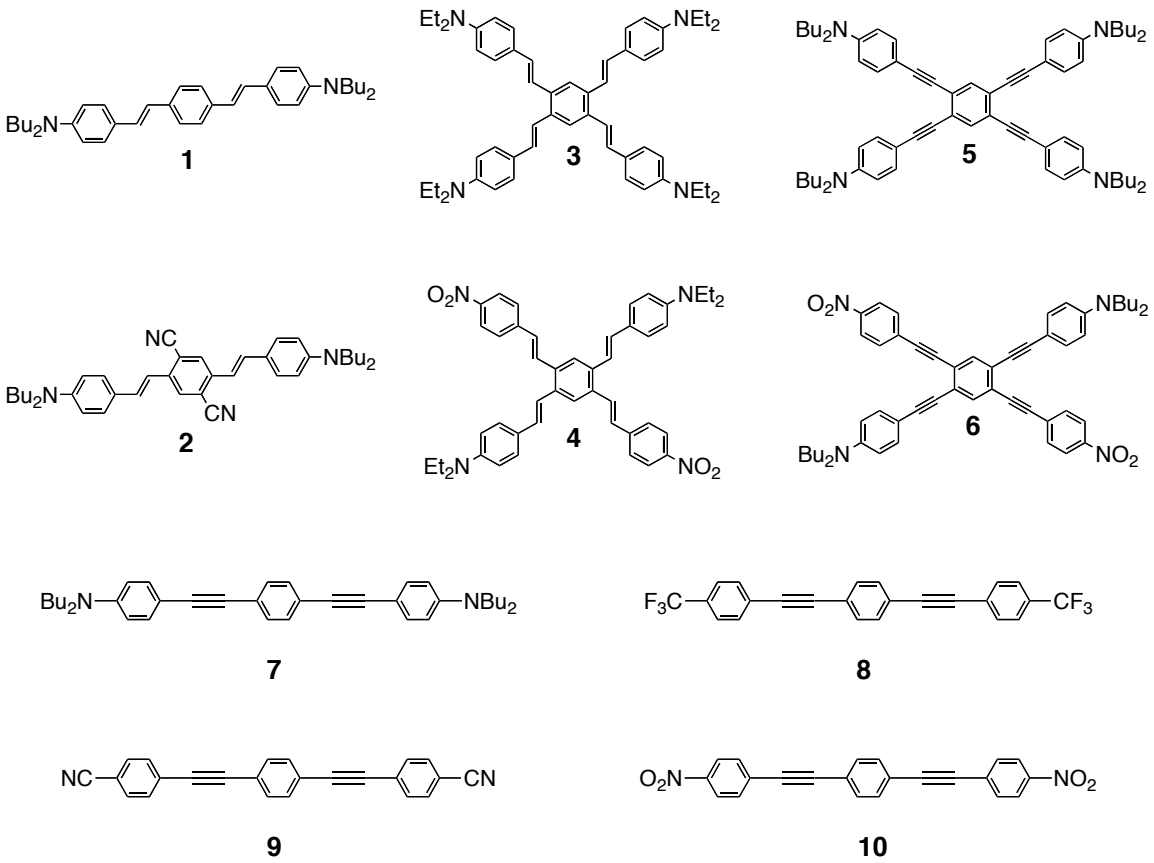

Figure 3.1: Structures of compounds reported in the literature and used as examples and comparisons in this chapter. Compounds **1** and **2** are DSB and CN-DSB, respectively, in Pond.[88] Compounds **3** and **4** are Ph-2Dx2D and Ph-2Dx2A, respectively, in Rumi.[72,73] Compounds **5** and **6** are TD-TPEB and para-TPEB, respectively, in Slepkov.[75,76] Compounds **7**-**10** were reported in Nguyen.[134]

dependent on the angle between the arms, and the strength and sign of the coupling interaction. Based on the estimate of the coupling obtained from the 1PA spectrum of **3**, the theoretical value of δ_{max} for **5** was actually smaller than the sum of the δ_{max} of the corresponding linear chromophores, in agreement with the observed spectra. This indicates that the cruciform architecture with degenerate conjugated arms is not itself sufficient to lead to an increase in δ_{max} for the low energy two-photon states. An alternate motif for constructing cruciform compounds is to use two different types of conjugated arms, including double bonded arms such as **1** and **2** and triple bonded arms such as **7**-**10**.

This chapter presents a detailed study of linear compounds **11** and **12** and of a series of cruciforms based on 1,4-distyryl-2,5-bis(phenylethynyl)benzene possessing non-degenerate conjugated arms (compound **13**) as well as four symmetrically substituted donor (D) groups (compound **14**) or varying donor/acceptor (D/A) substitution (compounds **15**-**20**) as shown in Figure 3.2. Such D/A substituted cruciforms, with conjugation via double bonds in one arm and triple bonds in the other, have been shown to exhibit interesting charge-transfer based metal-ion responsive optical properties.[65-68,70] Based on literature values for the Hammett parameters[135,136] of the substituents, the acceptor groups used in **16**-**20** increase in electron-accepting strength in the following pattern: *o*-CF_3 ≈ *p*-CF_3 < di-*m*-CF_3 ≈ *p*-CN < *p*-NO_2. There are several basic questions of interest regarding the optical properties of these cruciform systems including: 1) the role of electronic coupling for the case of two energetically non-degenerate chromophoric units; 2) the effect of the degree of charge transfer associated with variation of the strength of the electron accepting groups; and 3) the impact of coupling of pairs of charge-transfer pathways within the cruciforms, which we have addressed through a

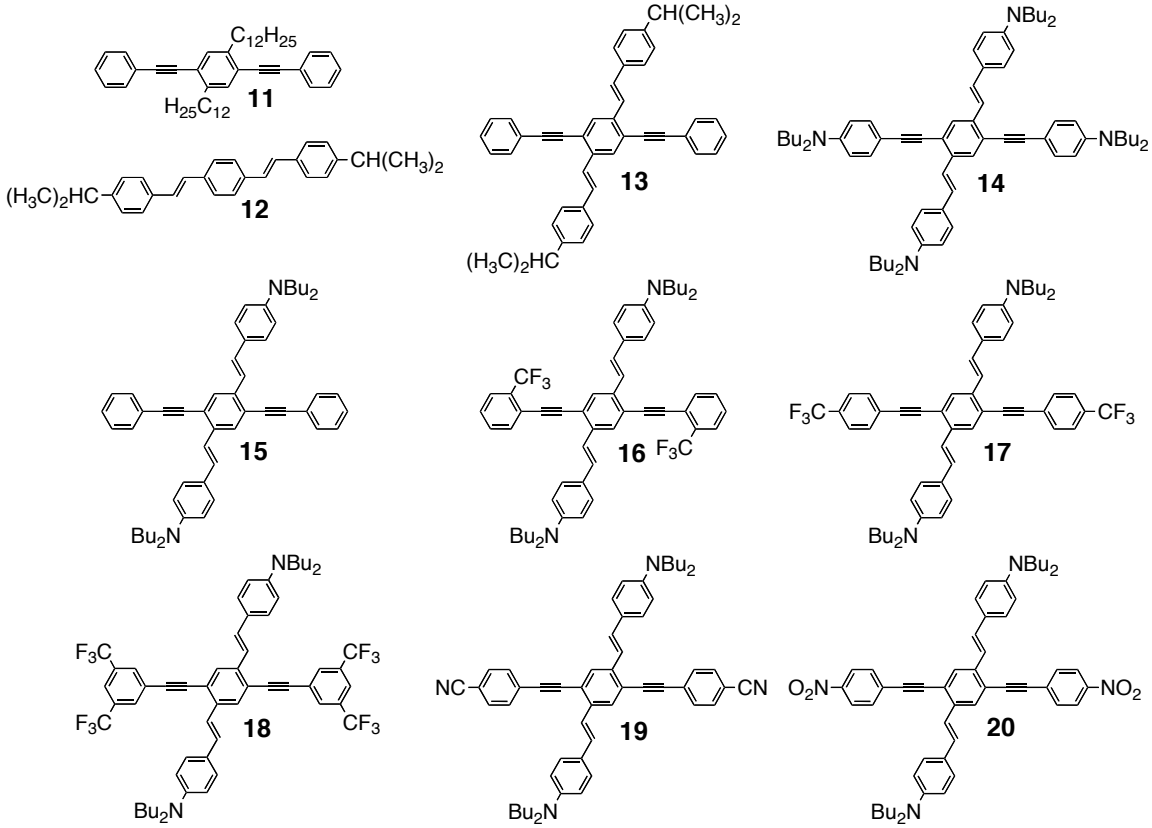

Figure 3.2. Structures of compounds **11**-**20**.

combination of one- and two-photon spectroscopic studies on a systematically varied set of cruciforms and double- or triple-bond containing linear model compounds.

3.2 Results

3.2.1 One-photon Spectroscopy

The one-photon absorption (1PA) spectra of compounds **11**-**14** are shown in Figure 3.3a. The spectra of compounds **11** and **12**, which serve as double bond and triple bond containing linear model compounds, show an absorption maximum at 329 nm for **11**, which is at somewhat higher energy than that of **12** (363 nm), as expected for a bis(phenylethynyl)-benzene chromophore as compared to a bis(styryl)-benzene chromophore. While the spectra of **11** and **12** each show only one prominent electronic absorption band in the wavelength range examined, both spectra exhibit vibronic structure, with a major vibrational frequency of about 1500 cm^{-1}. In contrast, the spectrum of the cruciform **13**, bearing no significant electron donor or acceptor groups, shows two distinct electronic absorption bands, with maxima at 332 nm and 376 nm, the latter of which has a smaller ε_{max} than the former, and also shows a low-energy shoulder similar to that observed in **12**. The symmetrically tetra-donor-substituted cruciform **14** also shows two distinct absorption bands**,** the higher (386 nm) and lower (430 nm) energy bands being bathochromically shifted by 4200 cm^{-1} and 2700 cm^{-1}, respectively, relative to those of **13**. This shift is a result of a reduction in the HOMO-LUMO gap caused by destabilization of the HOMO by the alkylamine groups. The fluorescence emission

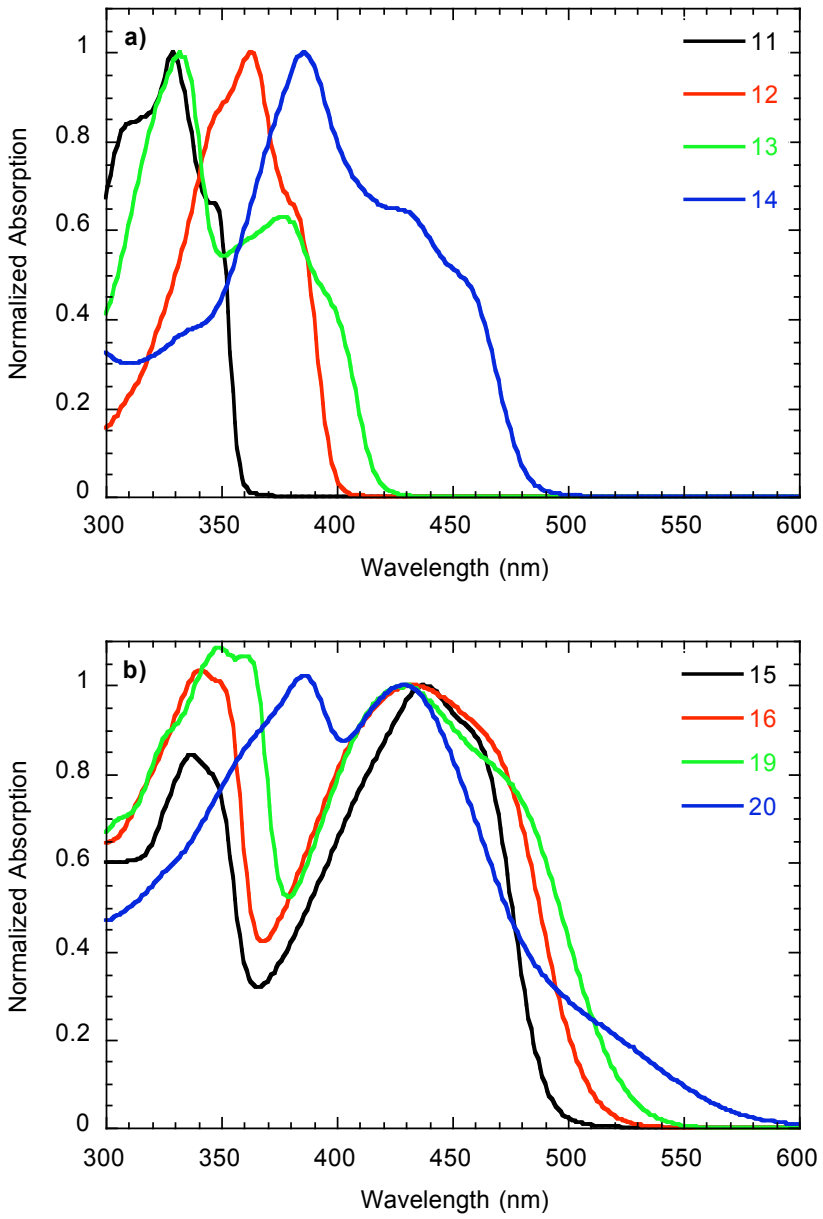

Figure 3.3: One-photon absorption (1PA) spectra of selected chromophores: **a)** Spectra for the linear model compounds (**11** and **12**) and the cruciform with no donor substituents (**13**) and four donor substituents (**14**). **b)** Spectra for cruciforms with electron-donor groups on the bis(styryl)phenylene arm and either no substituents (**15**) or electron acceptors on the bis(phenylethynyl)phenylene arm (**16**, **19** and **20**). [The 1PA spectra of **17** and **18,** which are very similar to those of **16** and **19**, respectively, are not shown.]

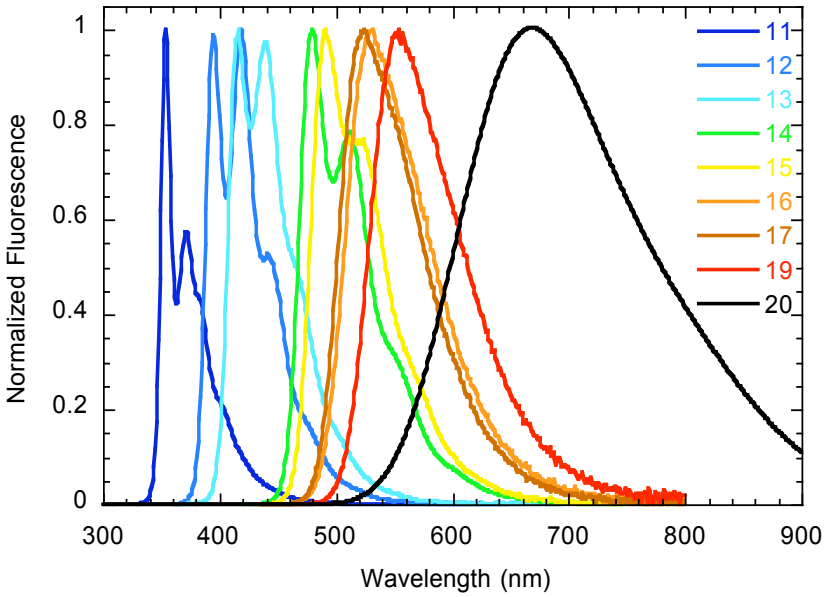

Figure 3.4: Fluorescence spectra of the linear model compounds **11** and **12** and cruciform compounds **13**-**17**, **19**, **20**. The spectrum of **18** is nearly identical to that of **19** and is omitted here for the sake of clarity. Note that the spectrum of **20** is a model consisting of a single Gaussian function fit by linear-least-squares to the non-noisy part of the experimental spectrum as collected on the fluorimeter.

Table 3.1. Experimental linear and two-photon spectroscopic properties of chromophores **11** - **20**.

Compound	$\lambda_{max}^{(1)}$ (nm)[a]	$\lambda_{s}^{(1)}$ (nm)[b]	ε_{max} (M^{-1} cm^{-1})[c]	$\lambda_{fl}^{(1)}$ (nm)[d]	η[e]	$\lambda_{max}^{(2)}$ (nm)[f]	δ_{max} (GM)[g]
11	329	350	49000	354	0.80	550	160
12	363	382	57000	396	0.95	580	120
13	332	400	80000	416	0.79	550	150
14	386	450	99000	480	0.64	700	1200
15	435	460	60000	491	0.66	770	740
16	433	470	50000	529	0.68	820	640
17	441	470	51000	524	0.71	810	730
18	431	475	49000	557	0.70	830	910
19	429	475	52000	554	0.67	830	950
20	430	515	59000	670	0.005	770	580

[a] For **11**-**14**, wavelength of the of the absorption maximum. For **15**-**20**, wavelength of the absorption maximum of the lower-energy band. [b] Approximate wavelength of the lowest-energy feature in the UV/vis absorption spectrum. [c] Molar extinction coefficient at $\lambda_{max}^{(1)}$. [d] Wavelength of the maximum in the fluorescence emission spectrum. [e] Fluorescence quantum yield. Uncertainty in η_{fl} is ± 5%. [f] Maximum of two-photon excited fluorescence excitation spectrum. [g] Peak two-photon cross section (1 GM = 10^{-50} cm^4 s $photon^{-1}$ $molecule^{-1}$). Uncertainty in δ is ± 15%.

spectra (see Figure 3.4) of all four of these compounds are very structured, with four vibronic transitions easily identifiable in each spectrum. A summary of the one-photon spectroscopic parameters of compounds **11**-**20** is presented in Table 3.1.

As can be seen in Figure 3.3b, donor/acceptor substitution of the nondegenerate cruciform backbone (**15**–**20)** results in significant changes in the 1PA spectra of the cruciforms. The addition of the two donor groups along the distyryl arm in **15** results in an absorption spectrum wherein the lowest energy feature is bathochromically shifted by about 3200 cm^{-1} compared to that of the non-D/A substituted analogue **13**, whereas the higher energy band of **15** is only slightly red-shifted by approximately 450 cm^{-1} relative to the overall peak of **13**. In the D/A substituted compounds **16** - **20**, in which the acceptor strength is increased, several changes occur: 1) the peak position of the lower energy 1PA band remains roughly constant (within 10 nm), 2) the band shape of the lower energy band broadens with an increasing splitting of the lower energy shoulder relative to **15**, and 3) the higher energy band (at approximately 340-350 nm) red-shifts increasingly as the strength of the electron-acceptor group(s) increases. The fluorescence spectra (Figure 3.4) of the cruciforms show a systematic red shift upon donor or D/A substitution (**14** – **20**) as compared to **13**, and **16**-**20** show significantly greater Stokes shifts and less vibronic structure than **13**-**15**, as expected for transitions with significant intramolecular charge transfer character. The fluorescence quantum yields of the D/A substituted cruciforms are all approximately 0.7 with the exception of the nitro-substituted cruciform **20**, which has a much lower quantum yield of 0.005.

3.2.2 Two-photon Spectroscopy

The 2PA spectra were determined by the two-photon excited fluorescence (2PEF) method. The 2PA data are summarized in Table 3.1. Figure 3.5a shows the spectra of the linear model compounds **11** and **12** compared to that of **13** (cruciform core with only *p*-isopropyl substituents on the styryl arms). The δ_{max} of **12** was measured as 110 GM at the 2PA peak wavelength ($\lambda_{max}^{(2)}$) of 580 nm. In the case of **11** and **13**, the position of the 2PA peak is at or below the shortest excitation wavelength accessed in this study, 550 nm. The largest values of δ in the range measured were 160 GM for **11** and 150 GM for **13** at 550 nm. The 2PA spectrum of **13** is not consistent with a bathochromic shift relative to the 2PA spectrum of **12**, although the longer wavelength sides of both spectra are qualitatively similar.

The addition of D/A groups to the arms of the cruciforms had significant effects on the 2PA spectra (Figure 3.5b). The spectrum of symmetrically tetra-donor substituted **14** has a δ_{max} of 1200 GM at a $\lambda_{max}^{(2)}$ of 700 nm, constituting an approximately 7.5-fold increase in δ_{max} and an approximately 3900 cm^{-1} bathochromic shift of $\lambda_{max}^{(2)}$, relative to that of **13**. The $\lambda_{max}^{(2)}$ is blue-shifted by 590 cm^{-1} and δ_{max} is slightly increased, when compared to those reported[40,72,73,88] for the bis-donor linear compound **1**. There is also a shoulder on the 2PA spectrum of **14** at 750 nm with a δ of 550 GM. In **15**, without donor groups on the triple-bonded arm of the cruciform core, the $\lambda_{max}^{(2)}$ shifts further to 770 nm, while the δ_{max} is reduced to 740 GM, still an approximately four-fold increase relative to the non-D/A substituted cruciform **13**. This $\lambda_{max}^{(2)}$ is red-shifted by 710 cm^{-1} and δ_{max} is reduced in magnitude compared to that of compound **1**. Interestingly, while the $\lambda_{max}^{(2)}$ of **15** is red-shifted by 1300 cm^{-1} from the peak of tetra-donor substituted **14**, it is rather close to the 2PA shoulder of **14** at 750 nm.

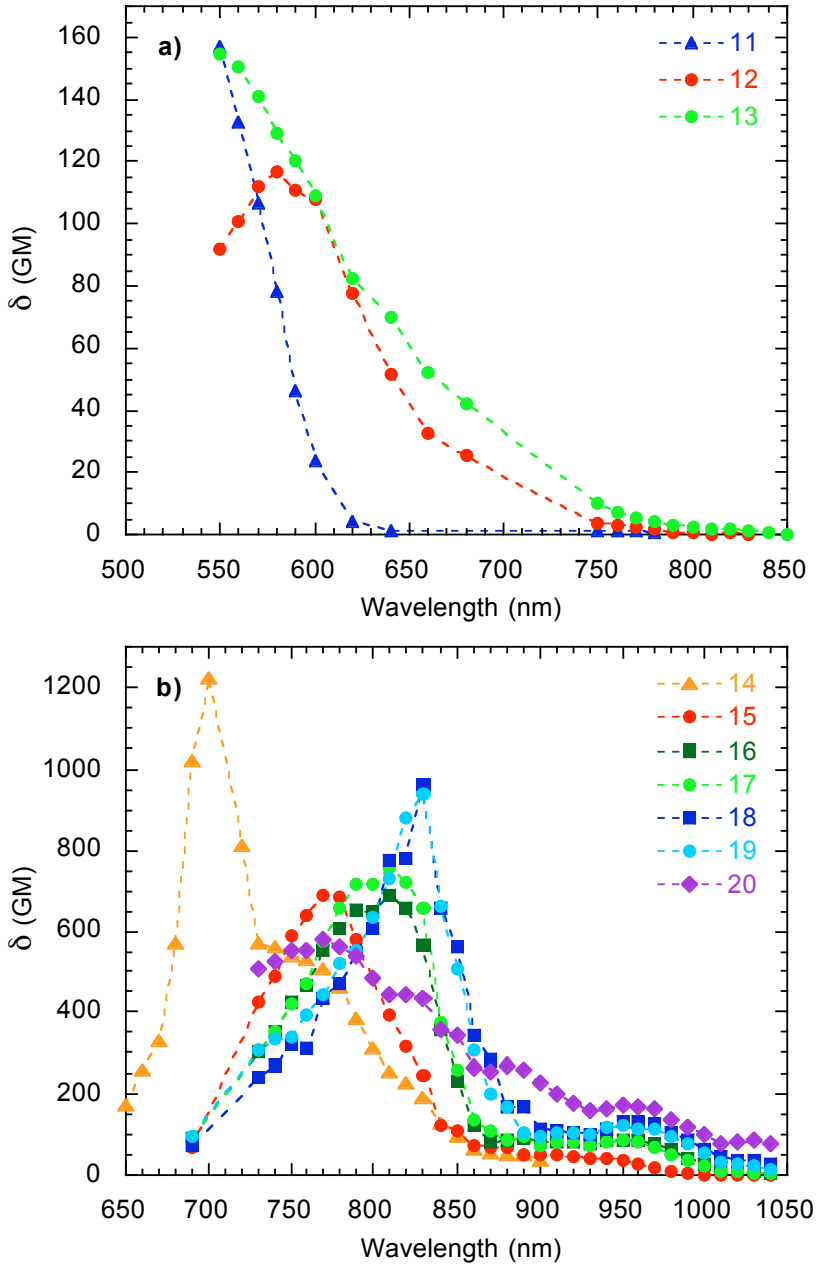

Figure 3.5. Two-photon absorption spectra of selected compounds. In all cases, the lines shown are not fits but are intended as guides for the eye. Shown in **a)** is the change in 2PA spectrum upon transitioning from the linear model compounds **11** and **12** to the unsubstituted cruciform **13**. In **b)** are 2PA plots of substituted cruciforms.

In **16** and **17**, the addition of inductive electron withdrawing CF_3 groups in the *ortho* or *para* positions on the terminal phenyls of the triple-bonded arm causes the phenyls to become electron deficient and act as weak electron acceptors. The $\lambda_{max}^{(2)}$ wavelengths display a red-shift with respect to **15** to about 810 nm, while the δ_{max} values are 640 GM and 730 GM, not significant changes given the experimental uncertainty in the measurement. When two CF_3 groups (in **18**) or one π-acceptor CN group (in **19**) are substituted on the same phenyl rings, the effective acceptor strength is increased. There is again a red shift of $\lambda_{max}^{(2)}$ (to 830 nm) but also an increase in δ_{max}, to 910 GM and 950 GM, respectively, and the 2PA band becomes somewhat narrower. However, upon addition of strong NO_2 electron acceptors in **20**, the $\lambda_{max}^{(2)}$ shifts to 770 nm, δ_{max} is reduced, and a weak band appears to rise at ~880 nm. The 2PA spectrum of **20** is rather broad overall with a weaker band at 970 nm. In the whole series of D/A cruciforms, there is a weak 2PA band that shifts from about 930 to 970 nm and increases in strength as the effective acceptor strength increases.

3.3 Discussion

The 1PA spectra of the cruciforms examined in this paper show shifts in band positions and splittings of bands that reflect the nature and extent of electronic interactions between the different arms of the cruciforms. There is an increase in the separation of the bands that are correlated with the lowest energy $\pi \rightarrow \pi^*$ transitions of the vinyl and ethynyl arms in the unsubstituted cruciform, **13**, relative to those of the

corresponding linear model compounds, which we ascribe to an electronic coupling and mixing of the ππ* excited states of the different arms. There is also a red-shift of the average position of the bands, which is due to an overall stabilization of the excited states upon coupling of the two arms. A similar trend is observed for the fully terminal donor substituted cruciform, **14**, although in this case the center of the band positions is significantly red-shifted compared to **13**, due to the donor substitution. These results are again consistent with a mixing of the π* excited states of the different arms. The structure in the lower energy band of **13** and **14** is attributed to a vibronic progression.

Cruciforms **15-19** have terminal donor substituted vinyl arms and different terminal acceptors on the ethynyl arms. In addition to the increase in the separation of the high and low energy bands of these compounds, there is a splitting of the low energy band that is too large to be assigned to a vibrational mode energy. For these compounds there is likely a significant charge transfer (CT) contribution to the low energy band and we believe that the splitting is associated with a coupling of the different possible charge transfer excitations in these cruciforms. The low energy band in **15-19** broadens as the strength of the acceptor group goes from weak (**15**) to moderate (**19**), while the peak position stays relatively constant, leading to significant bathochromic shifts of the lowest energy features of the spectra. The higher-energy band of the cruciforms is at a similar position to the analogous acceptor substituted triple-bonded linear compound, where comparative data is available.[134] To obtain insight into these observations, we have modeled the spectra of the cruciforms using a molecular exciton approach for the π* excited states of the two arms and for the CT excited states that involve transfer of electron density from the donors to the acceptors on the different arms. The 1PA spectra

were decomposed into sets of $\pi \rightarrow \pi^*$ and CT bands and the electronic transition energies were obtained by applying a Franck-Condon bandshape analysis. These results, together with the transition energies for the corresponding linear model compounds, were used to estimate the coupling energies and wavefunction mixing coefficients for the cruciforms.

3.3.1 Simple Exciton Treatment of Cruciform Electronic Spectra

In the molecular exciton model, when two chromophores are in close proximity or are attached to each other, their electronic interaction leads to a mixing of the excited state wavefunctions and shifts or splittings of the electronic absorption bands of the combined chromophore.[133,137] In the case of an excitonic coupling of two identical parallel units, two excitonic excited states are formed by symmetric and antisymmetric combinations of the excited state wavefunctions of the individual components. The excited state energy of each unit E_e^0 is stabilized by the Van der Waals interaction term V_{eg}^{diag}, and the energies of the exciton excited states, $E_{\pm}$, are split by $2V$ from this stabilized energy, where V is the coupling energy of the two arms:

$$E_{\pm} = E_e^0 + V_{eg}^{diag} \pm V \qquad (3.1)$$

We have divided the cruciforms into two nondegenerate linear components associated with the ethynyl and vinyl arms linked in *para*- fashion on the central phenyl ring, similarly to what has been used previously for compounds **3** and **4**.[72] This is somewhat approximate in that each arm shares the central phenyl ring. In these cruciforms the electronic states of the uncoupled arms have different electronic transition energies and thus the π and $\pi\pi^*$ states of each arm are energetically non-degenerate. Figure 3.6 diagrams the interactions of the excited states of nondegenerate chromophores

11a and **12a**, which model **11** and **12**. Since the π→π* transition dipoles of the components are at an angle to each other, they satisfy the conditions of an oblique exciton[133] and the component excited states mix to produce two 1PA-allowed excited states in **13a**.

3.3.2 Interaction of nondegnerate units in an exciton

A basis set for the ground state of an exciton composed of two different units is

$$\Phi_g = \psi_g^{(1)}\psi_g^{(2)} \tag{3.2}$$

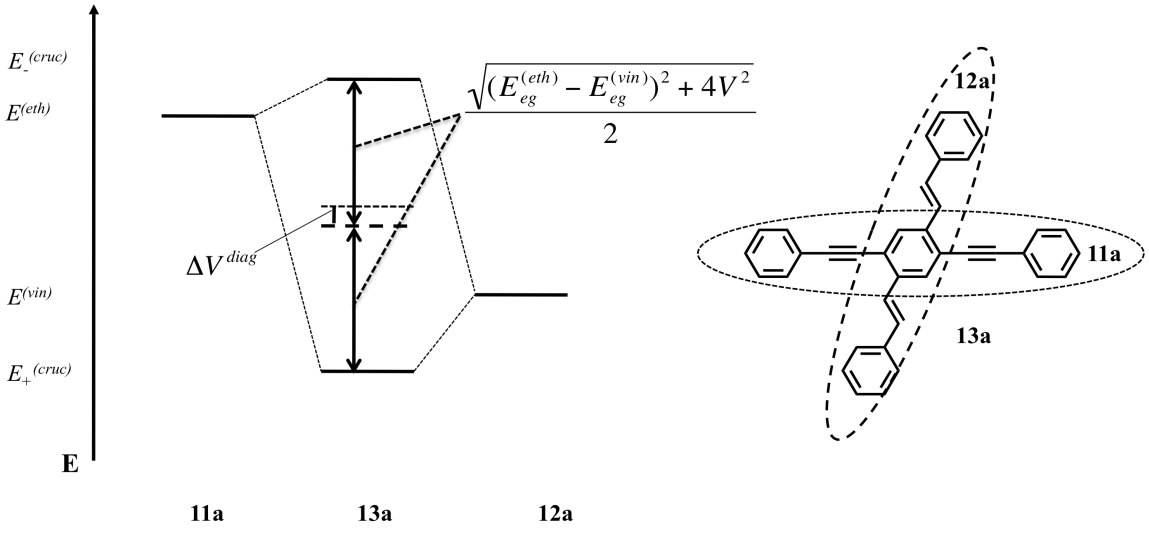

Figure 3.6: A diagram depicting the electronic excited states of the linear compounds **11a** and **12a** (similar to **11** and **12**, with alkyl groups omitted for clarity) and the joint cruciform molecular orbitals formed by their exciton mixing in the cruciform compound **13a**.

while a basis set for the excited states of the exciton that are formed from the interaction of the first excited states of the individual units can be described by exciting one unit while leaving the other unit in its ground state:

$$\Phi_e^{(1)} = \psi_e^{(1)}\psi_g^{(2)}$$
$$\Phi_e^{(2)} = \psi_g^{(1)}\psi_e^{(2)} \qquad (3.3)$$

In equations 3.2 and 3.3, the symbol Φ refers to the wavefunction of an exciton state with contributions from units 1 and 2, while $\psi^{(i)}$ refers to the wavefunctions of the individual units. Subscripts *g* and *e* refer to the ground and first electronic excited states, respectively.

The total Hamiltonian for this system is

$$H = H^{(1)} + H^{(2)} + H_{\text{int}} \qquad (3.4)$$

where H_{int} is the interaction Hamiltonian describing the coupling of the two units in the exciton. One part of H_{int} accounts for a diagonal energy shift due to Van der Waals interactions between units 1 and 2 in states *u* and *v*:

$$V_{uv}^{diag} = \left\langle \psi_u^{(1)}\psi_v^{(2)} \middle| H_{\text{int}} \middle| \psi_u^{(1)}\psi_v^{(2)} \right\rangle \qquad (3.5)$$

The energy of the ground state is then

$$E_g = \left\langle \Phi_g \middle| H \middle| \Phi_g \right\rangle = E_g^{(1)} + E_g^{(2)} + V_{gg}^{diag} \qquad (3.6)$$

The Hamiltonian of the matrix element for mixing of component states, allowing for overall diagonal shifts, is expressed in matrix form as:

$$H = \begin{pmatrix} E_e^{(1)} + E_g^{(2)} + V_{eg}^{diag} & V \\ V & E_g^{(1)} + E_e^{(2)} + V_{ge}^{diag} \end{pmatrix} \tag{3.7}$$

where V_{eg}^{diag} and V_{ge}^{diag} are the diagonal shifts of the excited state of unit 1 due to interaction with the ground state of unit 2, and vice versa. V is the coupling energy between units 1 and 2 in the excited state (the other part of H_{int}):

$$V = \left\langle \Phi_e^{(1)} \middle| H_{\text{int}} \middle| \Phi_e^{(2)} \right\rangle \tag{3.8}$$

$E_e^{(1)'}$ and $E_e^{(2)'}$ are defined as the excited state energies of the individual units including a diagonal energy shift due to Van der Waals interaction of the two units , i.e.:

$$\begin{aligned} E_e^{(1)'} &= E_e^{(1)} + E_g^{(2)} + V_{eg}^{diag} \\ E_e^{(2)'} &= E_g^{(1)} + E_e^{(2)} + V_{ge}^{diag} \end{aligned} \tag{3.9}$$

The secular determinant of for the excited states of an exciton composed of nondegenerate units 1 and 2 is then:

$$\begin{vmatrix} E_e^{(1)'} - E & V \\ V & E_e^{(2)'} - E \end{vmatrix} = 0 \tag{3.10}$$

which can be expanded to

$$E_e^{(1)'} E_e^{(2)'} - E(E_e^{(1)'} + E_e^{(2)'}) + E^2 - V^2 = 0 \tag{3.11}$$

This is a quadratic equation in E with

$$b = -(E_e^{(1)'} + E_e^{(2)'})$$

and

$$c = E_e^{(1)'} E_e^{(2)'} - V^2$$

The general solution for the quadratic equation leads to:

$$E = \frac{E_e^{(1)'} + E_e^{(2)'}}{2} \pm \frac{\sqrt{(-(E_e^{(1)'} + E_e^{(2)'}))^2 - 4(E_e^{(1)'} E_e^{(2)'} - V^2)}}{2} \tag{3.12}$$

which simplifies to the following expression for the energies of the in-phase and out-of-phase excited states of an exciton composed of non-degenerate units:

$$E_{\pm} = \frac{E_e^{(1)'} + E_e^{(2)'}}{2} \pm \frac{\sqrt{(E_{eg}^{(1)} - E_{eg}^{(2)} + \Delta V^{diag})^2 + 4V^2}}{2} \tag{3.13}$$

Where $E_{eg}^{(1)}$ is the $g \rightarrow e$ transition energy of component 1, $E_{eg}^{(2)}$ is the $g \rightarrow e$ transition energy of component 2, and $\Delta V^{diag} = V_{eg}^{\text{diag}} - V_{ge}^{\text{diag}}$. In Equation 3.13, the first term is the midpoint between the excited state energies of the components as influenced by their Van der Waals interactions in space and the second term is the splitting energy, in this case a function of the coupling term V and the difference in bandgaps of the two individual units.

In order to relate eq. 3.13 to the measurements made on the cruciforms, we consider the ethynyl arm to be component 1 and the vinyl arm to be component 2, and refer to the experimentally determined 0-0 transition energies $\Delta E_{\pm}^{(cruc)}$ of the cruciform compounds, $E_{eg}^{(eth)}$ of the triple-bonded model compounds and $E_{eg}^{(vin)}$ of the double bonded model compounds:

$$\begin{aligned} \Delta E_{\pm} &= E_{\pm} - E_g^{(cruc)} \\ &= \Delta E^{(unit)} + \Delta V^{diag'} \pm \frac{\sqrt{(E_{eg}^{(eth)} - E_{eg}^{(vin)} + \Delta V^{diag})^2 + 4V^2}}{2} \end{aligned} \tag{3.14}$$

Where

$$\Delta E^{(unit)} = \tfrac{1}{2}(E_{eg}^{(eth)} - E_{eg}^{(vin)})$$

and

$$\Delta V^{diag'} = \tfrac{1}{2}(V_{eg}^{diag} + V_{ge}^{diag} - 2V_{gg}^{diag})$$

The first term at the end of Equation 3.14 is the average transition energy of the uncoupled components, and the second term is the overall energy shift of the transition energies due to Van der Waals interactions between the states of the components. The third term is the splitting energy between the two exciton states, and is a function of the transition energies of the uncoupled units and the coupling term V. It should be noted that as ΔV^{diag} is usually small in comparison to the quantity $E_{eg}^{(eth)}$ - $E_{eg}^{(vin)}$, it does not influence appreciably the calculation of the electronic coupling or the wavefunction mixing coefficients and is neglected.[137] Taking the difference of ΔE_- and ΔE_+ and solving for V results in equation 3.15 below expressing V as a function of measurable parameters reported in this chapter:

$$V = \sqrt{\frac{(\Delta E_-^{(cruc)} - \Delta E_+^{(cruc)})^2 - (E_{eg}^{(eth)} - E_{eg}^{(vin)})^2}{4}} \tag{3.15}$$

The wavefunction mixing coefficients for the excitonic states in these cruciforms may be derived from the equation describing the exciton state wavefunctions of an exciton with non-degenerate components:[137]

$$\begin{aligned} \Psi_+ &= \cos(\gamma/2)\psi_e^{(eth)}\psi_g^{(vin)} + \sin(\gamma/2)\psi_g^{(eth)}\psi_e^{(vin)} \\ \Psi_- &= \sin(\gamma/2)\psi_e^{(eth)}\psi_g^{(vin)} - \cos(\gamma/2)\psi_g^{(eth)}\psi_e^{(vin)} \end{aligned} \tag{3.16}$$

where

$$\gamma = \arctan\left(\frac{2V}{E_{eg}^{(eth)} - E_{eg}^{(vin)}}\right) \tag{3.17}$$

3.3.3 Exciton analysis of cruciforms without D/A Substituent Pattern

The spectroscopic data were analyzed using a Franck-Condon (FC) bandshape analysis to obtain the 0-0 transition energies for the linear model compounds **11** and **12** and the cruciforms **13** and **14**. In the (FC) approximation for absorption band structure, the overall strength of a 1PA event is proportional to both the square of the transition dipole between electronic ground and excited states *g* and *e*, and to the square of the overlap integral of the nuclear wave functions of the initial and final vibrational states.[116,138] FC analysis was performed using equation 3.18:

$$\varepsilon(E) = \sum_{\upsilon''=0}^{m} \varepsilon_{0-0} \frac{S^{\upsilon''}}{\upsilon''!} \exp\left(-\frac{(E - E_{0-0} - \upsilon'' E_{vib})^2}{\Gamma^2}\right) \tag{3.18}$$

Equation 3.18 expresses the extinction coefficient ε(*E*) of a vibronic absorption band as *m*+1 vibronic components of a progression, with each component having a Gaussian line shape. The progression begins with a component at the energy $E_{0\text{-}0}$ between the $\upsilon'' = 0$ vibrational level in the electronic ground state *g* and the $\upsilon' = 0$ vibrational level in the electronic excited state *e*, and ends with the component at energy $E_{0\text{-}m}$ between the $\upsilon'' = 0$ vibrational level in *g* and the $\upsilon' = m$ vibrational level in *e*. Each component is assumed to have the same linewidth Γ and is separated from its neighboring components by the vibrational frequency ω_υ corresponding to the energy E_{vib}. Other assumptions made are that the potential energy surfaces of the *g* and *e* states are both harmonic, with minima separated from each other by ΔQ_e along the vibrational coordinate Q_e; and that ω_{uib} is the same in the electronic states *g* and *e*. The overall band amplitude is scaled by the factor $\varepsilon_{0\text{-}0}$. The *S* term is the Huang-Rhys factor:

$$S = \frac{\mu \omega_{vib} \Delta Q_e^2}{2\hbar} \tag{3.19}$$

which is proportional to the square of the change in geometry between the electronic ground and excited states.[88,116] Equation 3.19 thus allows ΔQ_e, the change in equilibrium vibrational coordinate between the ground and excited states, to determine the relative intensities of the FC components. In Equation 3.19, μ is the reduced mass of the vibrational mode being considered.[88,139]

The procedure used to fit a given band in the spectra of **11**-**15** involved first fitting the low energy portion of the band, which was truncated on the high-energy side of the peak in order to minimize the contribution of any higher-lying band, while still including the first two vibronic components so that the Huang-Rhys factor could be estimated. The bands were truncated on the high energy side of the band maximum at the position where $\varepsilon = 0.95*\varepsilon_{max}$, where ε_{max} is the molar extinction coefficient at the $\lambda_{max}^{(1)}$ of the band being fit. The truncated spectra were then fit by a linear least squares method to Equation 3.18 with $m = 3$. The sum of these components were subtracted from the complete spectrum to obtain the residual spectrum not accounted for by the fit.

In the cases of **13** and **14**, the lower-energy bands were fit first, by using the method described above. The higher energy bands, which were contained in the residuals, were fit by a method similar to that used for **11**, **12** and the lower-energy bands of **13** and **14**. However, in addition to the truncation on the high-energy side, they were also truncated on the low energy side at the location where $\varepsilon = 0.5*\varepsilon_{max}$. The low-energy truncation was necessary to minimize the effects of any contribution from the first band that might not have been accounted for fully by the first FC fit. Since the residuals were relatively featureless, the damping width was fixed at a nominal 0.1 eV before

performing the fit. The results of the Franck-Condon fitting for compounds **11**-**14** are shown in Figure 3.7 and Table 3.2.

The spectra of linear model compounds **11** and **12** are each reasonably modeled by an electronic transition with a single vibrational mode FC progression with each line having a Gaussian bandshape, for which a linewidth of 0.1 eV led to good agreement with the observed spectra. The spectrum of the cruciform **13** is decomposed into two bands: a low-energy band with a FC bandshape similar to that of **12**, and a high-energy band at a similar energy to that of **11,** although with a rather different overall bandshape. The spectrum of cruciform **14** has two bands with shapes very similar to those of **13**, although they are red-shifted by 0.5 eV (high-energy band) and 0.4 eV (low-energy band), which suggests that adding identical π-donor groups at all four terminal phenyl groups in the cruciform structure does not have a large impact on the nature of the inter-arm coupling, but destabilizes the HOMO of the cruciform as expected. Generally the bandshapes are consistent with moderate changes in geometry upon excitation as evidenced by the Huang-Rhys factors (~ 1.0 – 1.6), and damping widths of ~0.1 eV. The fitting of the high-energy band of **13** and **14** with Γ fixed at 0.1 eV was not definitive in terms of the vibrational frequency, Huang-Rhys factor or bandwidth. An alternative set of values obtained from a fit performed with Γ as an unconstrained fitting parameter also fit this peak well, but gave rise to a much larger vibrational frequency, lower Huang Rhys factor and an unusually large bandwidth. The values of the 0-0 energies for the low-energy and high-energy bands were quite consistent between the different fittings. The residual intensity between the two FC band fittings and the observed spectra of **13** and **14** were fairly small except in the higher energy region, which indicates the presence of

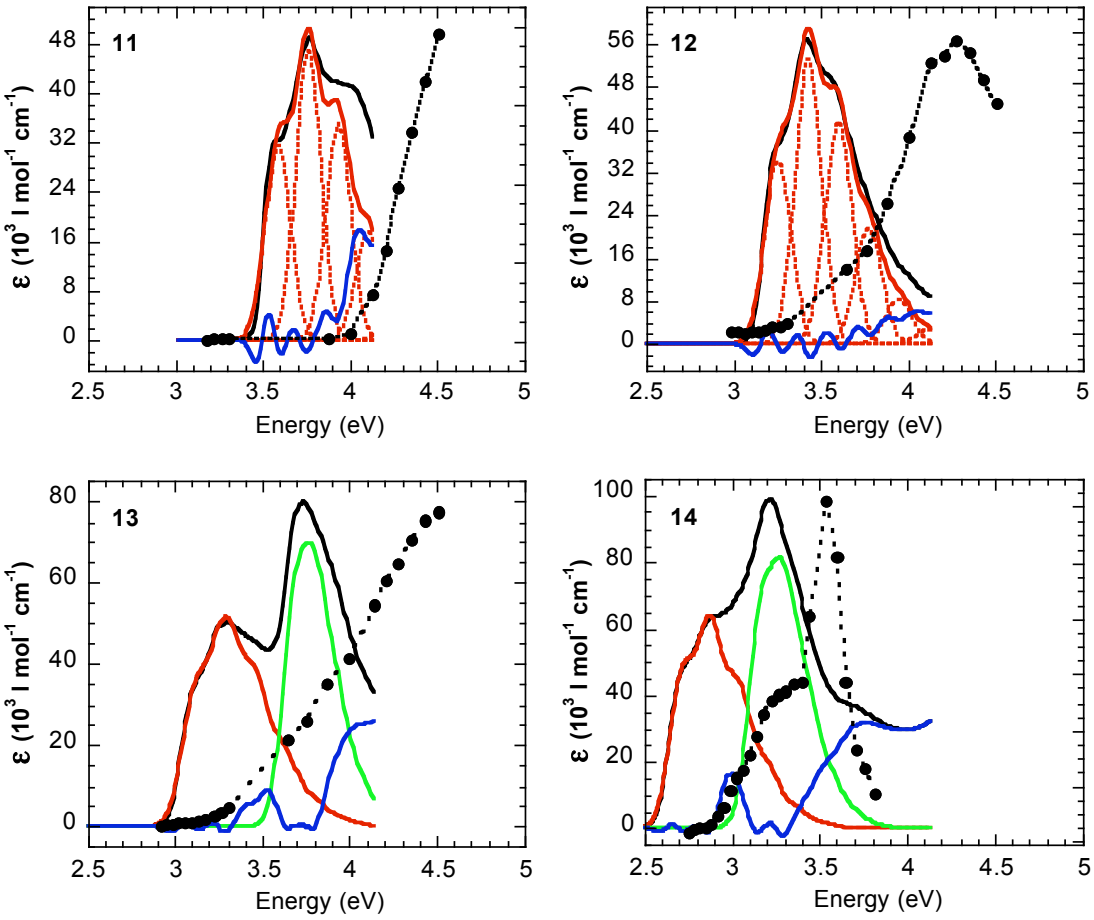

Figure 3.7: 1PA (black lines) and 2PA (black circles) spectra plotted as a function of transition energy, and results of the Franck-Condon bandshape analysis of the 1PA band for compounds **11**-**14**. For **11** and **12**, red dashed lines represent the six individual components of the Franck-Condon progression calculated. Individual Franck-Condon components are not included for **13** and **14** for the sake of clarity. In all plots, bold red solid lines represent the sum of the components of the Franck-Condon progression of the lowest-energy band. For **13** and **14**, green lines represent the total Franck-Condon fit of the higher energy component, while the blue lines are the total residuals (i.e. experimental spectrum – (total fit of lower-energy band) + (total fit of higher-energy band)).

Table 3.2. Parameters of Franck-Condon fitting of compounds **11**-**15**.

Compound	$\varepsilon_{0\text{-}0}$[c] (M^{-1} cm^{-1})	E_{vib} (cm^{-1})[d]	$E_{0\text{-}0}$ (eV)[e]	S[f]	Γ (eV)[g]
11	32,000	1400	3.59	1.49	0.10
12	34,000	1350	3.25	1.57	0.10
13[a] *low-energy band*	31,000	1360	3.12	1.46	0.11
13[a,b] *high-energy band*	49,000 (68,000)	1050 (1500)	3.69 (3.69)	1.04 (0.77)	0.1[h] (0.14)
14[a] *low-energy band*	44,000	1310	2.72	1.32	0.10
14[a,b] *high-energy band*	59,000 (60,000)	1090 (1290)	3.16 (3.19)	1.11 (0.79)	0.1[h] (0.14)
15[a] *low-energy band*	47,000	1290	2.68	1.14	0.10
15[a] *high-energy band*	35,000	1240	3.56	1.15	0.11

[a] For **13** and **14**, fit results are included for the low-energy band and the high-energy band. The spectrum of **15** was fit using three Franck-Condon bands; only the lowest and highest are reported here. The fit for the middle band of **15** (see body of paper) is included in Table 3.3 for sub-band 2 of compound **15**. [b] Top row of parameters was obtained from a fit with Γ fixed at 0.1 eV; parameters in parentheses were obtained with a fit with unconstrained Γ, as discussed in the text. [c] The molar extinction coefficient at the peak amplitude of the 0-0 vibronic transition in the Franck-Condon progression. [d] Vibrational frequency. [e] Energy of the peak of the 0-0 vibronic transition. [f] Huang-Rhys factor. [g] Damping width of the Gaussian components of the progression. [h] The damping width for the high-energy bands of **13** and **14** were fixed at 0.1 before performing the fit, as described in the text.

another electronic absorption band. In the case of **15**, in addition to a deviation at high energy, there is a significant area of residual intensity in between the main bands in the spectrum. As we will discuss below, the intensity of this residual band becomes more pronounced when there is a greater disparity in the electron donor and acceptor character of the terminal groups of the two arms.

With the $E_{0\text{-}0}$ values for all transitions in the spectra of **11**-**14** obtained from the FC analysis along with the $E_{0\text{-}0}$ value for **1** from the literature,[88] which is at 2.87 eV, and the lowest-energy feature of **7**,[134] which is at 3.18 eV and is a reasonable approximation for $E_{0\text{-}0}$ of **7**, we have calculated for **13** and **14** the ππ* excitonic coupling term V and the wavefunction mixing coefficient, sin(γ/2), using Equations 3.15 and 3.16. The values of V for **13** and **14** are 0.23 eV and 0.16 eV, respectively. Apparently, the symmetrical tetra-donor substitution leads to a smaller magnitude of the effective excitonic interaction energy and the wavefunction mixing. The square of the wavefunction mixing coefficient of the ethynyl arm in the low-energy exciton state is 0.20 for **13** and is 0.15 for **14**, showing that there is significant mixing of the π* excited states in both cases.

3.3.4 Charge transfer interactions in cruciforms with D/A substituent pattern

The low-energy band in the electronic spectra of **15**-**20** are broader than those of **13** and **14** and for **16**-**20** there is clear evidence for a splitting of the low-energy band which is too large to be due to a vibrational mode. We take this as evidence for a distinct excitonic interaction, relative to that in **13** and **14**, which is correlated with the presence of electron deficient terminal groups on the ethynyl arms; i.e. that this splitting is associated with a coupling of charge transfer transitions in the D/A cruciforms. In the

cases of the D/A substituted cruciforms **16**-**20**, as the degree of intramolecular charge transfer increases, the overall bandshape of the low-energy band evolves with a red-shift of the band edge and a redistribution of oscillator strength from the lower-energy component (sub-band 1) to the higher-energy component (sub-band 2) of this band. It should be noted that both the high-energy band (at approximately 340-350 nm) and the width of the low-energy band (at approximately 430 nm) are unique to D/A substituted cruciforms with non-degenerate conjugation in ethynyl and vinyl arms, as compared to those reported in the literature for **4** and **6** degenerate ethynyl or vinyl arms. This two-band structure is also not present in linear bis(dimethylaminostyryl)benzene compounds with acceptors substituted directly on the central phenyl ring; a comparison may be made of cruciform **19** to the linear compound **2**, which is analogous to **19** but with the cyano groups directly on the central phenyl ring, lacking the phenylethynyl linkers. The absorption spectrum of **2**[88] shows only one main electronic transition in the 1PA spectrum, lacking another transition corresponding to the higher-lying transition in **19**; the spectrum of **2** is also narrower and lacks the low-energy shoulder found in **19.**

In **20**, which has the strongest acceptor group (-NO_2), sub-band 2 is the dominant component of the low-energy band, whereas for the other acceptor substituted cruciforms and **15**, sub-band 1 is more intense. This trend may be explained by a greater contribution to the low-energy band from coupled charge-transfer states as the acceptor strength is increased. This is illustrated for the limiting case of a strong charge-transfer contribution in Figure 3.8: in this case, charge transfer excitations from the donors to the ortho-coupled acceptors are considered. Each charge-transfer excitation is assigned a transition dipole μ_i^{CT}. Since the charge-transfer transition dipoles are energetically degenerate and

anti-parallel, equation 3.2 may be applied to describe the excitonic interaction between the charge-transfer transitions; there is a one-photon allowed transition to the higher energy exciton state ψ_{-}^{CT} and a one-photon forbidden transition to the lower energy exciton state ψ_{+}^{CT}.[133]

While this interpretation provides a reasonable explanation of the 1PA spectrum of **20**, the intensity distributions of the sub-bands of compounds **15**-**19** (with weak to moderate acceptor groups) are not what would be expected from an antiparallel arrangement of degenerate charge-transfer chromophore units. The spectrum of

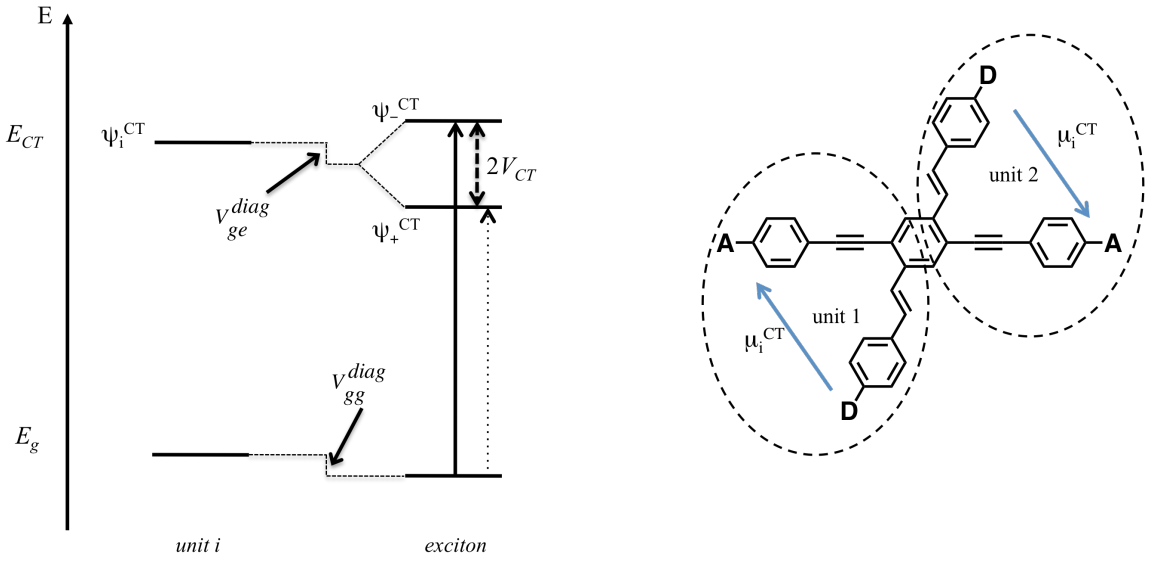

Figure 3.8. A diagram of the charge-transfer transitions in identical V-shaped components of D/A-substituted cruciforms. The energy-level diagram on the left is typical of the splitting of the exciton transitions in an H-aggregate. The allowed transition is represented by a solid arrow from the exciton ground state to ψ_{-}^{CT}, while the forbidden transition is represented by a light dashed arrow from the exciton ground state to ψ_{+}^{CT}.

compound **15**, with the lowest acceptor strength (an unsubstituted phenyl), appears to be similar to the spectra of **13** and **14**, which we described above using a ππ* exciton picture. There is one cruciform band near the transition energy of the ethynyl model compound **11**, and one cruciform band (sub-band 1) near the transition energy of the styryl model compound **1**. The low-energy side of the low-energy cruciform band can be fit reasonably well to a FC distribution very similar to that of model compound **1**[88] (see Table 3.2 for the parameters of the fit of the low energy side of the spectrum of **15**). Figure 3.9 shows that there is substantial residual intensity in between the low-energy and high-energy bands of the cruciform, upon subtraction of the two fitted FC bandshapes, which indicates the presence of an additional electronic band. We attribute this band to a higher energy sub-band (sub-band 2) as described for the D/A cruciform **16**-**20**.

Upon progressing to cruciforms with higher acceptor strengths in compounds **16**-**19**, the spectra of the low-energy band become increasingly similar to that of **20**, in which the coupling of the CT states dominates the low-energy band. The intensity distributions for intermediate cruciforms suggest that there are significant contributions of the ππ* exciton character (a lower energy band with significant oscillator strength) and CT exciton character (low oscillator strength in sub-band 1 and high intensity in sub-band 2). Even though the trend of the low-energy bands is complex we employ a simple splitting analysis to estimate the charge-transfer coupling term V_{CT} from the splitting of the sub-bands to correlate with the acceptor strength. A modified FC analysis was applied to the low-energy band, to obtain estimates of $E_{0\text{-}0}$ for each sub-band. First, the spectra were truncated at on the high-energy sides of their low-energy band peaks at $\varepsilon = 0.95 * \varepsilon_{max}$, as above. The low-energy bands were then fit to two separate FC distributions based

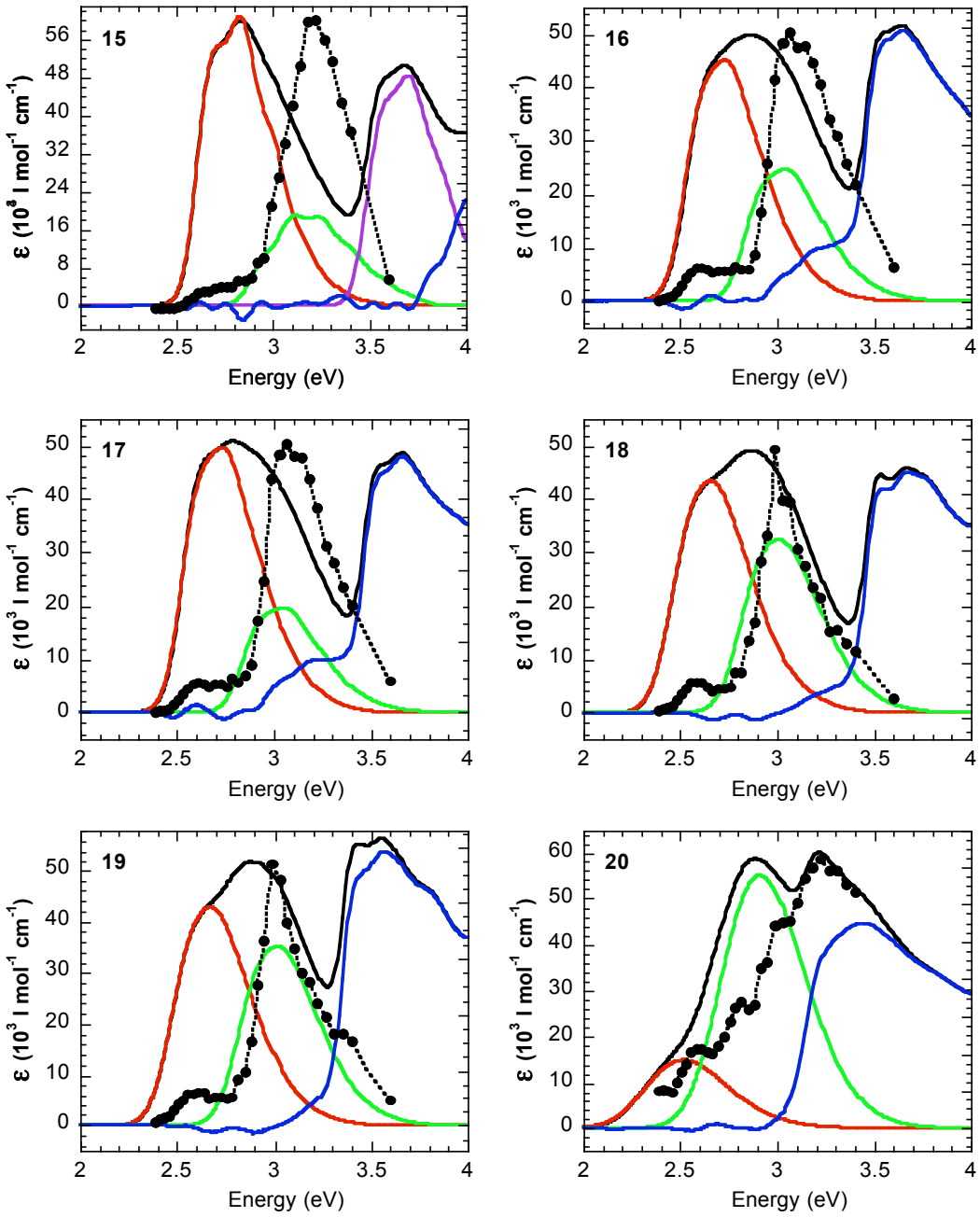

Figure 3.9: 1PA (black lines) and 2PA (black circles) spectra plotted as a function of transition energy, and results of the Franck-Condon bandshape analyses of compounds **15**-**20**. The plot for **15** displays the sums of the six vibronic components derived from Franck-Condon fits of the lowest energy band (red line), the middle band (green line) and phenylethynyl-derived band (purple line) along with the total residual (blue line). The plots for **16**-**20** display the results of the modified Franck-Condon (described in the Discussion): sub-band 1 (red line), sub-band 2 (green line), and residual (blue line).

on the FC parameters of the lowest energy transition in **15**, denoted sub-bands 1 and 2 in order of increasing 0-0 transition energy. The E_{vib} and S factors in the two sub-bands were the same as they are in the lowest-energy FC fit of **15**, while ε_{0-0} and E_{0-0} were allowed to vary independently in each sub-band; Γ was a fitting parameter, but it was constrained to assume the same value for both sub-bands. The first two components of a FC progression were used for each sub-band in the fitting procedure, for a total of four components. Fits were performed using the linear least squares method and 6-component FC progressions were then generated from the parameters obtained using the fitting procedure. Small adjustments were made by hand to achieve the best matches of the peak and shoulder wavelengths of the fits to the experimental spectra.

The results of the modified FC fits are given in Figure 3.9 and Table 3.3. The modified fitting procedure gave spectra in reasonably good agreement with the experimental spectra. As shown in Table 3.3, the values of ΔE_{0-0}, the gap between the E_{0-0} energies of sub-bands 1 and 2 were used to estimate the charge-transfer coupling term V_{CT} for the D/A substituted cruciforms. The value of V_{CT} increases with increasing acceptor strength, as does the ratio of the amplitudes $\varepsilon_{0-0}(1):\varepsilon_{0-0}(2)$. These trends indicate both stronger coupling between the CT transitions as well as the stronger influence of the coupled CT transitions on the overall character of the low-energy absorption band.

A coupling energy for the ππ* states may also be estimated for **15**-**20**. Using the centroid of the two sub-bands as the ΔE_{+}, and the lowest energy features reported[134] for acceptor substituted bis(phenylethynyl)benzenes **8**-**10**, which are 3.58, 3.46, and 3.26 eV, respectively, the ππ* coupling energies V of compounds **15**, **17**, **19** and **20** were calculated to be 0.096, 0.144, 0.195 and 0.268 eV, respectively. This increase of V

Table 3.3: Parameters of modified Franck-Condon fitting of compounds **15**-**20**.

Compound	$\varepsilon_{0\text{-}0}(1)$ (M^{-1} cm^{-1})[a]	$\varepsilon_{0\text{-}0}(2)$ (M^{-1} cm^{-1})[a]	ratio[b]	$E_{0\text{-}0}(1)$ (eV)[c]	$E_{0\text{-}0}(2)$ (eV)[c]	$\Delta E_{0\text{-}0}$ ($2V_{CT}$) (eV)[d]	Γ (eV)[e]
15	62,000	20,000	3.1	2.68	2.95	0.273	0.1*
16	32,000	17,000	1.9	2.61	2.93	0.322	0.13
17	37,000	15,000	2.5	2.6	2.92	0.321	0.12
18	27,000	20,000	1.4	2.54	2.89	0.352	0.14
19	26,000	22,000	1.2	2.55	2.89	0.343	0.14
20	7,000	27,000	0.26	2.39	2.78	0.393	0.20

[a]In this Table, $\varepsilon_{0\text{-}0}(1)$ and $\varepsilon_{0\text{-}0}(2)$ and are the peak molar extinction coefficients of the 0-0 vibronic transitions of the two sub-bands in the broad low-energy absorption band of the donor/acceptor substituted cruciforms **15**-**20**. Sub-band 1 is the lower energy of the two Franck-Condon fits used to describe the lowest-energy band and sub-band 2 is the higher energy Franck-Condon fit. [b]The ratio $\varepsilon_{0\text{-}0}(1)$: $\varepsilon_{0\text{-}0}(2)$, showing the increasing contribution of sub-band 2 to the composition of the low-energy band of the donor/acceptor substituted cruciforms. [c]The $E_{0\text{-}0}$ values of the sub-bands. [d]$\Delta E_{0\text{-}0}$ is the gap between the 0-0 vibronic transitions in the sub-bands, used to estimate the charge-transfer transition splitting term V_{CT}. [e]The damping width Γ is common to the Franck-Condon fits used in both sub-bands. *The independent fits of the sub-bands 1 (see Table 3.2) and 2 of **15** both returned a Γ of 0.1, even though they were not constrained to have the same value by the fitting procedure.

suggests an increase of electronic overlap between the ππ* excited states of the two arms with increasing acceptor strength. The corresponding ππ* mixing coefficients $\sin^2(\gamma/2)$ are 0.017, 0.036, 0.082 and 0.20. The coupling terms and mixing coefficients of **13**-**15**, **17**, **19** and **20** are shown graphically in Figure 3.10.

3.3.5 2PA spectra of linear compounds and cruciforms without D/A substituent pattern

The $\lambda_{max}^{(2)}$ and δ_{max} of **12** are close to the well-characterized and extremely similar molecule BMSB[86,87] (in cyclohexane). The larger HOMO-LUMO gap of **11** causes its 2PA peak to be shifted hypsochromically (relative to **12** and BMSB) too far to be observable with the set-up used. Since the $\lambda_{max}^{(2)}$ of **13** was also outside of the set-up measurement range, it is not possible to determine if the 2PA excited states of the component arms of **13** interact in the same way as the 1PA excited states. Over the wavelength range studied, the shape of the 2PA spectrum of **13** is relatively similar to that of the sum of **11** and **12**, although the magnitude of δ is less for **13** than for the sum of **11** and **12** between 550 – 600 nm. This suggests that there is relatively little coupling between the 2PA excited states of the linear components of **13**, and the lower magnitude of the 2PA spectrum of **13** than the sum of **11** and **12** is consistent with the exciton description of Rumi et al.[72]

It is possible to gain more insight into the coupling of the 2PA excited states by examining **14**. The δ_{max} of **14** is 1200 GM at 700 nm, while there is a shoulder with δ = ~550 GM at approximately 750 nm, in distinction to the 2PA spectra of **3** and **5**, each of which have one peak and no obvious shoulder. We attribute this to the differing conjugated arms in **14** as opposed to the identical conjugated arms in **3** and **5**. Equations

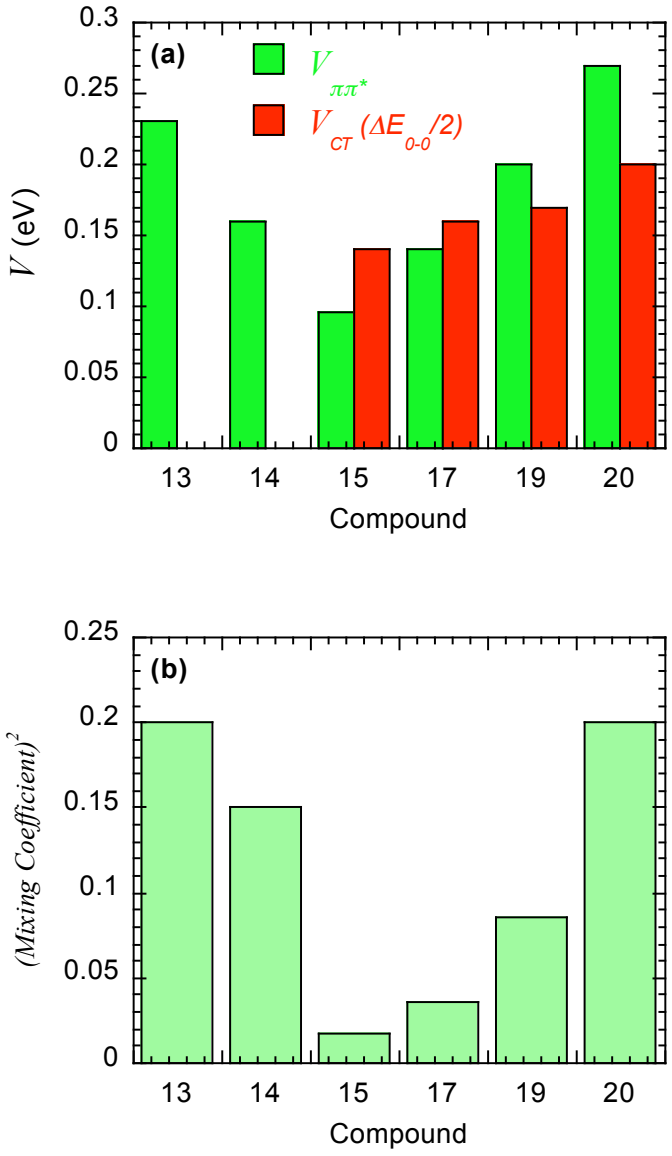

Figure 3.10. Plots of the coupling terms and mixing coefficients for selected cruciforms. For the ππ* mixing, the coefficient shown is the sin(γ/2) term. For the charge-transfer transition mixing, the coefficient is the value given by theory, $2^{-1/2}$.

analogous to equations 3.1 and 3.13 may be written for the $g \rightarrow e'$ 2PA transition energies of excitons composed of identical (equation 3.20) or nonidentical (equation 3.21) units:

$$E_{(\pm)'} = E^0_{e'} + V^{diag}_{e'g} \pm V' \tag{3.20}$$

$$E_{(\pm)'} = \frac{E^{(1)'}_{e'} + E^{(2)'}_{e'}}{2} \pm \frac{\sqrt{(E^{(1)}_{e'g} - E^{(2)}_{e'g} + \Delta V^{diag''})^2 + 4(V')^2}}{2} \tag{3.21}$$

In equation 3.21, $E_{e'g}{}^{(1)}$ is the $g \rightarrow e'$ transition energy of component 1, $E_{e'g}{}^{(2)}$ is the $g \rightarrow e'$ transition energy of component 2, and $\Delta V^{diag''} = V_{e'g}{}^{\text{diag}} - V_{ge'}{}^{\text{diag}}$. Rumi et al.[72] showed that the splitting energy for 2PA transitions in cruciforms such as **3** composed of identical units is near zero, since the splitting energy is equal to the coupling term V'. As $V' = \langle \Phi_{e'}{}^{(1)} | H_{\text{int}} | \Phi_{e'}{}^{(2)} \rangle$ is zero or near zero for 1PA-forbidden transitions to the e' state of a cruciform composed of identical arms, the small splitting energy leads to only one apparent 2PA band. In the case of differing units here, the splitting energy is a function not only of V but of $E_{e'g}{}^{(\text{eth})} - E_{e'g}{}^{(\text{vin})}$ as well. In fact, if both $\Delta V^{diag''}$ and V' are neglected, the splitting term in equation 3.21 is simply half of the quantity $E_{e'g}{}^{(\text{eth})} - E_{e'g}{}^{(\text{vin})}$. For a qualitative comparison, we refer to the 2PA spectra of **1B**[40,88] and **7B**[140] (see Figure 3.11). While the donor groups of these chromophores are not identical to those of **14**, the $\lambda_{max}{}^{(2)}$ of **1B** is shifted by only 0.04 eV from that of compound **1**. To a first order approximation, we assume that a similar shift is present between the $\lambda_{max}{}^{(2)}$ of **7B** and that of **7**, and use the difference between the peak 2PA trantition energies of **1B** and **7B** to approximate $E_{e'g}{}^{(\text{eth})} - E_{e'g}{}^{(\text{vin})}$ for **7** and **1**. The peak 2PA transition energy of **7B** is at 3.56 eV, while the peak 2PA transition energy of **1B** is at 3.33 eV, resulting in a splitting energy of 0.115 eV. Using the wavelengths of the 2PA peak and shoulder of **14** to approximate the

cruciform "excitonic" 2PA transition energies 3.54 and 3.30 eV, the actual splitting of the features in the spectrum of **14** is 0.12 eV from the center energy, consistent with the approximated splitting energy derived from the $\lambda_{max}^{(2)}$ of **1B** and **7B**. This strongly suggests that in the absence of strong coupling of the 2PA excited states of the non-degenerately conjugated linear arms of cruciforms such as **14**, there are two cruciform "exciton" 2PA transitions attributable to the differing linear arms, with little wavefunction mixing. This interpretation is consistent with previous work indicating low mixing of 2PA excited states in cruciforms with degenerate arms[72] and in paracyclophane-linked linear chromophores.[94]

3.3.6 2PA spectra of cruciforms with D/A substituent pattern

The 2PA spectra of the D/A-substituted cruciforms **15-20** all show evidence of more than one 2PA transition in the range investigated, a main peak between 770-830 nm and a secondary band at approximately 950 nm. These transitions correlate with the two sub-bands calculated in the modified FC fitting (see Figure 3.9). Specifically, the

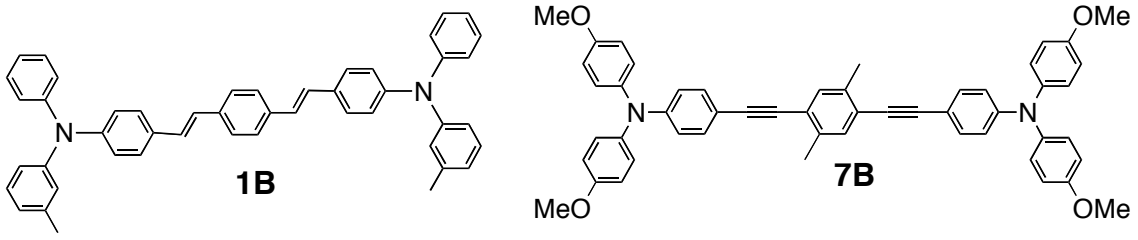

Figure 3.11. Model chromophores for the linear components of cruciform **14**.

strongest 2PA band corresponds to sub-band 2, while the weaker 2PA band correlates with sub-band 1, for compounds **15**-**19**. As the acceptor strength increases from **15** to **19**, the δ_{max} and the peak δ of the lower energy 2PA band increase in magnitude (see Figure 3.5), while $\lambda_{max}^{(2)}$ shows a slight red-shift (see Table 3). As the charge-transfer character of the lower energy states grows with increasing acceptor strength, the magnitude of the lower energy 2PA bands increase, as has been observed for quasi-linear conjugated donor-acceptor-donor systems.[33] On the other hand, **20**, with -NO_2 acceptors, exhibits a substantially broadened and blue shifted 2PA spectrum with both a lower δ_{max} and a blue-shifted $\lambda_{max}^{(2)}$ compared to **19**, which has -CN acceptors. Compounds **4**[72,73] and **6**[75,76] also display relatively broad 2PA spectra, although the low-energy 2PA transitions of both are slightly redshifted from the energy of their main 1PA transitions. Unlike **4**, **6** and cruciforms **15** - **19**, the peaks of the 2PA spectrum of **20** are blue shifted relative the to the 1PA peaks of the sub-bands. This may be due to the presence of overlapping additional bands that give apparent shifts in the positions of the maxima, possibly including the 2PA band from the ππ* excited state of the ethynyl arm. The CT exciton model would predict that the lower energy excited state would be of A_g symmetry and the upper state B_u, consistent with the relative intensities of the 1PA bands, and would indicate that sub-band 2 would show little or no 2PA activity. With the lowering of the energy of the ππ* excited state of the ethynyl arm upon –NO_2 substitution there may be additional state mixings of CT and ππ* states that have not been accounted for by the independent exciton models described above and may result in redistribution of two-photon intensity into higher energy states. Further theoretical studies will be needed to explain the 2PA spectrum of **20**.

The δ_{max} of **15** (740 GM) and **19** (950 GM) show significant reductions from their respective linear bis(styryl)benzene model compounds **1** (995 GM) and **2** (1750 GM). There is also a bathochromic shift of the $\lambda_{max}^{(2)}$ of cruciform **15** (770 nm) with respect to the peak of the linear compound **1** (730 nm); there is no such bathochromic shift in the $\lambda_{max}^{(2)}$ of **19** relative to **2** ($\lambda_{max}^{(2)}$ = 830 nm for both). This indicates the cruciform architecture with both double- and triple-bond arms does not inherently lead to enhanced values of δ_{max} (for the all-parallel polarization tensor component) relative to similar linear compounds that have identical donor and acceptor substituents but lack a phenylene-ethynylene bridge to the electron acceptor. The D/A cruciform motif does provide some ability to tune 2PA band positions and bandwidths, which can be useful for some applications.

3.4 Summary and assignment of state symmetries

The results and modeling of the one and two photon absorption spectroscopy of the cruciforms examined lead to the following overall description: for the unsubstituted or tetra-donor substituted cruciforms, which do not possess substantial intramolecular charge-transfer character, coupling of non-identically conjugated linear units results in some mixing of the ππ* excited states. The interaction of the linear units in the cruciform produces two cruciform excited states with increased splitting over the splitting of the excited states of the independent units. For the cruciform with strong dialkylamino donors and nitro acceptors **20**, there is strong mixing of pairs of charge-transfer states

associated with different CT pathways, which gives rise to a strong splitting of the low-energy 1PA band into a low energy weak band (A_g excited state) and a much stronger band (B_u excited state) at higher energy. In the cruciforms with weak to moderate acceptor strength, **15**-**19**, the transitions appear to be of mixed ππ* and CT exciton character and with the CT character of the lower energy states (that correlate with the donor substituted vinyl arm ππ* state in the limit of weak acceptor strength) increasing as the acceptor strength is increased. The high-energy band (that correlates with the bis(phenylethynyl)benzene arm ππ* excited state) is stabilized by acceptor substitution and appears to be less influenced by the CT interaction.

The trends in the evolution of the state energies of the compounds in this study is illustrated in Figure 3.12. Assignments of the excited states were made based on the observed locations of 1PA and 2PA bands and symmetry selection rules for the D_{2h} point group. In centrosymmetric chromophores such as these cruciforms, 1PA transitions from the ground $1A_g$ state are allowed to excited states with different parity, such as B_u states; 2PA transitions are allowed to higher-lying excited states with the same A_g symmetry. Thus in Figure 3.11, the energies of the $1B_u$ and $2B_u$ states are derived from the peaks in the 1PA spectra, while the energies of the $2A_g$, $3A_g$ and $4A_g$ states are derived from the 2PA peaks. When moving from the linear **11** and **12** to the cruciform **13**, the most notable change is the inferred lowering of the $2A_g$ state from 4.3 eV to ~4 eV, while the remainder of the state energies do not change greatly. The D/A cruciform **15** shows a significant lowering of both the double-bond arm derived $1B_u$ and $2A_g$ states, while the triple-bond arm derived $2B_u$ and $3A_g$ states show relatively little change. Increasing the acceptor group strength in **16**-**19** results in the further lowering of both the $1B_u$ and $2B_u$

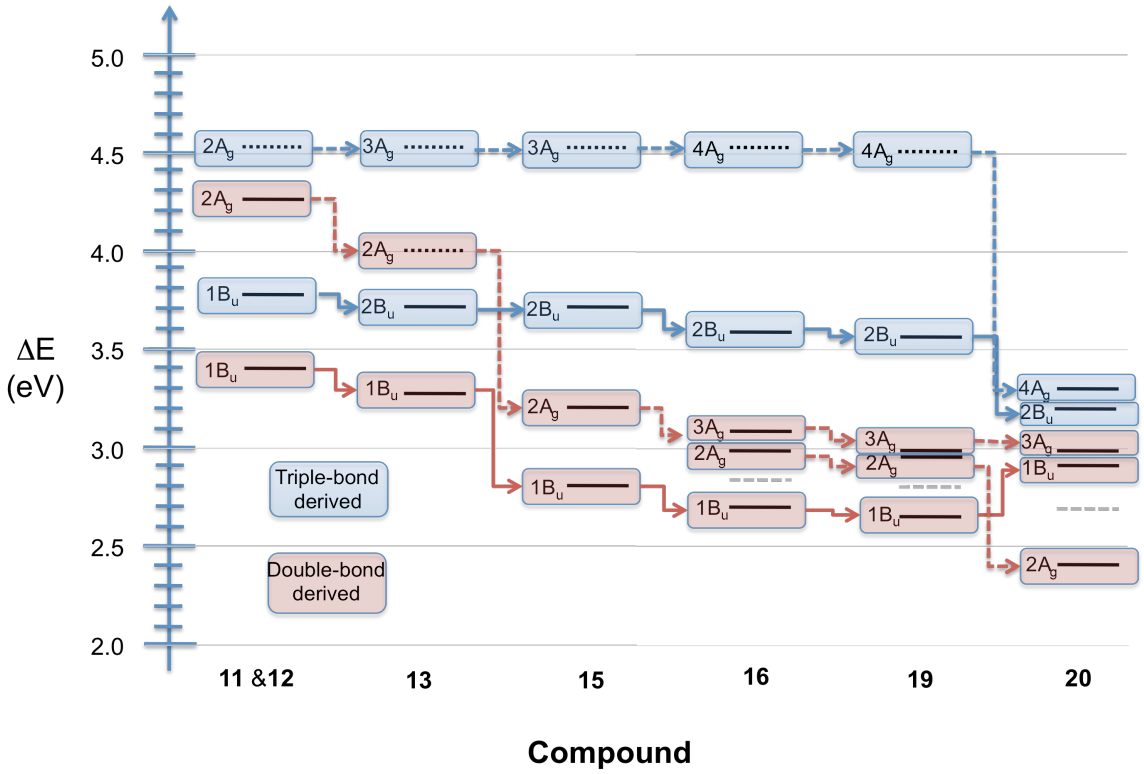

Figure 3.12. State energy diagram of selected linear model and cruciform compounds. The ΔE axis represents the energy of electronic transitions between the ground state and excited states in the compounds. Blue highlighted states are those localized on the bis(phenylethynyl)benzene arm, while red highlighted states are those localized on the bis(styryl)benzene arm. Solid arrows are used to connect B_u states, and dashed arrows to connect A_g states. Dashed pink lines represent the centroid of the sub-bands of in the D/A cruciforms. Dashed black lines are used to describe states whose energies were not indentified in the reported work.

state (δ_{max}). In **20** the $2B_u$ state is at the lowest energy of any of the cruciforms, while the highest-energy 2PA state ($4A_g$) can be identified.

3.5 Conclusions

We have reported the linear absorption, fluorescence and two-photon excited fluorescence properties of eight cruciforms with one bis(styryl)benzene and one bis(phenylethynyl)benzene arm as well as of two linear model compounds representing each non-degenerate arm. The linear- and two-photon absorption spectra of the cruciform with no electron donor or acceptor groups or a cruciform with identical electron-donor substituents on each arm are explained within a ππ* exciton framework. The spectra of the cruciforms substituted with electron-donors on the bis(styryl)benzene arm and electron-acceptors on the bis(phenylethynyl)benzene arm are explained as a superposition of a weakly-mixed ππ* exciton with an intramolecular H-aggregate exciton associated with degenerate charge-transfer transitions between the electron-donors and electron-acceptors. The two-photon absorption cross-sections reported for our cruciforms are on the same order of magnitude as those reported for similar cruciform compounds with degenerate arms;[72,73,75,76] the incidence and systematic variation in the strength of a secondary 2PA band at 950 nm due to a 1PA forbidden transition is reported here for the first time.

The composite ππ* and CT exciton model description for conjugated cruciforms with non-degenerate arms provides useful insight into the nature of the electronic

transitions in the visible and near-IR range and may be useful in the design of two-photon absorption based sensing chromophores that can take advantage of the shift from weak mixing between arms to strongly coupled charge-transfer transitions involving both arms. While the use of strong donor groups and strong acceptor groups might be expected to provide the strongest and most red-shifted 2PA peaks, these objectives would both be best achieved with strong donors and moderate acceptors.

CHAPTER 4: RESPONSE OF CRUCIFORM CHROMOPHORES TO ACID AND ZINC ION BINDING

4.1 Introduction

The cruciform chromophores studied in Chapter 3 utilize differing conjugated arms and substitution with electron donors and acceptors to tailor their linear and two-photon absorption properties. One of the uses that these types of chromophores have been studied for is as components in ion sensor arrays,[66,67] in which the donor or acceptor groups in each cruciform bind to certain metal ions, changing the linear absorption and fluorescence properties of the chromophores and the pattern seen in the sensor array in ways specific to each metal ion. The convergence of ion sensitivity of cruciforms with the 2PA properties shown in Chapter 3 of this work suggest that cruciform compounds might be useful candidates for development into sensing dyes for two-photon microscopy. In this chapter the 1PA, fluorescence and 2PA of a set of cruciforms is studied in the presence and absence of acid or Zn^{2+} ions to provide insight into the potential use of cruciforms as metal binding chromophores for two-photon microscopy.

Many ion-selective moieties that are currently in use are based on amine groups, which act as electron donors.[141] In an example from the literature, chromophores reported in Pond et al.[107] used aza-crown-ether binding moieties attached by the nitrogen atom to the 4 and 4′ positions of the terminal phenyl rings of bis(styryl)benzene (BSB) backbones. In the absence of metal ions, the aza-crown-ether substituted BSB chromophore had a 2PA spectrum indistinguishable from those of the analogous

dibutylamine substituted chromophore **2**, while the introduction of Mg^{2+} ions led to significant reductions in the 2PA spectrum in the range of 720 – 860 nm. This was attributed to "turn-off" of charge donation by the nitrogen atoms of the aza-crown-ether groups, and showed that the strongly electron donating dialkylamine groups were attractive targets for use in switching 2PA properties in centrosymmetric chromophores. However, a preferred modality in 2PLSM dyes is turning on of 2PA, and a method for using metal ion binding to strong acceptor groups to increase 2PA in some portion of the 700 – 1000 nm range useful for 2PLSM would be of significant utility in designing new 2PLSM chromophores.

In Chapter 3, the linear and two-photon absorption properties of cruciform compounds such as those in Figure 4.1 were investigated. In particular, the cruciforms reported demonstrated relatively strong 2PA with δ_{max} and $\lambda_{max}^{(2)}$ strongly dependent on the pattern of electron-donor and –acceptor substitution at the terminal phenyl groups. Other groups have reported[65-69,77,79] changes in linear optical properties of these and similar cruciforms upon ion or amine binding to the donor or acceptor groups that help them achieve their 2PA strength. Additionally, the modular nature of these types of chromophores makes it relatively simple to construct libraries of chromophores with different optical and ion-responsive properties, and attractive prospect for use in multi-color 2PLSM. However, to date no systematic study has been done to determine the effects of metal binding to 2PA properties of cruciform chromophores. In Chapter 3, cruciform chromophores based on **13** have been explained as being composed of two individual chromophores interacting in an exciton-like manner. In the limiting case of a cruciform with no electron donating or withdrawing/accepting substituents, the two linear

arms couple weakly, resulting in two weakly mixed, relatively localized ππ* excited states, each concentrated mostly on one arm. In the limiting case of a cruciform with strong donors at the terminal positions of the double-bonded arm and strong acceptors on the terminal phenyls of the triple-bonded arm, an excited state with a high degree of intramolecular charge transfer between the D and A groups leads to a strong mixing of the excited states of the two arms, resulting in significantly different optical properties. Cruciforms with moderate strength substituents show properties that have characteristics intermediate to the weakly and strongly coupled regimes. A key finding was the rise of a second 2PA band between 900 – 1000 GM that increased with increasing acceptor strength. In the four-donor compound **14**, no 2PA was measured beyond 900 nm. In **15**, which has only two donors, the slight charge-transfer character imparted by the electronic asymmetry resulted in a weak but present 2PA band between 900 - 1040 nm. This suggests using two out of the four donor groups on a compound like **14** as ion-binding groups could lead to a turn-on of 2PA induced fluorescence in the excitation region at higher wavelength than 900 nm, if the other two donor groups were prevented from binding. Alternatively, increases in the 2PA-induced fluorescence from excitation at wavelengths longer than 900 nm could be achieved by the use of two non-binding donor groups on one arm and two weak acceptor groups on the other arm to serve as binding sites for metal ions that could increase the charge transfer upon binding. The research described in this chapter utilizes the D/A groups as ion binding sites and explores the effects of switching cruciform chromophores between differing coupling regimes in order to understand how to use the cruciform structure as a framework for creating new

libraries of dyes that could be used in 2PLSM. Additionally, a strong donor group used in some 2PA chromophores is evaluated for its resistance to metal binding.

4.2 Results and Discussion

4.2.1 Titrations of cruciforms and model compounds with trifluoromethanesulfonic acid

Titrations of **15**, **22**, and **1B** with trifluoromethanesulfonic acid in methanol were performed in order to model the ion responses of two types of substituted cruciforms as well as diphenylamine, a candidate for use as a non-binding strong donor. The results are shown in Figure 4.2. Protonation of the dialkylamine donor groups of **15** leads to the disappearance of the lower-energy band in the linear absorption spectrum as well as a hypsochromic shift of the higher-energy band. The apparent absorbance of the higher energy band also increases; however, this is likely due to the introduction of the shoulder at 360 nm. Overall, the spectrum of the protonated **15** is very similar to the spectrum of the non-substituted **13** in toluene as shown in Figure 3.3, suggesting strongly that the protons binding to the alkylamine donor groups effectively turn off charge donation by the donors and switch **15** from the moderate inter-arm mixing regime to the weak inter-arm coupling regime. The spectrum of **22** in the absence of acid is very similar to that of **13** and protonated **15**; the titration resulted in a shift of the peak as well as the rise of a second absorption band at approximately 440 nm, near the lower energy band of **15** that has significant charge transfer character. This result suggests that the pyridyl groups are not strong electron acceptors until the electron lone pairs of the pyridyl nitrogen are

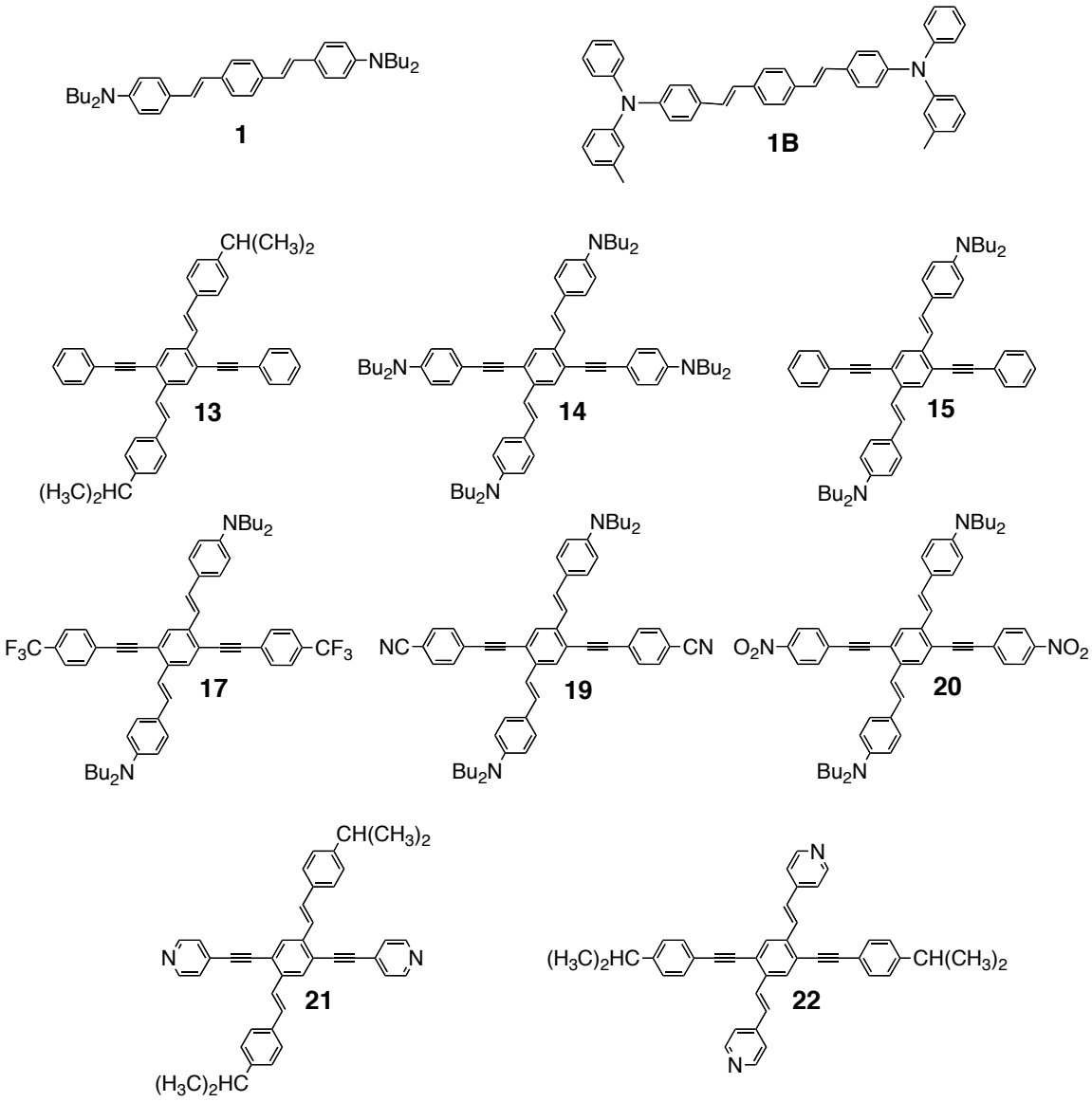

Figure 4.1. Chromophores studied in this chapter.

protonated; the binding event switches the cruciform from the weak-coupling regime to a mixed regime with some charge transfer character. The titration of **1B** resulted in no significant spectral changes at an acid concentration similar to that of the final step of the titration of **15**, suggesting that the diphenylamine group may serve as electron donor groups significantly more resistant to switching by ion binding than dibutylamino groups.

4.2.2 Effects of Zinc ion binding on spectral properties of linear model compounds

Linear and two-photon spectroscopic spectra of the compounds shown in Figure 4.1 were taken at concentrations of 10 μM in dichloromethane in the absence and presence of Zn^{2+} ions, with the exception of **14**, which was studied at 5 μM in the presence of Zn^{2+}. Zinc trifluoromethanesulfonate was added to solutions of the compounds in approximately 5-fold molar excess for all except **14**, which was added in approximately 10-fold molar excess. These ratios correspond to 2.5 fold molar excess with respect to the binding groups on each chromophore. Summaries of the 1PA and fluorescence data are found in Table 4.1, and of the 2PA data in Table 4.2.

4.2.3 Comparative effects of Zn^{2+} ions on spectra of linear compounds with dibutylamine and diphenylamine donor groups

As can be seen in Figure 4.3, the 1PA and fluorescence spectra of **1** and **1B** are very similar to each other in the absence of Zn^{2+}. The 1PA peaks of the compounds are within 5 nm of each other, and the peak positions of the spectra are similar as well to those reported in the literature[40,88] for these compounds in toluene. The fluorescence

spectra reported here have a considerably larger Stokes shift and less vibronic structure than those reported previously for these compounds in toluene, as a result of the more

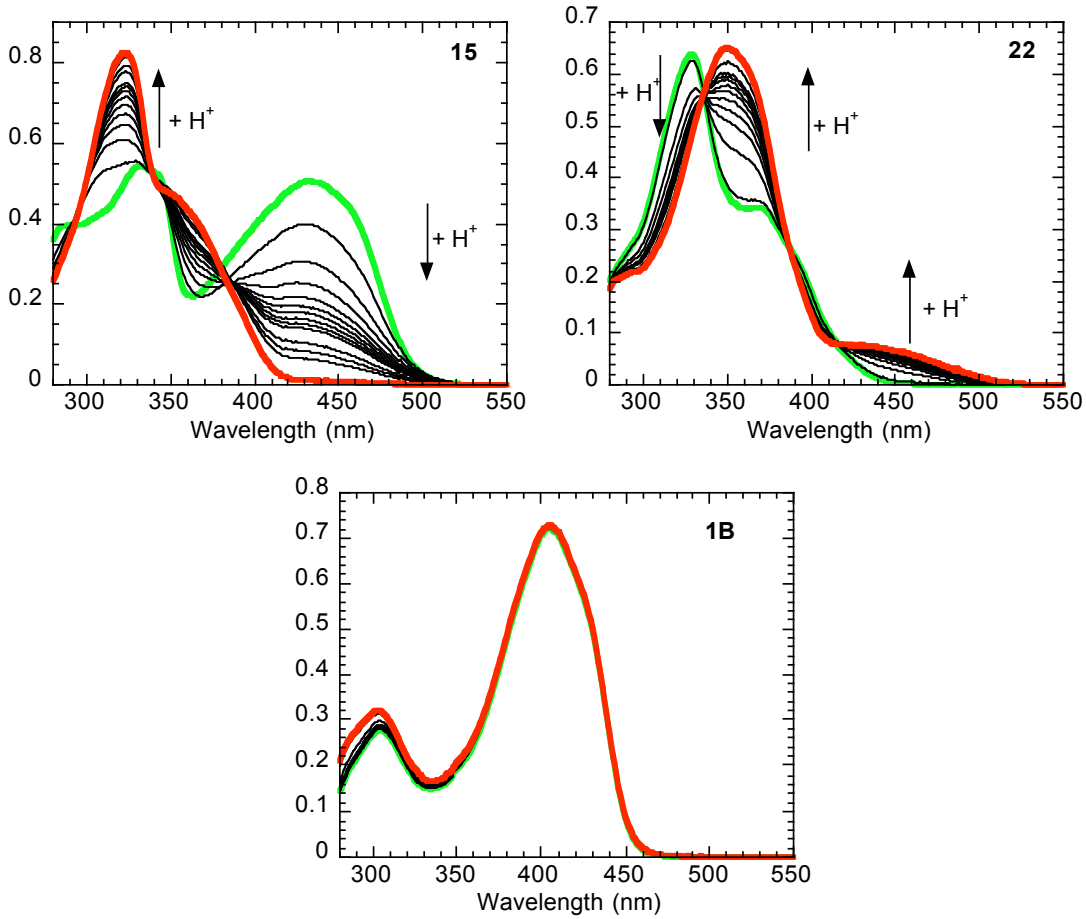

Figure 4.2: Titrations of 10 μM solutions of **15**, **22** and **1B** with trifluoromethanesulfonic acid in methanol. Concentrations of acid in the titration of 15 range between 0-20 molar equivalents; in the titration of 22 between 0-6 molar equivalents; and in the titration of 1B from 0-25 molar equivalents.

polar solvent used here. The 2PA spectra have $\lambda_{max}^{(2)}$ of 730 and 740 nm, respectively, identical within experimental error to those published for these compounds in toluene, although the δ_{max} are significantly reduced, from 995 GM and 805 GM to 315 GM and 450 GM, respectively. The general reduction in δ_{max} is attributable to the polar solvent environment, likely affecting **1** more than **1B**.

The addition of Zn^{2+} to the solutions resulted in no appreciable change for **1B**, while all spectral features of **1** displayed significant hypsochromic shifts; the absorption peak also decreased in magnitude compared with the chromophore in the absence of Zn^{2+}. The ratio of the peak absorbances, 1.23, is similar to the ratio of ε_{max} of compounds **1** and **12** in toluene, which is 1.3. The Stokes shift also decreases, accompanied by a fluorescence spectrum with clear vibronic structure. The spectra of **1** in the presence of Zn^{2+} are very similar to those of compound **12** as reported in Chapter 3, indicative of a total "turn off" of the electron donation from the dialkylamino donor groups to the π-electron system.

4.2.4 Effects of Zn^{2+} on spectral properties of cruciforms

For purposes of direct comparison, the linear absorption spectra of all of the cruciforms studied are shown in Figure 4.4. The spectra of **13**, **14**, **15**, **17**, **19** and **20** in the absence of Zn^{2+} bear great overall similarities to the spectra of the same compounds in toluene as reported in Chapter 3. The spectra of **21** and **22** differ significantly from each other and from **13**, with lower-energy transitions not as distinct or as strong as those of **13**. The overall magnitudes of the bands of **21** and **22** are also significantly lower than **13**, suggesting that while the pyridyl groups are strong enough acceptors to affect the 1PA spectrum, they are not enough by themselves to switch the cruciforms from ππ*

Table 4.1. Linear absorption and fluorescence data for quadrupolar and cruciform compounds studied in dichloromethane, in the absence and presence of Zn^{2+}.

Compound	$\lambda_{max}^{(1)}$ (nm)[a]	$\lambda_{max}^{(1)}$ (nm) (Zn^{2+}) [b]	$\lambda_{fl}^{(1)}$ (nm)[c]	$\lambda_{fl}^{(1)}$ (nm) (Zn^{2+}) [d]	η_{fl}[e]	η_{fl} (Zn^{2+})[f]
1	417	360	484	417	0.57	0.73
1B	412	411	498	495	0.89	0.85
13	332	330	441	441	0.73	0.72
14	390	332	513	414	0.42	0.43
15	338 (444)	330	532	427	0.60	0.65
17	338 (451)	338	574	414	0.68	0.80
19	348 (433)	338	621	427	0.35	0.68
20	387 (433)	353	n/a	n/a	n/a	n/a
21	329	357	458	610	0.49	0.065
22	330	342	443	559	0.39	0.47

[a]Linear absorption peak wavelength of highest energy feature of the chromophores in dichloromethane in the absence of Zn^{2+} ions. Parenthetical values are the peak wavelengths of the lower energy bands of the cruciforms, where applicable. Error in the wavelengths reported in this Table is ± 1 nm. [b]Linear absorption peak wavelength of the chromophores in presence of Zn^{2+}. [c]Fluorescence peak wavelength of the chromophores in the absence of Zn^{2+}. [f]Fluorescence peak wavelength of the chromophores in the presence of Zn^{2+}. [e]Fluorescence quantum yield of the chromophores in the absence of Zn^{2+}. [f]Fluorescence quantum yield of the chromophores in the presence of Zn^{2+}. Error in reported quantum yield measurements is ± 5%.

Table 4.2. Two-photon absorption properties of quadrupolar and cruciform chromophores studied in dichloromethane, in the absence and presence of Zn^{2+} ions.

Compound	$\lambda_{max}^{(2)}$ (nm)[a]	$\lambda_{max}^{(2)}$ (nm) (Zn^{2+}) [b]	δ_{max} (GM)[c]	δ_{max} (GM) (Zn^{2+})[d]
1	730	570	315	130
1B	740	740	450	470
13	550	550	70	70
14	720	570	485	290
15	790	550	415	150
17	820 (950)	550	515 (230)	130
19	820 (970)	550	625 (310)	180
21	610	730	120	230
22	550	720	105	90

[b]Wavelength of largest two-photon absorption cross-section of the chromophores in absence of Zn^{2+}, over the wavelength region studied. Parenthetical values are the peak wavelengths of the lower energy 2PA bands of the cruciforms, where applicable. [b]Wavelength of largest two-photon absorption cross-section of the chromophores in presence of Zn^{2+}, over the wavelength region studied. [c]Two-photon cross-section at $\lambda_{max}^{(2)}$ of highest energy feature of the chromophores in dichloromethane in the absence of Zn^{2+} ions. Parenthetical values are 2PA cross-sections at $\lambda_{max}^{(2)}$ of the lower energy 2PA bands of the cruciforms, where applicable. [c]Two-photon cross-section at $\lambda_{max}^{(2)}$ of the chromophores in presence of Zn^{2+}. Errors in $\lambda_{max}^{(2)}$ are ± 10 nm, while errors in δ_{max} are ± 15% with the exception of **21** in the presence of Zn^{2+}, where the error is > ± 50%.

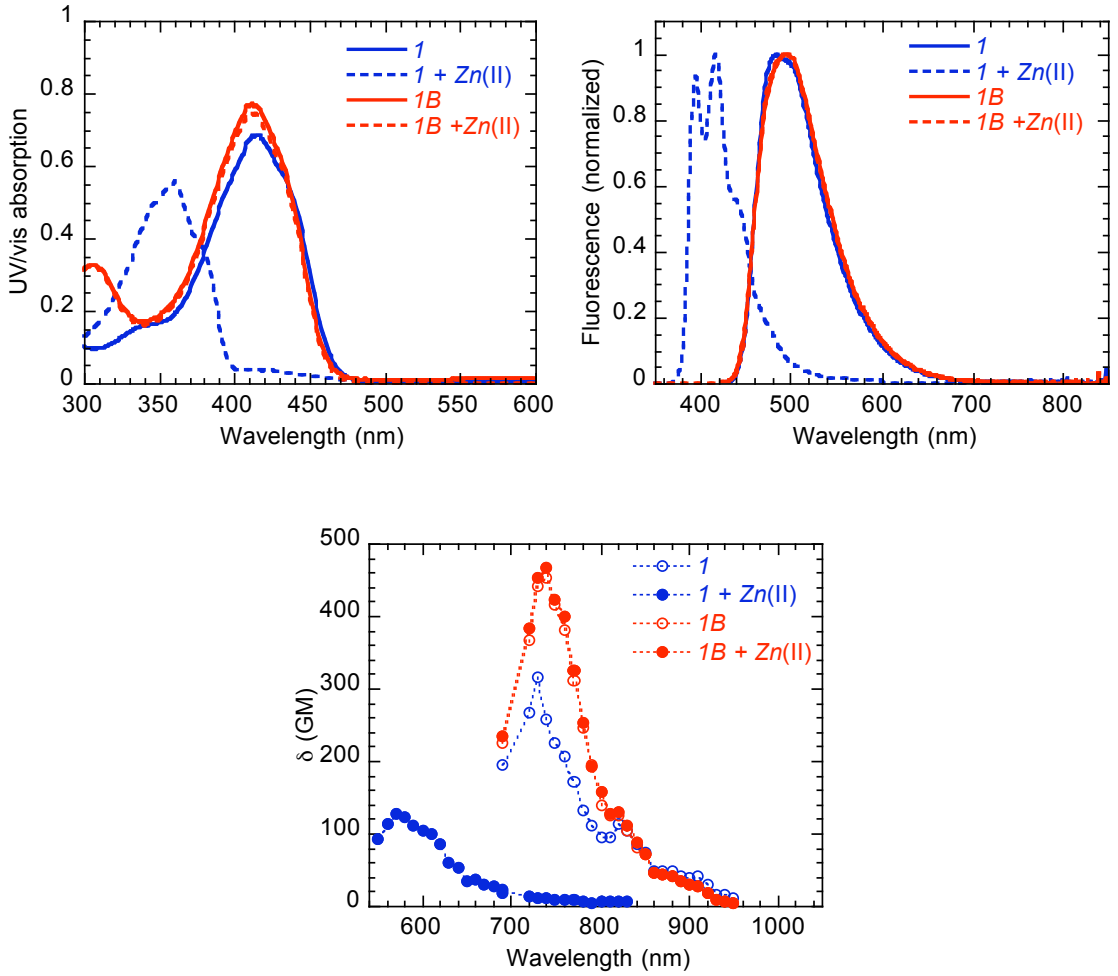

Figure 4.3. 1PA, fluorescence and 2PA spectra of compounds **1** and **1B** in the absence and presence of Zn^{2+}.

excitonic coupling to charge-transfer coupling.

The introduction of Zn^{2+} ions to the solutions caused significant shifts in the absorption spectra of all compounds except **13**. The spectra of compounds **14**, **15**, **17**, **19** and **20** all show evidence of turn-off of the electron donation from the terminal alkylamine groups, as the absorption band in the region of 400-550 nm is largely eliminated. The residual intensity in that area is likely due to incomplete association of the cruciform alkylamine groups with the Zn^{2+} ions. The main features of **14** in the presence of Zn^{2+}, the overall peak at ~330 nm and the shoulder at ~370 nm, are at similar locations to those of **13**, but the ratios of the relative absorptions at those wavelengths are significantly different, which may again be attributed to incomplete association of all alkylamine groups with Zn^{2+} ions. In the range of 300-420 nm, the spectra of **15** and **17** are nearly identical to that of **13**, suggesting that the trifluoromethyl group by itself is not a strong enough acceptor to impact the electronic structure of the cruciform without contribution of an electron donor. This may be contrasted to the spectra of **19** and **20**, which are markedly different from that of **13**. The peaks of **19** and **20** are red-shifted by 700 and 2000 cm^{-1} compared to **13**, indicating that the cyano and nitro acceptor groups have a significant perturbative effect on the state energies of the cruciforms. The spectrum of **21** shows one main peak bathochromically shifted by 2300 cm^{-1} from its value in the absence of Zn^{2+}, and has little apparent vibronic structure. This may be a result of the stabilization of the ethynyl arm state energies by electron donation form the pyridine nitrogen lone pair to the Zn^{2+} ion, causing the transition energies of the individual ethynyl and styryl arms to overlap more with each other. An opposite effect is seen in the spectrum of **22**, in which there is greater separation between the two

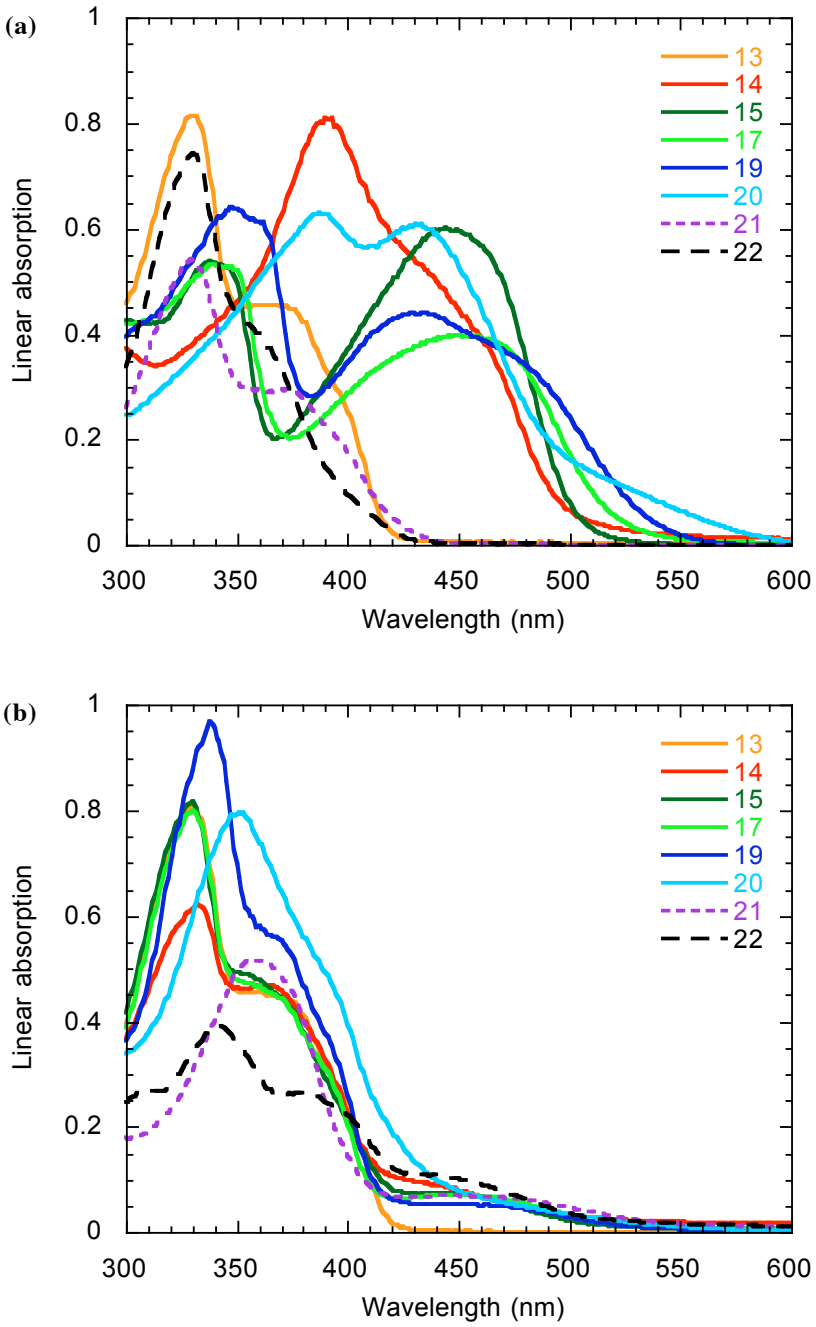

Figure 4.4. 1PA spectra of 10 μM solutions of cruciform compounds in dichloromethane in (a) absence and (b) presence of Zn^{2+}. Note that the spectrum of **14** in (b) is the spectrum of a 5 μM chromophore solution multiplied by two. The concentration of Zn^{2+} in each solution in (b) was 52 μM, corresponding to a 2.5-fold ratio of Zn^{2+} ions to alkylamine or pyridyl groups.

transitions that there was in the absence of Zn^{2+}, due to energy lowering of the styryl arm states resulting from electron donation from the styryl arm pyridine nitrogen lone pair to the Zn^{2+} ion. In both **21** and **22**, there is absorption between 440 – 520 nm that is not seen in the absence of Zn^{2+}, which we ascribe to a weak charge-transfer transition.

4.2.5 Turn-off of charge donation in tetra-donor and bis-donor cruciforms

As can be seen in Figure 4.5, the spectra of **13** are effectively identical with or without Zn^{2+}, as expected for a compound without D/A groups to serve as binding sites. Overall, the spectra of **13** in dichloromethane are very similar to the spectra in toluene. While the 1PA and fluorescence spectra of **14** in the presence of Zn^{2+} show evidence of incomplete binding (significant absorption between 420 nm and 500 nm, as well as the fluorescence band at 600 nm), the spectra of the zinc-bound form are otherwise very similar to those of **13**, a result of the "turn off" of the charge-transfer from the donor groups. In particular, the fluorescence spectra of **14** and **15** in the presence of Zn^{2+} would be indistinguishable from that of **13** in 2PLSM applications.

As shown in Figure 4.5, the 2PA spectra of **13**, **14** and **15** without Zn^{2+} are similar in shape and peak location to those reported for toluene solution in Chapter 3, with the exception of 400 cm^{-1} bathochromic shifts of δ_{max}. The δ values of the spectra overall are approximately half the corresponding values in toluene solution, although both **14** and **15** have a significantly stronger secondary band between 900 - 1000 nm than was measured in toluene solution, particularly for **14**, which showed no noticeable 2PA from 900 - 1000 nm in toluene. This is indicative of stabilization of charge-transfer 2PA excited states by the more polar solvent. Upon Zn^{2+} binding and turn off of charge donation from the

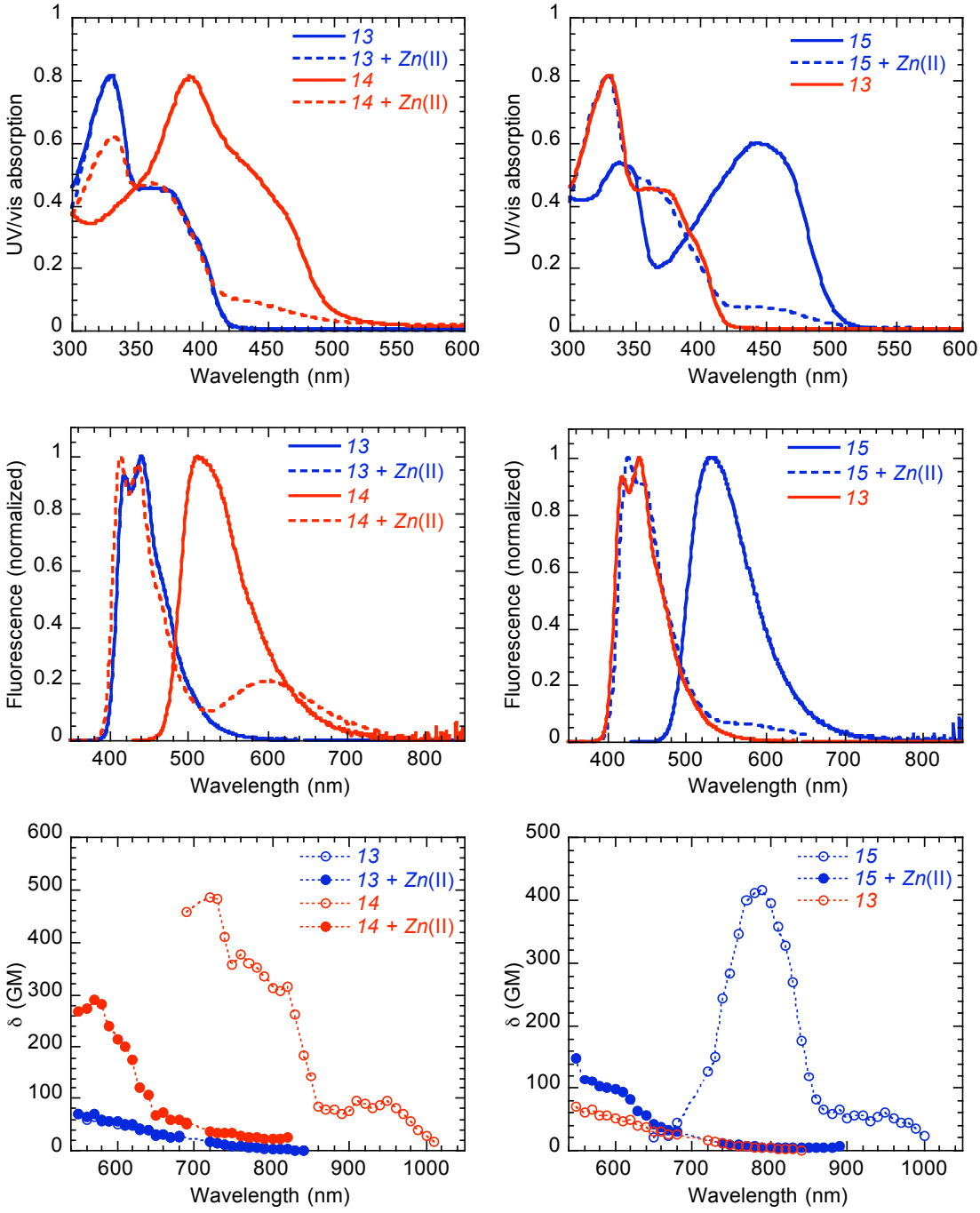

Figure 4.5. 1PA, fluorescence and 2PA spectra of compounds **13**, **14** and **15** in the absence and presence of Zn^{2+}. Spectra of **13** in the absence of Zn^{2+} are included for comparison. Note that the 1PA spectrum of **14** in the presence of Zn^{2+} is of a 5 μM solution of **14** multiplied by a factor of 2.

terminal amine groups, the 2PA spectra show an extreme blue shift, effectively turning off 2PA in the range of 800 – 1000 nm. All told, these results suggest that use of a motif of "turning off" two out of four donor groups would not have the desired effect of switching on 2PA at longer wavelengths for 2PLSM; both the four-donor chromophore **14** and the two-donor chromophore **15** have equivalent 2PA spectra in the range of 800 - 1000 nm, and there is not enough difference between them either in the 2PA or fluorescence to distinguish them.

4.2.6 Turn-off of charge donation in cruciforms with donor groups and acceptor groups

The patterns seen for **15** are extended in the spectra of **17** and **19**, as shown in Figure 4.6. In addition to the differences in 1PA spectra in the presence and absence of Zn^{2+}, the fluorescence spectra of **17** and **19** in the presence of Zn^{2+} are both extremely similar to that of **13**, and would be impossible to differentiate between in 2PLSM. The 2PA spectra of **17** and **19** without Zn^{2+} are significantly different from the spectra of the neat compounds in toluene. The $\lambda_{max}^{(2)}$ is at approximately the same energy, but there is again a reduction in the δ_{max} of the main peak of nearly a factor of 2. The secondary band between 900 - 1040 nm is also significantly increased both in absolute strength and relative to the main peak from the values in toluene solution. Together these observations indicate that while the stabilization of charge transfer states by the polar solvent changes the 2PA properties of the cruciform chromophores significantly, the acceptor groups do not have a large impact on the 1PA, fluorescence and 2PA spectra of the cruciforms when the electron donors are switched off.

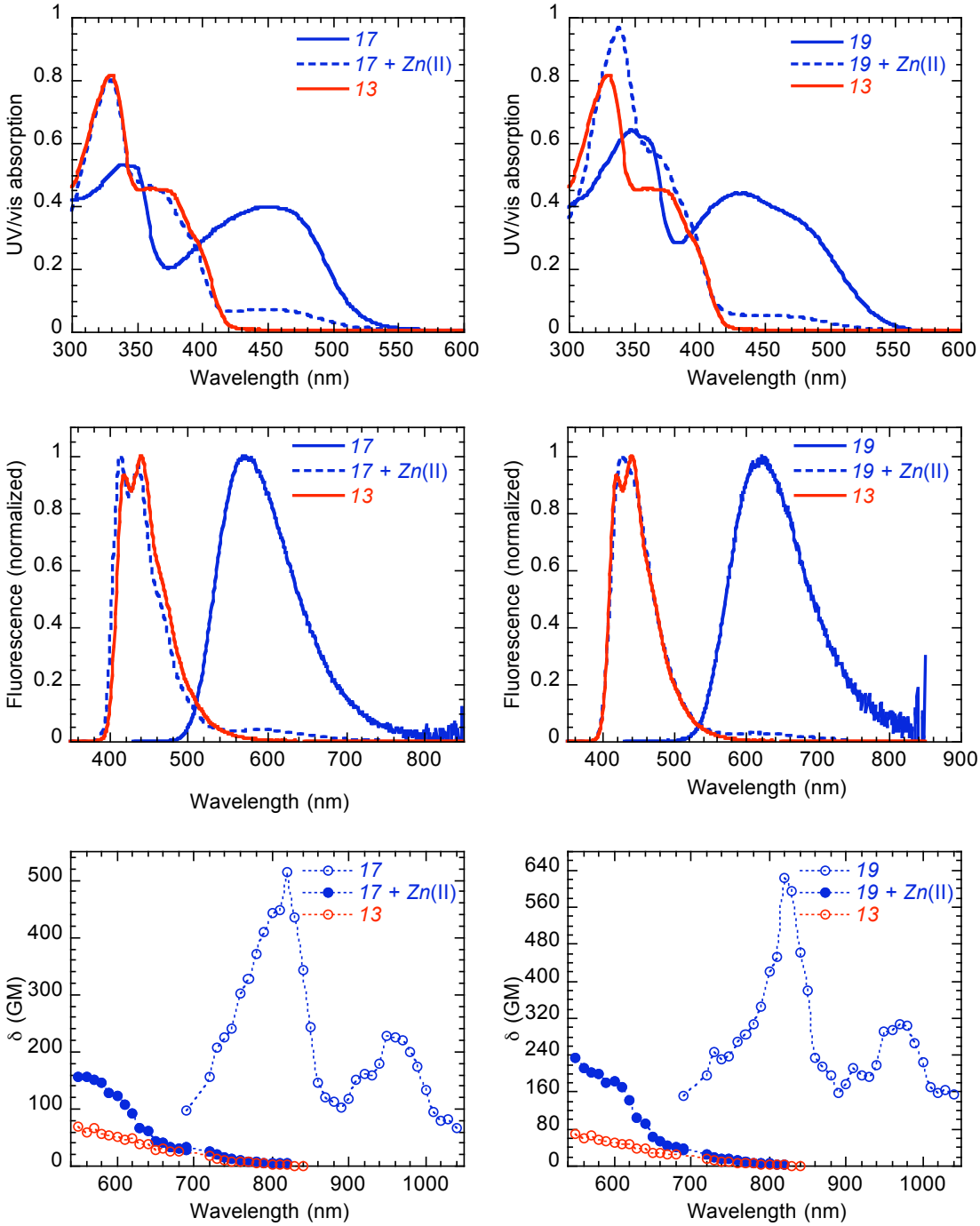

Figure 4.6. 1PA, fluorescence and 2PA spectra of compounds **17** and **19** in the absence and presence of Zn^{2+}. Spectra of **13** in the absence of Zn^{2+} are included for comparison.

4.2.7 Turn-on of acceptor groups

The spectra of **21** and **22** show significantly different changes from those in **14**, **15**, **19** and **20** with respect to the presence or absence of Zn^{2+} ions. As noted, the pyridyl groups act as electron acceptors when bound to Zn^{2+} ions, so these cruciforms display spectral changes associated with turn-on of charge-transfer instead of turn-off. The changes in the 1PA spectra were noted earlier, and in Figure 4.7 the changes in fluorescence and 2PA spectra are shown as well. The fluorescence spectra of **21** and **22** in the presence of Zn^{2+}, with peaks at 610 and 559 nm, respectively, are markedly different from each other. This has two implications: that the pyridine-Zn^{2+} group is a very strong electron acceptor even in the absence of an electron donor in the compound, and that the conjugation non-degeneracy of the arms may be used in concert with choice of electron donors and acceptors to create sensing dyes using the same binding motif that have fluorescence spectra distinguishable from each other under 2PLSM conditions.

The 2PA spectra of **21** and **22** in the presence of Zn^{2+} are intermediate between the spectra of **13** and Zn^{2+}-bound D/A cruciforms on the one hand, and the spectra of the Zn^{2+}-free D/A cruciforms on the other. The $\lambda_{max}^{(2)}$ are 730 and 720 nm, respectively, with δ_{max} of 210 for **21** and 90 for **22**. While these δ_{max} are not as high as those of **14** and Zn^{2+}-free D/A cruciforms, they do have isosbestic points of 2PA at 690 nm and 680 nm, within the operating range of most 2PLSM apparatus. Additionally, the overlapping 2PA bands and distinguishable fluorescence bands could be used for coexcitation of dyes based on **21** and **22** with different pyridine-based sensing moieties targeted at different metal ions or analytes.

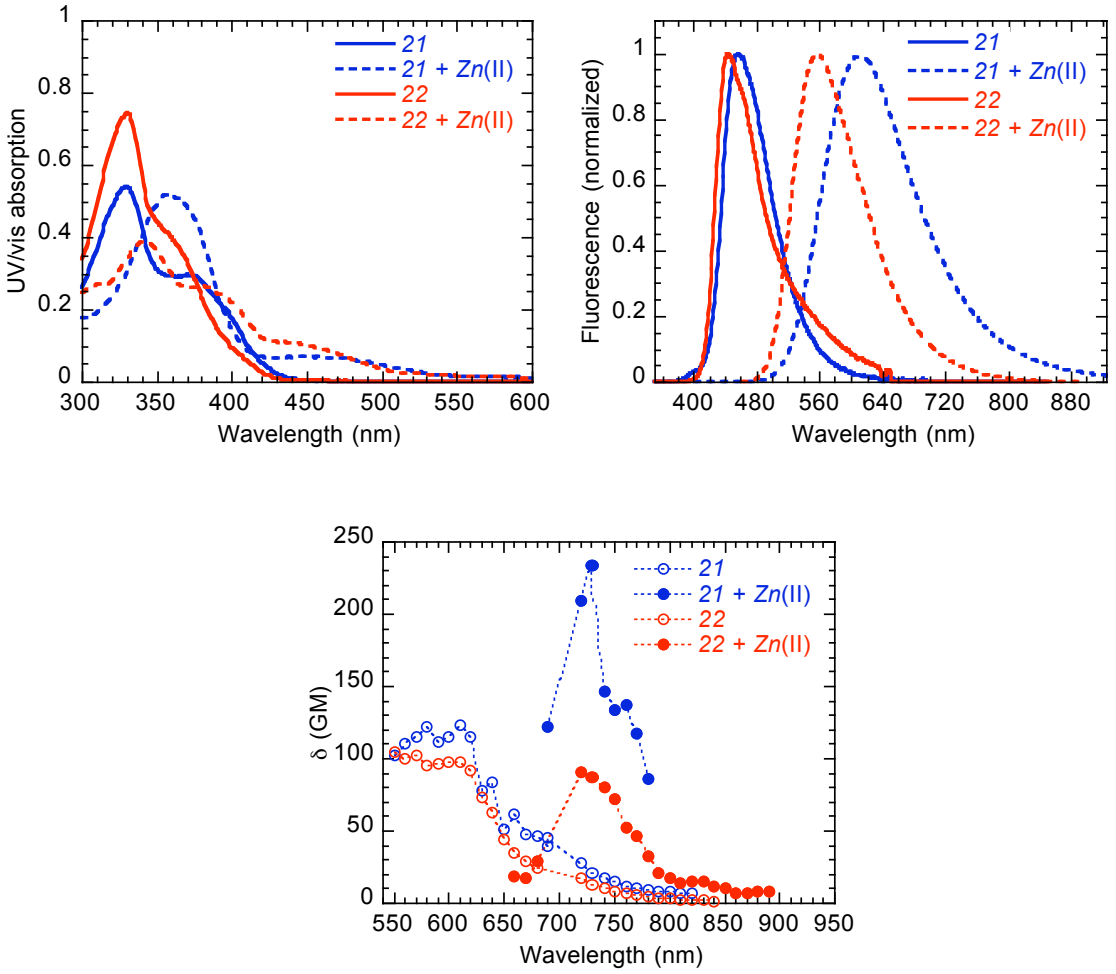

Figure 4.7. 1PA, fluorescence and 2PA spectra of **21** and **22** in the absence and presence of Zn^{2+}. Note that the error in δ for **21** in the presence of Zn^{2+} is on the order of ± 50%.

4.3 Conclusions

The use of cruciform compounds for two-photon excited fluorescence based metal ion sensing has been investigated by linear absorption, fluorescence and two-photon absorption spectroscopy in dichloromethane, both in the absence and presence of Zn^{2+}. In general, the spectra of Zn^{2+}-free cruciforms were relatively similar to the spectra of the same compounds in toluene, with differences congruent with the polar nature of the dichloromethane solvent used here. In cruciforms with dibutylamino donor groups on the styryl arms and the same groups or acceptor groups on the ethynyl arms, binding of Zn^{2+} resulted in switching off of intramolecular charge transfer and in accompanying blue shifts of all spectra and reductions of 2PA strength in the 2PLSM region of interest. The presence of trifluoromethyl or cyano acceptor groups on the terminal phenyl of the ethynyl arms did not render the 2PA or fluorescence bands of these cruciforms distinguishable from each other when bound to Zn^{2+}.

In cruciforms without donor substitution but with weak acceptor pyridyl groups on either the ethynyl arms or styryl arms, spectral properties in the absence of Zn^{2+} were similar to that of an unsubstituted cruciform, showing that pyridyl groups by themselves have relatively little impact on the electronic structure of cruciform compounds. The addition of Zn^{2+} resulted in significant changes in all spectral properties explained by the turn on of intramolecular charge transfer. In particular, the 2PA peaks moved into the wavelength region of interest for 2PLSM, with δ_{max} values comparable to currently used 2PLSM chromophores. The fluorescence spectra in the presence of Zn^{2+} were also readily distinguishable from each other under typical 2PLSM conditions. The use of non-

degenerate conjugation in the arms was shown to provide a potential pathway toward creating libraries of chromophores with sensing moieties based on the same donor or acceptor groups.

Finally, a strong electron donor group was identified for use as a non-binding donor group capable of increasing δ_{max} values in the cruciform structure. The use of this impervious strong donor group or other, moderately strong non-binding donor groups along with pyridyl-based sensing groups, could result in a set of chromophores with strong 2PA and readily distinguishable fluorescence, that could provide a valuable complement to 2PLSM chromophores already available.

CHAPTER 5: DIPOLAR OXAZOLE AND THIAZOLE CHROMOPHORES FOR ZINC ION SENSING

5.1 Introduction

As discussed in Chapter 1, the structure and composition of cells and biological materials as well as of transport of biologically relevant molecules are topics of much current study. One of the tools that has attained widespread use in recent years is two-photon laser scanning microscopy (2PLSM).[5,6,10,11,96,97] In order to further develop 2PLSM, it is necessary to develop chromophores that possess both strong two-photon absorption (2PA) and biological interaction moieties; many of the chromophores currently used for 2PLSM are optimized for biological activity and linear optical properties but are not designed for 2PA.[115] Desired characteristics of 2PLSM dyes are strong 2PA in the near-infrared region of interest of approximately 700 – 1000 nm, effectiveness as a fluorescence turn-on sensor[142,143] upon analyte binding, relatively large fluorescence quantum yield, and significant spectral shifts upon analyte binding.

5.1.1 Role of zinc ions in biological processes

One biologically important analyte for which novel 2PLSM chromophores have been recently developed[112-115,144] is the Zn^{2+} ion. Zinc is the second most abundant transition metal in the human body, and the highest concentration of Zn^{2+} is in the brain, where it has concentrations as much as 10^4 higher than some neurotransmitters.[145] Zinc ions play an important role in many other biological systems such as the immunological,

endocrine and gastroenterological systems,[146] and is an important part of many proteins and enzymes. The most well known zinc-containing proteins are the zinc-finger proteins, which play important roles as DNA transcription factors.[145] However, even though the total concentration of zinc in the body is high, only approximately 10% is labile or free zinc that is not bound up in some biological system or process.[145] In order to better understand the many physiological roles of zinc, it is important to develop sensitive techniques to image labile Zn^{2+} ions. As Zn^{2+} ions are difficult to observe with many techniques, one of the most important tools for Zn^{2+} imaging is the use of fluorescent dyes whose fluorescence undergoes profound changes when bound to Zn^{2+}.[146] Furthermore, the assessment of local and transient concentrations of Zn^{2+} would provide more important information than simple knowledge of the presence or absence of Zn^{2+}. Thus, ratiometric sensing is a sensing modality particularly important for imaging on zinc ions in cells and tissues.

5.1.2 Ratiometric sensing

Ratiometric imaging[147-150] is a technique that is useful for analyte sensing in microscopy due to numerous advantages over other methods used to track concentrations and trafficking of analytes in biological systems. Chiefly, artifacts due to variations in illumination intensity, photobleaching and local concentration of the sensing dye are eliminated by the use of a ratio of two signals. In ratiometric imaging, two separate spectral measurements are made; one is of a spectral property of the free ligand form of the sensor, and the other is of the same spectral property of the analyte-bound form. While the property measured my be the excitation efficiency of fluorescence at a given

wavelength by excitation at different wavelengths (excitation ratiometry), this method requires two excitations of the sample and two readouts of the fluorescence signal generated. In practice, it is preferable to use only one excitation pulse to avoid the potential of having the excitation light pulse or sample differ change between pulses. This requires that the free and bound forms of the dye in use each must have significant fluorescence intensity in a region in which the other form of the dye has relatively low fluorescence intensity, i.e. large fluorescence contrast at two wavelengths. If these conditions are met, then the sample may be illuminated with excitation light at the isosbestic point of absorption of the two forms of the dye. The resulting fluorescence signal may be filtered to separate the fluorescence emissions, each belonging primarily to one form of the dye; this is emission ratiometry. The ratio of these signals may then be used to calculate local concentration of the analyte in question using the following equation:[147]

$$[M] = K_d \left(\frac{(F_1/F_2) - (S_{f1}/S_{f2})}{(S_{b1}/S_{b2}) - (F_1/F_2)} \right) \left(\frac{S_{f2}}{S_{b2}} \right) \tag{4.1}$$

with the measured fluorescence intensities F_1 and F_2 defined by:

$$\begin{aligned} F_1 &= S_{f1}c_f + S_{b1}c_b \\ F_2 &= S_{f2}c_f + S_{b2}c_b \end{aligned} \tag{4.2}$$

In equation 4.1, $[M]$ is the concentration of the analyte in question and K_d is the effective dissociation constant. In both equations 4.1 and 4.2, the S factors are proportionality coefficients derived from the excitation intensity, extinction coefficient of the dye, path length of the excitation in the sample, fluorescence quantum yield and collection

efficiency of the detection system. The subscripts *f* and *b* refer to the free ligand and bound form, and subscripts 1 and 2 refer to the two fluorescence wavelengths or bands used. The concentrations of the free and bound forms of the dye are represented by c_f and c_b.

5.1.3 Choice of dipolar backbone and use of 2PA dye π-electron acceptor as sensing moiety

With the aforementioned motivation in mind, there have recently been a number of ratiometric dyes developed for Zn^{2+} sensing,[146,151-155] as well as several developed for Zn^{2+} sensing and 2PA.[112-114]The chromophores discussed in this chapter are based on dipolar oxazole chromophores shown to display both ratiometric response to pH[156] and relatively strong 2PA figures of merit[109,110] in the 2PLSM region of interest. These chromophores were modified by incorporating the pyridyl group of the chromophore into a tris(picolyl) metal chelating unit.[115] The choice of a dipolar structure was made with several reasons in mind. Quadrupolar chromophores with a D-π-D or D-π-A-π-D structure, which often have very high δ_{max}, have two binding groups, rendering them more complicated for use in ratiometric imaging due to the need to account for two different analyte-bound chromophore species. In these types of dye, metal binding to the donor groups also results in a reduction of intramolecular charge transfer, consequently causing a shift in the 2PA peak position and reducing δ_{max} as well. It has also been suggested that ions are ejected or displaced from the donor groups in these chromophores when they are in the excited state, causing fluorescence shifts between the free and analyte-bound chromophores that are too small to be useful for emission ratiometric

imaging.[107,108] Dipolar chromophores only have one binding site, making their use in ratiometric imaging simpler. Additionally, their lack of centrosymmetry means that their $\lambda_{max}^{(2)}$ is relatively easy to predict based on their $\lambda_{max}^{(1)}$. However, to address the last two issues, a strategy for analyte binding was employed that is different than most.

Most sensing chromophores rely on using analyte binding groups based on electron donor groups; the binding of analyte results in a reduction of intramolecular charge transfer and reduced δ in the region of interest. As seen in Figure 5.1, a different method is to use as the binding group an electron acceptor such as pyridine; binding of the metal would in this case increase intramolecular charge transfer and δ, and provide a significant bathochromic shift of all spectra.

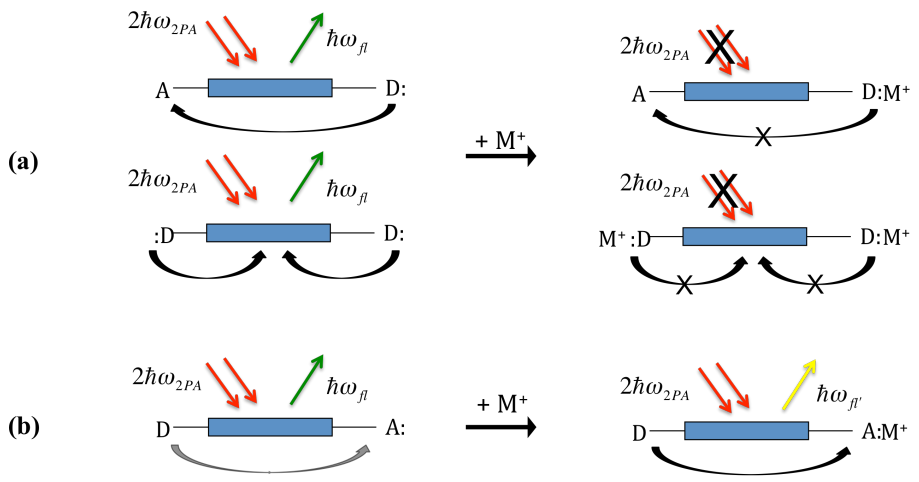

Figure 5.1. Use of electron donors and acceptors as binding groups. In (a), electron donor groups of a D-A or D-π-D chromophore are used as metal ion binding sites. As the metal binds, the electron lone pairs that were the source of high δ through intramolecular charge transfer are prevented from taking part in charge transfer, and two-photon excited fluorescence is reduced or eliminated. In (b), the acceptor group binds to a metal ion, causing it to become more electron deficient and increasing intramolecular charge transfer, δ and redshifting the fluorescence emission.

The strategy of chromophore design for the chromophores in this chapter was to develop dyes with the following properties for ratiometric 2PLSM sensing of zinc:

- Strong 2PA and 2PLSM figures of merit $\eta\delta$ in the 2PLSM region of interest of 700 – 1000 nm.
- Isosbestic point of 2PA in the 2PLSM region of interest.
- Distinguishable fluorescence spectra of free and bound form.
- Selectivity for Zn^{2+}.

5.2 Oxazole chromophores results and discussion

The structures of the oxazole chromophores discussed in this section are shown in Figure 5.2. The **YW2-068** chromophore features a pyridine group attached to an oxazole backbone. The pendant group attached at the carbon adjacent to the pyridine nitrogen serves to make the chromophore selective for Zn^{2+}. The methoxyphenyl group attached to the oxazole serves to extend the π-conjugation of the system, with weak electron donation from the methoxy group. The **SL35** chromophore[115] features fluorine atoms on the pendant group pyridyl groups to discourage formation of 2:1 complexes of **SL35**:Zn^{2+},

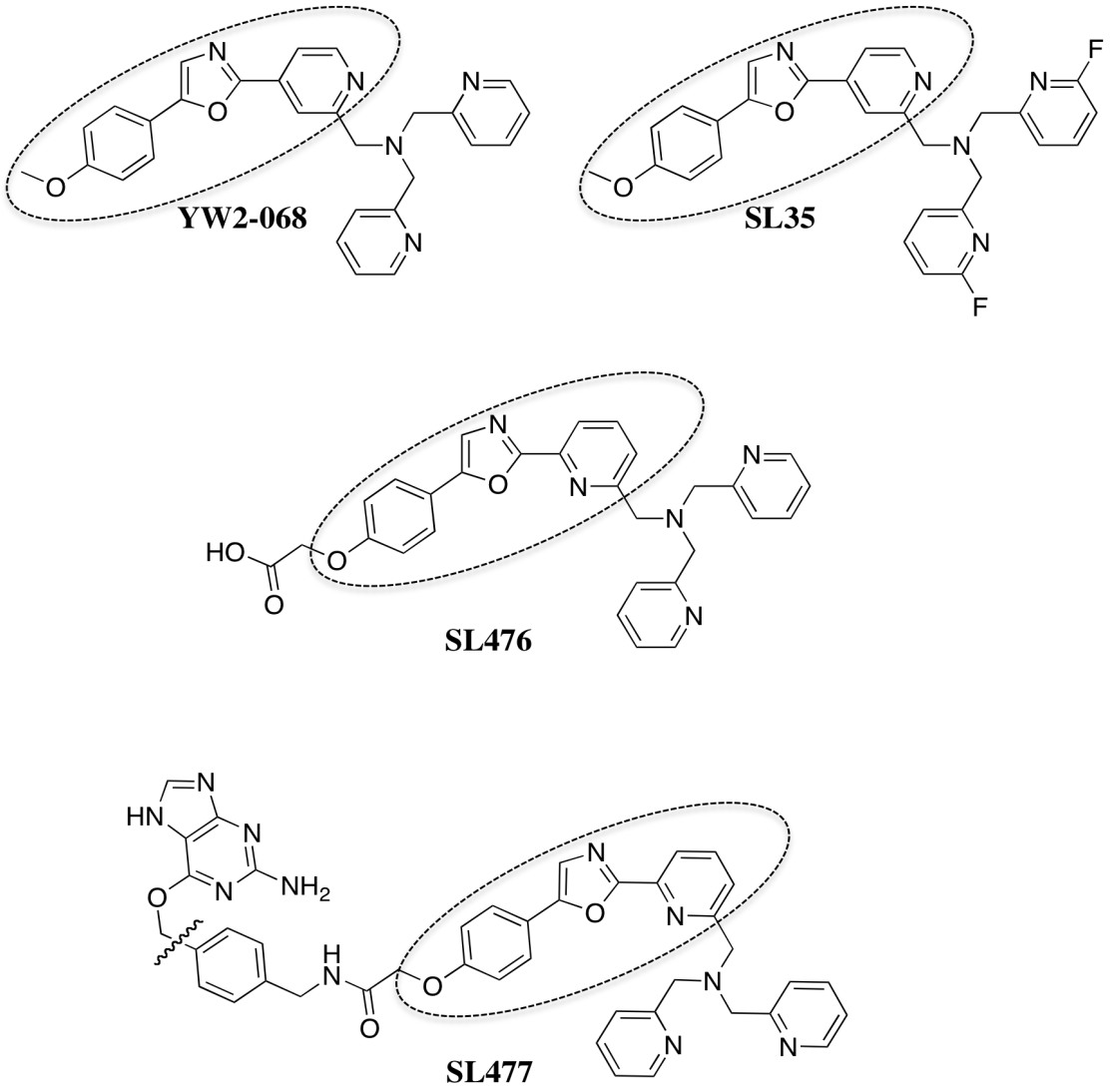

Figure 5.2. Oxazole-based chromophores studied in this chapter. The chromophore unit is indicated by the dashed oval, while the bond broken to attach **SL477** to a protein is indicated by the wavy line.

which were observed with **YW2-068**. **SL476** is significantly different in that the attachment of the pyridine group to the oxazole is at the ortho position to the pyridine nitrogen instead of at the para position as in **SL35**. This was pursued as an alternate way to discourage 2:1 complex formation by using the steric bulk of the chromophore along with the pendant pyridyl groups to shield the Zn^{2+} ion from other chromophores, and to reduce the pKa of the pyridine nitrogen and thus the risk of excited state protonation. **SL477** is based on **SL476**, but is attached to a leaving group through an amide bond. **SL477** is designed to be attached to a protein to investigate the function of the chromophore in proximity to protein. In cells, the leaving group is removed by an enzyme at the position indicated by the curved line and attached to a sulfur residue of a protein.[157] The 2PA spectra of **SL477** was obtained after its attachment to an artificial model protein. Linear absorption and fluorescence characteristics are summarized of the oxazole chromophores are summarized in Table 5.1, while 2PA spectroscopic data are summarized in Table 5.2.

5.2.1 1PA, fluorescence and 2PA spectra of YW2-068

YW2-068 was studied in both water and methanol, showing 1PA spectra for the free and Zn^{2+} species that were not affected greatly by the choice of solvent (see Figure 5.3a). However, as can be seen in Figure 5.3b, upon changing the solvent from methanol to water, significant red shifts of the fluorescence spectra were observed, along with a reduction in the quantum yields of both the free and Zn^{2+} chromophore. The fluorescence spectrum of free **YW2-068** in water also shows evidence at longer wavelengths of more

Table 5.1. Linear absorption and fluorescence measurements of oxazole chromophores

Compound (solvent)	$\lambda_{max}^{(1)}$ **(nm)**[a]	$\lambda_{max}^{(1)}$ **(nm)** (Zn^{2+})[b]	$\lambda_{max}^{(fl)}$ **(nm)**[c,h]	$\lambda_{max}^{(fl)}$ **(nm)** (Zn^{2+})[d,h]	η_{fl} [e,h]	η_{fl} (Zn^{2+})[f,h]
YW2-068 (MeOH)	338	363	441	491	0.4	0.66
YW2-068 (H_2O)[g]	336	356	478	515	0.17	0.47
SL35 (Methanol)	338	362	441	497	0.35	0.71
SL476 (H_2O)[g]	332	337	445	~500	0.3	0.56
SL477 (H_2O)[g]	334	349	n/a	n/a	n/a	n/a

[a]Linear absorption peak of free chromophore. [b]Linear absorption peak of zinc-bound chromophore. [c]Fluorescence peak of free chromophore. [d]Fluorescence peak of zinc-bound chromophore. [e]Fluorescence quantum yield of free chromophore. [f]Fluorescence quantum yield of zinc-bound chromophore. [g]Solution contained buffer as described in Chapter 2. [h]Fluorescence spectra and quantum yield measurements were performed by Dr. Sumalekshmy.

Table 5.2. Two-photon absorption data for oxazole compounds.

Compound (Solvent)	$\lambda_{max}^{(2)}$ **(nm)**[a]	$\lambda_{max}^{(2)}$ **(nm)** (Zn^{2+}) [b]	**2PA isosbestic point (nm)**[c]	δ_{max} **(GM)**[d]	δ_{max} **(GM)** (Zn^{2+})[e]	$\eta\delta_{max}$ **(GM)**[f]	$\eta\delta_{max}$ **(GM)** (Zn^{2+})[g]
YW2-068 (MeOH)	700	720	650	34	90	14	60
YW2-068 (H_2O)	690	720	n/a	37	101	6.4	47
SL35 (MeOH)	690	730	655	21	77	11	55
SL476 (H_2O)[h]	700	720	705	15	17	4.5	9.5
SL477 (H_2O)[h]	700	720	n/a	n/a	n/a	3	23

[a]Peak wavelength of two-photon absorption of free chromophore. Error is ± 10 nm. [b]Peak wavelength of two-photon absorption of zinc-bound chromophore. Error is ± 10 nm. [c]Isosbestic point of two-photon absorption. [d]Peak two-photon absorption cross-section of free chromophore. Error in δ is ± 15%. [e]Peak two-photon absorption cross-section of zinc-bound chromophore. Error in δ is ± 15%. [f]Two-photon microscopy figure of merit for free chromophore, including η_{fl}, the fluorescence quantum yield. [g]Two-photon microscopy figure of merit for the zinc-bound chromophore, including η_{fl}, the fluorescence quantum yield. [h]These solutions were buffered water as discussed in Chapter 2.

than one species being present, complicating the assessment of **YW2-068**. Further, **YW2-068** was determined to bind Zn^{2+} in a 2:1 ratio, rendering it unsuitable for ratiometric imaging. This occasioned the need to move to chromophore structures designed to prevent formation of 2:1 complexes, such as **SL35** and **SL476**. Figure 5.3c and 5.3d show the 2PA spectra of the free and Zn^{2+} bound **YW2-068** in both methanol and water. The δ_{max} and $\lambda_{max}^{(2)}$ of **YW2-068** are not affected greatly by the difference of solvent between methanol and water, although the $\eta\delta_{max}$ are very different due to the lower η of both forms of the chromophore in water. A qualitative assessment that may be made about this general chromophore is that changing the solvent from methanol to water affects the $\eta\delta$ more by the reduction in η than by changing δ, serving as grounds for assessing chromophores for their potential in 2PLSM based on their characteristics in methanol solution.

5.2.2 Linear absorption and fluorescence spectra of SL35, SL476 and SL477

The response of **SL35** to titration with Zn^{2+} in methanol is shown in Figure 5.4. Increasing the concentration of Zn^{2+} from 0 to 1.2 molar equivalents resulted in a bathochromic shift of the 1PA peak from 338 nm to 362 nm, with a well-defined isosbestic point at 348 nm. There was a corresponding red shift of the fluorescence peak from 441 nm to 491 nm, and the fluorescence quantum yield η also increased significantly from 0.35 to 0.71. The significant redshift of the fluorescence band of the Zn^{2+} complex is sufficient to enable use of this chromophore for emission ratiometry.

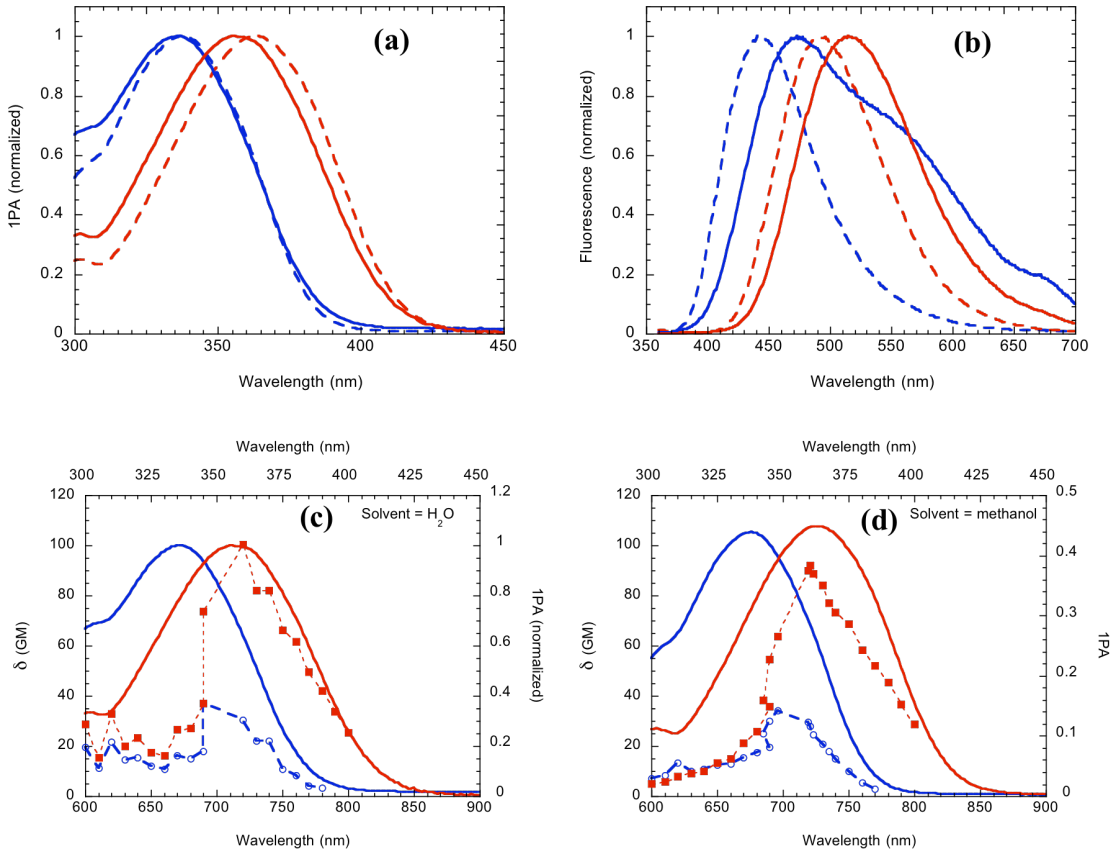

Figure 5.3. (a) Linear absorption and **(b)** fluorescence spectra of **YW2-068** in methanol and buffered H_2O; 2PA spectra of **YW2-068** in **(c)** buffered H_2O and **(d)** methanol. In **(a)** and **(b)**, dashed blue lines are spectra of free **YW2-068** in methanol, and dashed red lines are the Zn^{2+}-bound **YW2-068** in methanol; solid blue lines are spectra of free **YW2-068** in H_2O, and solid red lines are the Zn^{2+}-bound **YW2-068** in H_2O. In **(c)** and **(d)**, solid blue and red lines refer to the 1PA spectra of the free and Zn^{2+}-bound **YW2-068** (top and right axes), while the blue circles and red squares refer to the 2PA spectra of the free and Zn^{2+}-bound **YW2-068** (bottom and left axes); the dashed lines are a guide for the eye.

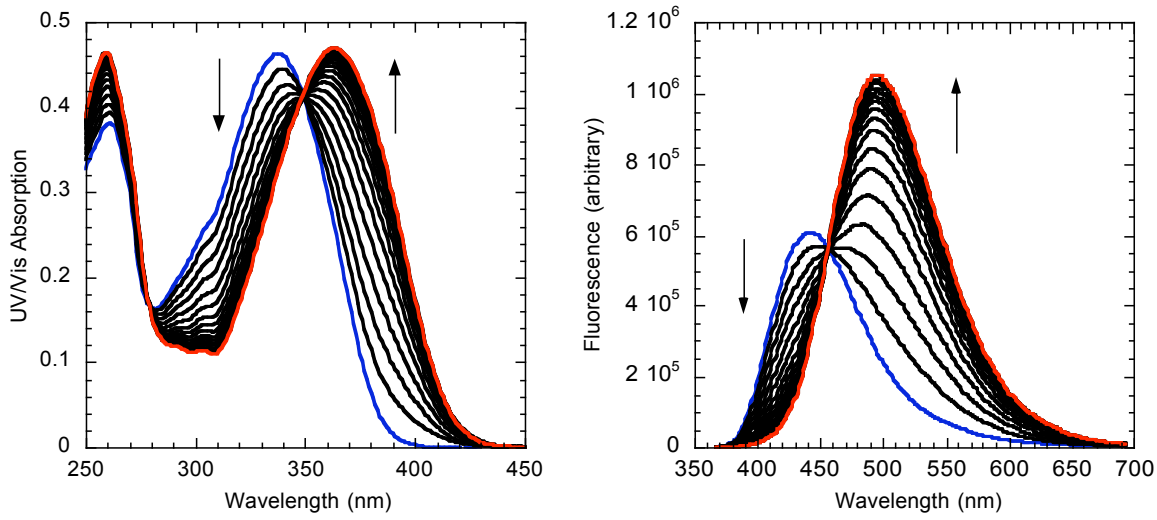

Figure 5.4. Titration of **SL35** in methanol studied by 1PA and fluorescence spectroscopy. The spectra in blue are of the free ligand, while the spectra in red are of the Zn^{2+} bound form. Black spectra are intermediate titration steps. Data was taken by Dr. S. Sumalekshmy.

The 1PA spectra of **SL476** and **SL477** in water are shown in Figure 5.5 along with the fluorescence spectra of **SL476**. The 1PA peak of **SL476** shows less of a red shift than **SL35** with Zn^{2+} binding, which is likely the result of the different attachment position of the pyridine ring to the oxazole, rather than the change to aqueous solution. Interestingly, the 1PA peak of **SL477** shows a greater shift than **SL476**, suggesting the anchoring to the protein has a measurable effect on the spectroscopic properties of the dye. The fluorescence spectra of **SL476** behave similarly to those of **SL35**, with a red shift from 445 to 500 nm upon Zn^{2+} binding. While the η values of both forms are reduced compared to **SL35** in methanol, this is to be expected from the use of water as the solvent. Fluorescence spectra and quantum yields were not obtained for MV477 due to the difficulty of preventing decomposition of the sample during the measurements.

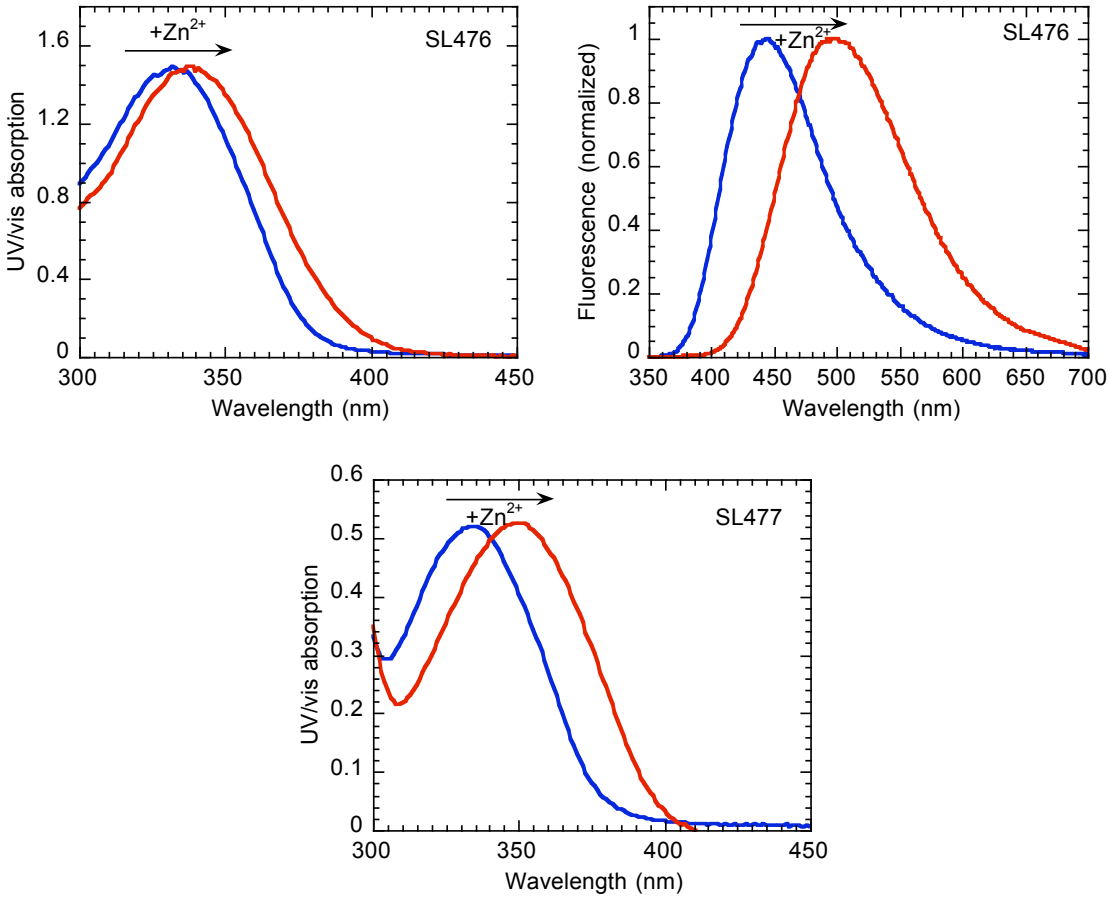

Figure 5.5. Linear absorption spectra of **SL476** and **SL477**, and fluorescence spectra of **SL476**. Blue spectra belong to the free ligands, while red spectra belong to the Zn^{2+} bound species.

5.2.3 Two-photon absorption spectra of SL35 and SL476

Two-photon absorption spectra of **SL35** in methanol and **SL476** in buffered H_2O were determined by the nanosecond 2PEF method both in the absence and presence of

Zn^{2+}. The results are shown graphically in Figure 5.6. In **SL35**, the increase in δ_{max} with Zn^{2+} binding is approximately fourfold, and the $\lambda_{max}^{(2)}$ appears to shift about 40 nm bathochromically, although a precise assessment of the shift is difficult to make due to the relative lack of data between 690 – 730 nm. The figure of merit for 2PLSM, $\eta\delta_{max}$, shows an even larger increase due to the doubling of η on going from the free chromophore to the Zn^{2+}-bound species. However, the isosbestic point of 2PA, which is the optimal wavelength for ratiometric imaging using 2PLSM, is at ~655 nm, not within the excitation range of most 2PLSM systems. By contrast, the 2PA spectrum of Zn^{2+}-free **SL476** in water is relatively similar to that of **SL35** in methanol, although δ is reduced somewhat. Upon adding Zn^{2+} to **SL476** in water, the 2PA spectrum increases only slightly, a result we attribute this to steric effects of the Zn^{2+} binding. The binding of Zn^{2+}

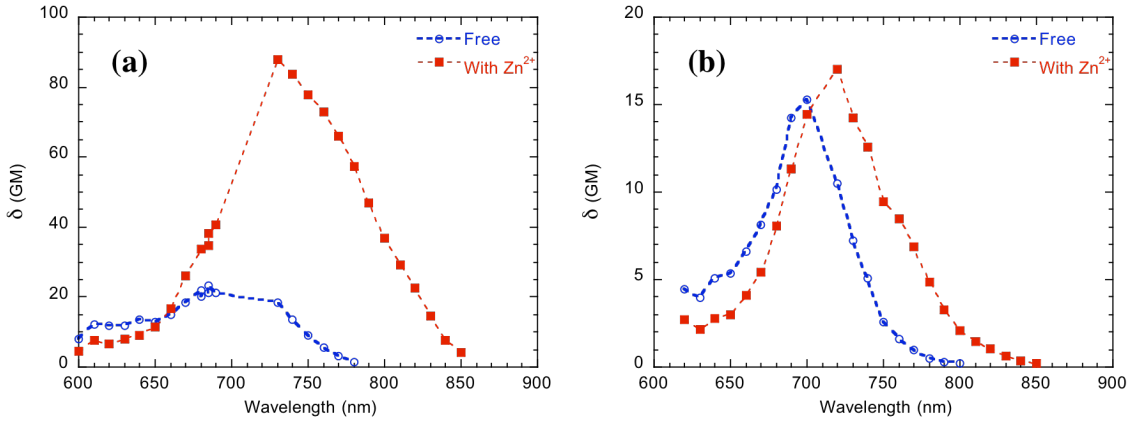

Figure 5.6. Two-photon absorption spectra of (a) **SL35** in methanol and (b) **SL476** in buffered H_2O. The dashed lines are guides for the eye.

is likely to induce some twisting or curvature of the chromophore backbone, reducing the conjugation and intramolecular charge transfer of the chromophore backbone. While this suggests that the brightness of **SL476** is lower than that of **SL35**, it does move the isosbestic point of 2PA to approximately 705 nm, within the range of typical 2PLSM excitation sources.

5.2.4 Performance of SL477 chromophore attached to peptide

Without knowing the fluorescence quantum yield of **SL477**, it was not possible to determine δ. However, 2PA spectra were taken of the protein-bound **SL477** in buffered water to examine the effects of the local environment near the protein on the 2PLSM brightness of the chromophore, which is essentially identical to **SL476**. As seen in Table 5.2 and Figure 5.7, the 2PLSM figure of merit $\eta\delta$ of the free chromophore is slightly decreased in **SL477**, while the $\eta\delta$ of the Zn^{2+}-bound chromophore is approximately doubled. While interpretation of this increase is complex, it is consistent with the effects a more hydrophobic environment would be expected to have on both η and δ. The results indicate that attaching these chromophores to relatively hydrophobic structures in cells could be a method of achieving higher-contrast performance in 2PLSM.

5.3 Thiazole Chromophores Results and Discussion

The set of thiazole-based chromophores shown in Figure 5.8 was characterized by 1PA, fluorescence and 2PA spectroscopy. The thiazole moiety was chosen to replace the

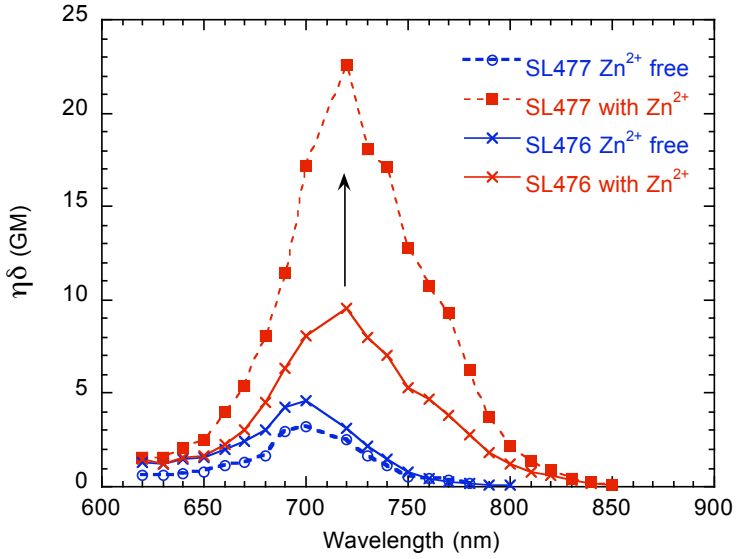

Figure 5.7. Two-photon microscopy figure of merit $\eta\delta$ for **SL476** and **SL477**.

oxazole moiety of the other chromophores in order to destabilize the HOMO of the chromophore and shift the spectra further to the red. The thiazole chromophores were also designed to test the effects of using longer conjugation lengths (**SL407**, **MV170**) and a stronger donor group (**MV170**).

5.3.1 Linear absorption and fluorescence spectra

The 1PA and fluorescence spectra of **SL327**, **SL407** and **MV170** were taken in buffered H_2O, methanol, and ethanol, respectively. The results are presented in Table 5.3 and Figure 5.9. The change in the conjugation length from methoxyphenyl chromophore

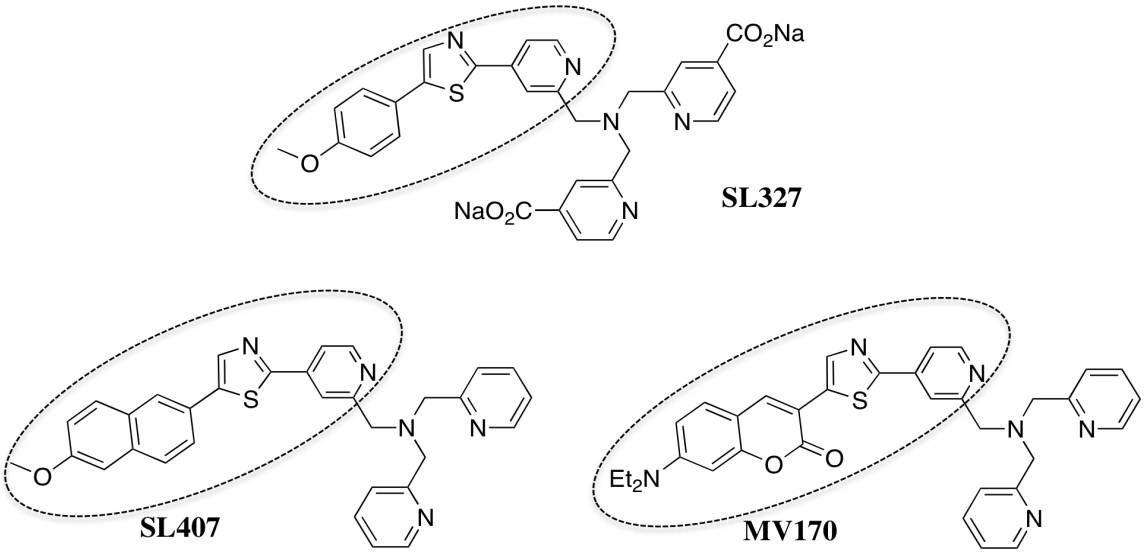

Figure 5.8. Thiazole chromophores studied in this chapter. The dashed lines enclose the chromophore units.

SL327 to the methoxynaphthyl chromophore **SL407** had the effect of a slight bathochromic shift on 1PA and fluorescence peaks of the Zn^{2+} free forms, with larger shifts for the Zn^{2+} bound forms. The use of the strong charge-transfer coumarin unit in **MV170** led to large bathochromic shifts of approximately 90 nm in the 1PA spectra of both the Zn^{2+}-free and Zn^{2+} bound forms relative to those of **SL407**, while the fluorescence spectra of the Zn^{2+}-free and Zn^{2+} bound forms showed smaller bathochrominc shifts of ~ 35 and ~ 55 nm relative to those of **SL407**. The fluorescence quantum yields of **SL327** and**SL407** followed the pattern of the oxazole chromophores, with increases in yield upon going from the free chromophore to Zn^{2+} bound, although in

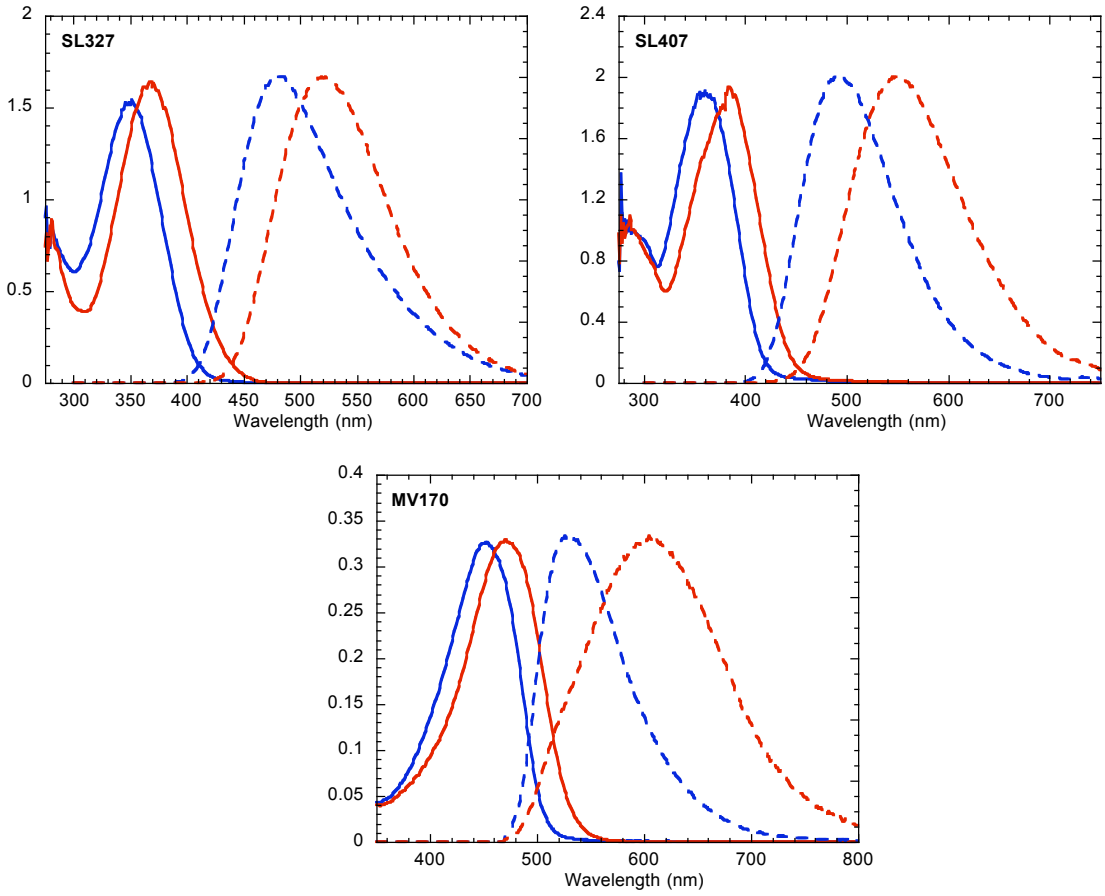

Figure 5.9. Linear absorption and fluorescence spectra of thiazole chromophores. Solid and dashed blue lines are the 1PA and fluorescence of the Zn^{2+}-free chromophores, while solid and dashed red lines are the 1PA and fluorescence of the Zn^{2+}-bound chromophores

Table 5.3. Linear absorption and fluorescence measurements of thiazole chromophores

Compound (solvent)	$\lambda_{max}^{(1)}$ **(nm)**[a]	$\lambda_{max}^{(1)}$ **(nm)** (Zn^{2+})[b]	$\lambda_{max}^{(fl)}$ **(nm)**[c,h]	$\lambda_{max}^{(fl)}$ **(nm)** (Zn^{2+})[d,h]	η_{fl} [e,h]	η_{fl} (Zn^{2+})[f,h]
SL327 (H_2O)[g]	350	367	481	521	0.31	0.63
SL407 (Methanol)	360	384	489	549	0.47	0.57
MV170 (Ethanol)	453	472	526	605	0.92	0.63

[a]Linear absorption peak of free chromophore. [b]Linear absorption peak of zinc-bound chromophore. [c]Fluorescence peak of free chromophore. [d]Fluorescence peak of zinc-bound chromophore. [e]Fluorescence quantum yield of free chromophore. [f]Fluorescence quantum yield of zinc-bound chromophore. [g]Solution contained buffer as described in Chapter 2. [h]Fluorescence spectra and quantum yield measurements were performed by Dr. Sumalekshmy for **SL327** and **SL407**, and by Dr. Manjusha Verma for **MV170**.

the case of **MV170** this trend is reversed. The fluorescence spectra themselves, however, are still resolvable into bands that could be used for ratiometric imaging.

5.3.2 2PA spectra of thiazole chromophores

Two-photon absorption spectra of **SL327**, **SL407** and **MV170** in buffered H_2O, methanol, and ethanol, respectively, were determined by the nanosecond 2PEF method both in the absence and presence of Zn^{2+}. The results are shown in Figure 5.10 and Table 5.4. The change from the methoxyphenyl end group in **SL327** to the methoxynaphthyl end group in **SL407** led to increases in the δ_{max} of both forms of the chromophore. There is also a greater red shift of $\lambda_{max}^{(2)}$ upon Zn^{2+} binding in **SL407** as opposed to **SL327**. A more significant finding is that the isosbestic point of 2PA changed from a wavelength of

710 nm to 740nm, and the δ at the isosbestic point increased from ~ 15 GM to ~ 35 GM, potentially allowing for greater brightness form ratiometric 2PLSM. The coumarin end group in **MV170** led to the largest bathochromic shifts of any of the chromophores studied, with $\lambda_{max}^{(2)}$ of 960 nm and 970 nm. The δ_{max} of both forms increased to over 110 GM. There are also two isosbestic points of 2PA with potential for use in ratiometric 2PLSM, one in the region of 780 nm with a δ of ~ 18 GM, and another one at ~ 965 nm with a δ of ~ 105 GM. Given this second isosbestic point with its high δ and position much further into the 2PLSM region of interest than the other chromophores reported here, **MV170** is a promising candidate as a platform for further study and development as a sensor for ratiometric 2PLSM.

5.4 Conclusions

The linear absorption, fluorescence and two-photon absorption properties of a series of chromophores designed for ratiometric sensing in two-photon microscopy have been reported. The dipolar oxazole or thiazole based chromophore unit displays ion-responsive 2PA and fluorescence behavior suitable for ratiometric sensing. The 2PA strength of these chromophores rivals or exceeds most chromophores currently used for 2PLSM. Several factors have been identified to affect the overall properties of these chromophores. Attachment of the pyridyl sensing group to the chromophore backbone at

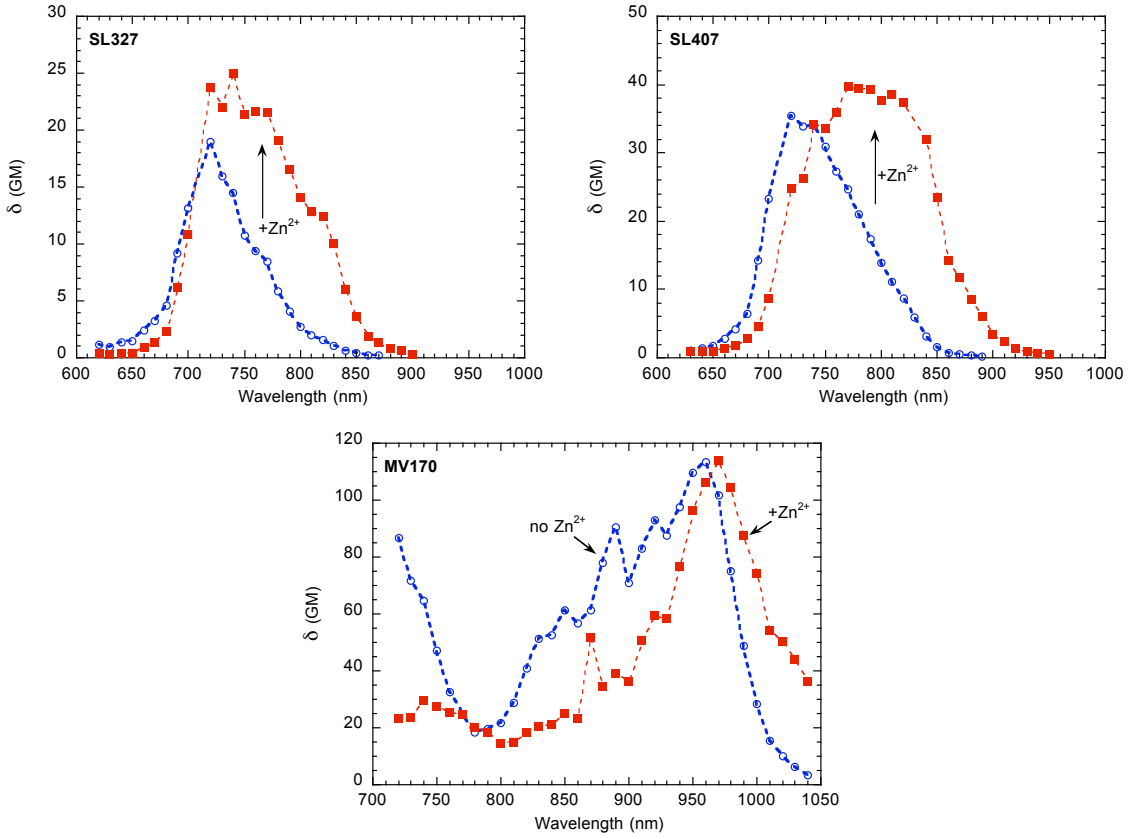

Figure 5.10. Two-photon absorption spectra of thiazole chromophores. Blue circles are for the free chromophores, red squares are for the Zn^{2+}-bound chromophores. The lines are guides for the eye.

Table 5.4. Two-photon absorption data for thiazole chromophores.

Compound (Solvent)	$\lambda_{max}^{(2)}$ **(nm)**[a]	$\lambda_{max}^{(2)}$ **(nm)** **(Zn^{2+})** [b]	**2PA isosbestic point (nm)**[c]	δ_{max} **(GM)**[d]	δ_{max} **(GM)** **(Zn^{2+})**[e]	$\eta\delta_{max}$ **(GM)**[f]	$\eta\delta_{max}$ **(GM)** **(Zn^{2+})**[g]
SL327 (H_2O)[h]	720	740	710	19	25	5.9	16
SL407 (Methanol)	720	770	740	35	40	16	25
MV170 (Ethanol)	960	970	965[i]	113	114	104	72

[a]Peak wavelength of two-photon absorption of free chromophore. Error is ± 10 nm. [b]Peak wavelength of two-photon absorption of zinc-bound chromophore. Error is ± 10 nm. [c]Isosbestic point of two-photon absorption. [d]Peak two-photon absorption cross-section of free chromophore. Error in δ is ± 15%. [e]Peak two-photon absorption cross-section of zinc-bound chromophore. Error in δ is ± 15%.[f]Two-photon microscopy figure of merit for free chromophore, including η_{fl}, the fluorescence quantum yield. [g]Two-photon microscopy figure of merit for the zinc-bound chromophore, including η_{fl}, the fluorescence quantum yield. [h]These solutions were buffered water as discussed in Chapter 2. [i]There is another region with an apparent isosbestic point between770 – 790 nm.

the *ortho* position to the pyridyl nitrogen rather than the *para* position had the effect of decreasing δ_{max}, but also helped to eliminate non-ratiometric binding of the chromophores with Zn^{2+} ions, and served to move the isosbestic point of 2PA into the region accessible with common 2PLSM excitation sources. When attached to a protein, the *ortho*-linked chromophore showed significant increase in two-photon brightness upon Zn^{2+} binding, suggesting that *ortho*-linked chromophores may be more suitable for sensing when anchored to a relatively hydrophobic biological structure such as a protein or lipid membrane. In otherwise similar *para*-linked chromophores **SL35** and **SL327**, the shift from an oxazole to a thiazole backbone had an effect on $\lambda_{max}^{(2)}$ and the 2PA isosbestic point similar to the switch from a *para*-linked oxazole in **SL35** to an *ortho*-linked oxazole in **SL476**, although the δ_{max} of both forms of **SL327** was higher than those of **SL476**. The use of longer conjugation pathways in **SL407** and **MV170** and a strong donor in **MV170** further improved 2PA characteristics, culminating in the **MV170** chromophore with excellent characteristics for ratiometric 2PLSM.

CHAPTER 6: CONCLUSIONS AND FUTURE WORK

The continued interest in technologies utilizing two-photon absorption demonstrates a clear need to develop new chromophores optimized for particular 2PA applications. Design principles for optimizing δ_{max} and $\lambda_{max}^{(2)}$ of linear quadrupolar and dipolar chromophores are well known. Extension of the π-conjugated backbone of these compounds and substitution of electron donating and withdrawing groups along the backbone both lead to increases in δ_{max} and $\lambda_{max}^{(2)}$. However, significant work remains to be done on understanding the effects of using branched chromophore structures, and on designing chromophores with high figures of merit for two-photon laser scanning microscopy. In particular, the use of non-degenerate conjugation pathways along with symmetric electron donor and acceptor substitution in cruciform compounds leads to interesting linear absorption properties. The effects of the electronic state structures of these compounds on 2PA are complex and lead to 2PA properties differing significantly from those of linear compounds and cruciform compounds with degenerate conjugation pathways. Additionally, the use of donor and acceptor groups of these chromophores as sensing moieties programmed to affect two-photon induced fluorescence potentially could provide new routes toward creating 2PLSM chromophore libraries. Another approach to creating 2PLSM chromophores is the use of linear donor/acceptor substituted dipolar backbones with the acceptor serving as the sensing moiety. Determining the

parameters that optimize the 2PLSM characteristics of these dyes is critical for the furtherance of two-photon microscopy techniques.

The work presented in this thesis addresses these questions and provides new insights into the ways in which the spectral properties of cruciform chromophores can be understood, as well as into the modalities of analyte sensing that are available with the cruciform platform and a purpose-developed dipolar chromophore. In Chapter 3, cruciform compounds composed of linear 1,4-bis(styryl)benzene and 1,4-bis(phenylethynyl)benzene arms sharing a common central phenyl group were studied by linear and two-photon absorption spectroscopy. The terminal electron-donor and -acceptor substitution pattern ranged from none at all, to four identical donors, to donors on the styryl arm, to donors on the styryl arm and acceptors of various strengths on the ethynyl arm. Exciton models were developed to provide insights into the interactions of the arms in the cruciform. The use of non-degenerate conjugation conjugation pathways with no donor substitution or with substitution by four identical donors was described by a single "oblique" exciton system, shown to lead to moderate electronic interactions of the 1PA excited states of the arms, although the two excitonic excited states were each still localized mostly along one linear arm. It was shown that the 2PA excited state energies were relatively unaffected by the coupling of the two linear arms in the cruciform. By contrast, the electronic state structure of cruciform with both strong donors and strong acceptors was described by an exciton model using the anti-parallel charge-transfer transitions of the donor and acceptor groups on arms substituted *ortho*- to each other on the central ring. Compounds with donor groups on the styryl arms and acceptors of intermediate strength on the ethynyl arms were best described by a combination of

these two exciton models. The effects of the different types of interactions on the 1PA, fluorescence and 2PA spectra were profound. The oblique exciton interaction led to 1PA spectra with one main split band in the region of 300-600 nm, sharp and vibronically featured fluorescence spectra and relatively narrow 2PA spectra. As more electronic asymmetry was introduced with the donor/acceptor substituent groups, the 1PA developed two distinct bands, one of which contained two sub-bands resulting from the increasing influence of antisymmetric charge transfer transitions. The fluorescence spectra shifted to the red and grew less featured. The 2PA peak also shifted to lower energy, and a secondary 2PA band grew in the region of 900 – 1040 nm, the strength of which was correlated with the acceptor strength.

Proceeding form here, a worthwhile course of action would be to examine the properties of D/A substituted cruciforms with longer arms, such as five-ring arms, coupled through their central ring. Knowledge of the effects that the longer distance between the D and A groups on adjacent arms have on the charge-transfer nature of the cruciform transitions would help refine the understanding of their electronic structure.

When cruciforms were exposed to Zn^{2+} ions in dichloromethane, the "turn-off" of the charge donation from the donor groups resulted in the Zn^{2+}-bound cruciforms behaving essentially as if they had no donor or acceptor groups attached to them at all. This, coupled with the close similarity of the 2PA and fluorescence spectra of the four-donor system to those of the two-donor system, indicated that the turning off of the two donor groups on the termini of one arm would not be an effective method of constructing chromophores for "turn-on" of two-photon induced fluorescence in the range of 900 – 1000 nm. However, the placement of ion-binding acceptor groups at the terminal

positions of the arms did result in "turn-on" of 2PA in the range of 700 – 800 nm. Further, the fluorescence emission spectrum of the pyridyl-ethynyl cruciform **21** was distinguishable from that of the pyridyl-styryl cruciform **22**, a factor that can be taken advantage of in designing libraries of new chromophores. Future work in this area should concentrate on designing and creating water-soluble cruciforms with ion-selective acceptor-based binding groups for use in multicolor 2PLSM. It is also worth investigating whether placement of non-binding donor groups of various donor strengths on the arm opposite to the acceptor-substituting arm is another way to favorably influence the fluorescence and 2PA properties.

The 2PA properties of dipolar small molecule Zn^{2+}-sensing dyes have also been assessed. These dyes have favorable properties for ratiometric sensing of Zn^{2+} in 2PLSM. The use of a 2PA "turn-on" sensing modality resulted in bathochromic shifts of both 2PA and fluorescence upon complexation of the dyes with Zn^{2+} ions. There are several aspects of the overall design of the dye that had significant impact on the 2PA spectra. Changing the point of attachment of the sensing group to the chromophore unit, and changing the central chromophore unit from an oxazole group to a thiazole group both had the effect of reducing the increase in 2PA upon Zn^{2+} complexation, but did move the isosbestic point of 2PA into the wavelength region commonly used for 2PLSM. However, the most significant changes arose from the choice of electron donor group. Replacing the methoxyphenyl donor group in **SL327** with a longer methoxynaphthyl donor group in **SL407** resulted in small red-shifts of the 2PA spectrum of the Zn^{2+} complex and in the 2PA isosbestic point to. However, the use of a strongly donating coumarin unit in **MV170** resulted in significant increases in the 2PA strength and red-shifts of the 2PA

spectra of both the free dye and the Zn^{2+} complex, although these results were obtained in ethanol. In order to render these dyes more suitable for 2PLSM in biological systems such as cells and tissue, important work remains to be performed to design and characterize dyes that incorporate and maintain all the desirable characteristics above in aqueous environments.

REFERENCES

(1) Butcher, P. N.; Cotter, D. *The Elements of Nonlinear Optics*; Cambridge University Press: Cambridge, UK, 1998.

(2) Shen, Y. R. *Principles of Nonlinear Optics*; Wiley-Interscience: Hoboken, 1984.

(3) Goppert-Mayer, M. *Annalen der Physik* **1931**, *9*, 273.

(4) Kaiser, W., and Garrett, C. G. B. *Physical Review Letters* **1961**, *7*, 229.

(5) Denk, W.; Strickler, J.; Webb, W. *Science* **1990**, *248*, 73.

(6) Strickler, J.; Webb, W. *Proceedings of SPIE* **1991**, *1398*, 107.

(7) Xu, C.; Zipfel, W.; Shear, J.; Williams, R.; Webb, W. *Proceedings of the National Academy of Sciences* **1996**, *93*, 10763.

(8) Xu, C.; Webb, W. *Topics in Fluorescence Spectroscopy* **1997**, *5*, 471.

(9) Nakamura, O. *Microscopy Research and Technology* **1999**, *47*, 165.

(10) So, P.; Dong, C.; Masters, B.; Berland, K. *Annual Review of Biomedical Engineering* **2000**, *2*, 399.

(11) Svoboda, K.; Yasuda, R. *Neuron* **2006**, *50*, 823.

(12) Oheim, M.; Michael, D.; Geisbauer, M.; Madsen, D.; Chow, R. *Advanced Drug Delivery Reviews* **2006**, *58*, 788.

(13) Maruo, S.; Nakamura, O.; Kawata, S. *Optics Letters* **1997**, *22*, 132.

(14) Cumpston, B.; Ananthavel, S.; Barlow, S.; Dyer, D.; Ehrlich, J.; Erskine, L.; Heikal, A.; Kuebler, S.; Lee, I.; McCord-Maughon, D. *Nature* **1999**, *398*, 51.

(15) Belfield, K.; Schafer, K.; Liu, Y.; Liu, J.; Ren, X.; Stryland, E. *Journal of Physical Organic Chemistry* **2000**, *13*.

(16) Zhou, W.; Kuebler, S.; Braun, K.; Yu, T.; Cammack, J.; Ober, C.; Perry, J. W.; Marder, S. R. *Science* **2002**, *296*, 1106.

(17) Lee, K.; Yang, D.; Park, S.; Kim, R. *Polymers for Advanced Technologies* **2006**, *17*, 72.

(18) Lee, K.; Kim, R. H.; Yang, D.; Park, S. H. *Progress in Polymer Science* **2008**, *33*, 631.

(19) Haske, W.; Chen, V.; Hales, J.; Dong, W.; Barlow, S.; Marder, S. R.; Perry, J. W. *Optics Express* **2007**, *15*, 3426.

(20) Mendonca, C.; Correa, D.; Baldacchini, T.; Tayalia, P.; Mazur, E. *Applied Physics A* **2008**, *90*, 633.

(21) Sun, H.; Kawata, S. *Advances in Polymer Science* **2004**, *170*, 169.

(22) Lafratta, C.; Fourkas, J.; Baldacchini, T.; Farrer, R. *Angewandte Chemie International Edition* **2007**, *46*, 6238.

(23) He, G.; Xu, G.; Prasad, P.; Reinhardt, B.; Bhatt, J.; Dillard, A. *Optics Letters* **1995**, *20*, 435.

(24) He, G.; Gvishi, R.; Prasad, P.; Reinhardt, B. *Optics Communications* **1995**, *117*, 133.

(25) He, G.; Zheng, Q.; Yong, K.; Ryasnyanskiy, A.; Prasad, P. N.; Urbas, A. *Applied Physics Letters* **2007**, *90*, 181108.

(26) Ehrlich, J.; Wu, X.; Lee, I.; Hu, Z.; Röckel, H.; Marder, S. R.; Perry, J. W. *Optics Letters* **1997**, *22*, 1843.

(27) Oberle, J.; Bramerie, L.; Jonusauskas, G.; Rulliere, C. *Optics Communications* **1999**, *169*, 325.

(28) Lei, H.; Wang, H.; Wei, Z.; Tang, X.; Wu, L.; Tung, C.; Zhou, G. *Chemical Physics Letters* **2001**, *333*, 387.

(29) Morel, Y.; Irimia, A.; Najechalski, P.; Kervella, Y.; Stephan, O.; Baldeck, P.; Andraud, C. *The Journal of Chemical Physics* **2001**, *114*, 5391.

(30) Lemercier, G.; Mulatier, J.; Martineau, C.; Anémian, R.; Andraud, C.; Wang, I.; Stéphan, O.; Amari, N.; Baldeck, P. *Comptes rendus-Chimie* **2005**, *8*, 1308.

(31) Charlot, M.; Izard, N.; Mongin, O.; Riehl, D.; Blanchard-Desce, M. *Chemical Physics Letters* **2006**, *417*, 297.

(32) Maguire, P.; Barry, L.; Krug, T.; Guo, W.; Lynch, M.; Bradley, A. L.; Donegan, J. F.; Folliot, H. *Journal of Lightwave Technology* **2006**, *24*, 2683.

(33) Albota, M.; Beljonne, D.; Brédas, J.; Ehrlich, J. E.; Fu, J.; Heikal, A. A.; Hess, S. E.; Kogej, T.; Levin, M. D.; Marder, S.; McCord-Maughon, D.; Perry, J. W.; Rockel, H.; Rumi, M.; Subramaniam, G.; Webb, W. W.; Wu, X.; Xu, C. *Science* **1998**, *281*, 1653.

(34) Reinhardt, B. A.; Brott, L. L.; Clarson, S. J.; Dillard, A. G.; Bhatt, J. C.; Kannan, R.; Yuan, L.; He, G. S.; Prasad, P. N. *Chemistry of Materials* **1998**, *10*, 1863.

(35) He, G. S.; Tan, L.; Zheng, Q.; Prasad, P. N. *Chemical Reviews* **2008**, *108*, 1245.

(36) Rumi, M.; Barlow, S.; Wang, J.; Perry, J. W.; Marder, S. *Advances in Polymer Science* **2008**, *213*, 1.

(37) Pawlicki, M.; Collins, H.; Denning, R.; Anderson, H. *Angewandte Chemie International Edition* **2009**, *48*, 3244.

(38) Kasha, M. *Discussions of the Faraday Society* **1950**, *9*, 14.

(39) Kogej, T.; Beljonne, D.; Meyers, F.; Perry, J. W.; Marder, S. R.; Brédas, J. L. *Chemical Physics Letters* **1998**, *298*, 1.

(40) Rumi, M.; Ehrlich, J. E.; Heikal, A. A.; Perry, J. W.; Barlow, S.; Hu, Z.; McCord-Maughon, D.; Parker, T. C.; Rockel, H.; Thayumanavan, S.; Marder, S. R.; Beljonne, D.; Brédas, J. *Journal of The American Chemical Society* **2000**, *122*, 9500.

(41) Andraud, C.; Fortrie, R.; Barsu, C.; Stéphan, O.; Chermette, H.; Baldeck, P. *Advances in Polymer Science* **2008**, *214*, 149.

(42) Beljonne, D.; Wenseleers, W.; Zojer, E.; Shuai, Z.; Vogel, H.; Pond, S. J. K.; Perry, J. W.; Marder, S.; Brédas, J. L. *Advance Functional Materials* **2002**, *12*, 631.

(43) Chung, S.; Kim, K.; Lin, T.; He, G. S.; Swiatkiewicz, J.; Prasad, P. N. *the Journal of Physical Chemistry B* **1999**, *103*, 10741.

(44) Chung, S.; Lin, T.; Kim, K.; He, G. S.; Swiatkiewicz, J.; Prasad, P. N.; Baker, G. A.; Bright, F. V. *Chemistry of Materials* **2001**, *13*, 4071.

(45) Cho, B.; Son, K.; Lee, S.; Song, Y.; Lee, Y.; Jeon, S.; Choi, J.; Lee, H.; Cho, M. *Journal of The American Chemical Society* **2001**, *123*, 10039.

(46) Concilio, S.; Biaggio, I.; Günter, P.; Piotto, S.; Edelmann, M.; Raimundo, J.; Diederich, F. *Journal of The Optical Society of America B* **2003**, *20*, 1656.

(47) Porrès, L.; Mongin, O.; Katan, C.; Charlot, M.; Pons, T.; Mertz, J.; Blanchard-Desce, M. *Organic Letters* **2004**, *6*, 47.

(48) Katan, C.; Terenziani, F.; Mongin, O.; Werts, M.; Porres, L.; Pons, T.; Mertz, J.; Tretiak, S.; Blanchard-Desce, M. *The Journal of Physical Chemistry A* **2005**, *109*, 3024.

(49) Terenziani, F.; Mongin, O.; Katan, C.; Bhatthula, B.; Blanchard-Desce, M. *Chemistry - A European Journal* **2006**, *12*, 3089.

(50) Katan, C.; Tretiak, S.; Werts, M.; Bain, A.; Marsh, R.; Leonczek, N.; Nicolaou, N.; Badaeva, E.; Mongin, O.; Blanchard-Desce, M. *The Journal of Physical Chemistry B* **2007**, *111*, 9468.

(51) Terenziani, F.; d'Avino, G.; Painelli, A. *ChemPhysChem* **2007**, *8*, 2433.

(52) Terenziani, F.; Le Droumaguet, C.; Katan, C.; Mongin, O.; Blanchard-Desce, M. *ChemPhysChem* **2007**, *8*, 723.

(53) McDonagh, A. M.; Humphrey, M. G.; Samoc, M.; Luther-Davies, B. *Organometallics* **1999**, *18*, 5195.

(54) Drobizhev, M.; Karotki, A.; Rebane, A.; Spangler, C. W. *Optics Letters* **2001**, *26*, 1081.

(55) Drobizhev, M.; Karotki, A.; Dzenis, Y.; Rebane, A.; Suo, Z.; Spangler, C. W. *The Journal of Physical Chemistry B* **2003**, *107*, 7540.

(56) Drobizhev, M.; Rebane, A.; Suo, Z.; Spangler, C. W. *Journal of Luminescence* **2005**, *111*, 291.

(57) Varnavski, O.; Leanov, A.; Liu, L.; Takacs, J.; Goodson, T. *The Journal of Physical Chemistry B* **2000**, *104*, 179.

(58) Varnavski, O.; Yan, X.; Mongin, O.; Blanchard-Desce, M.; Goodson, T. *The Journal of Physical Chemistry C* **2007**, *111*, 149.

(59) Goodson, T. *Accounts of Chemical Research* **2005**, *38*, 99.

(60) Ramakrishna, G.; Bhaskar, A.; Bauerle, P.; Goodson, T. *The Journal of Physical Chemistry A* **2008**, *112*, 2018.

(61) Kondo, K.; Yasuda, S.; Sakaguchi, T.; Miya, M. *Journal of the Chemical Society, Chemical Communications* **1995**, 55.

(62) Wilson, J. N.; Josowicz, M.; Wang, Y.; Bunz, U. H. *Chemical Communications* **2003**, 2962.

(63) Wilson, J. N.; Smith, M. D.; Enkelmann, V.; Bunz, U. H. *Chemical Communications* **2004**, 1700.

(64) Wilson, J.; Hardcastle, K.; Josowicz, M.; Bunz, U. *Tetrahedron* **2004**, *60*, 7157.

(65) Wilson, J. N.; Bunz, U. H. F. *Journal of The American Chemical Society* **2005**, *127*, 4124.

(66) Zucchero, A. J.; Wilson, J. N.; Bunz, U. H. *Journal of The American Chemical Society* **2006**, *128*, 11872.

(67) Hauck, M.; Schönhaber, J.; Zucchero, A. J.; Hardcastle, K. I.; Müller, T. J.; Bunz, U. H. *Journal of Organic Chemistry* **2007**, *72*, 6714.

(68) Brombosz, S. M.; Zucchero, A. J.; Phillips, R. L.; Vazquez, D.; Wilson, A.; Bunz, U. H. *Organic Letters* **2007**, *9*, 4519.

(69) McGrier, P.; Solntsev, K.; Miao, S.; Tolbert, L.; Miranda, O.; Rotello, V.; Bunz, U. *Chemistry - A European Journal* **2008**, *14*, 4503.

(70) Tolosa, J.; Zucchero, A. J.; Bunz, U. H. *Journal of The American Chemical Society* **2008**, *130*, 6498.

(71) Tolosa, J.; Solntsev, K. M.; Tolbert, L. M.; Bunz, U. H. F. *Journal of Organic Chemistry* **2009**, *75*, 523.

(72) Rumi, M.; Pond, S. J. K.; Meyer-Friedrichsen, T.; Zhang, Q.; Bishop, M.; Zhang, Y.; Barlow, S.; Marder, S. R.; Perry, J. W. *The Journal of Physical Chemistry C* **2008**, *112*, 8061.

(73) Rumi, M.; Pond, S.; Zhang, Q.; Bishop, M.; Zhang, Y.; Barlow, S.; Marder, S.; Perry, J. *Proceedings of SPIE* **2008**, *6891*, 689104.

(74) Marsden, J. A.; Miller, J. J.; Shirtcliff, L. D.; Haley, M. M. *Journal of The American Chemical Society* **2005**, *127*, 2464.

(75) Slepkov, A. D.; Marsden, J. A.; Miller, J. J.; Shirtcliff, L. D.; Haley, M. M.; Kamada, K.; Tykwinski, R. R.; Hegmann, F. A. *Proceedings of SPIE* **2005**, *5934*, 593405.

(76) Slepkov, A.; Hegmann, F.; Tykwinski, R. R.; Kamada, K.; Ohta, K.; Marsden, J. A.; Spitler, E. L.; Miller, J. J.; Haley, M. *Optics Letters* **2006**, *31*, 3325.

(77) Spitler, E. L.; Shirtcliff, L. D.; Haley, M. M. *Journal of Organic Chemistry* **2007**, *72*, 86.

(78) Samori, S.; Tojo, S.; Fujitsuka, M.; Spitler, E. L.; Haley, M. M.; Majima, T. *Journal of Organic Chemistry* **2007**, *72*, 2785.

(79) Spitler, E. L.; Haley, M. M. *Tetrahedron* **2008**, *64*, 11469.

(80) Spitler, E. L.; Monson, J. M.; Haley, M. M. *Journal of Organic Chemistry* **2008**, *73*, 2211.

(81) Sun, Y.; Zhao, K.; Wang, C.; Luo, Y.; Ren, Y.; Tao, X.; Jiang, M. *Journal of Molecular Structure: THEOCHEM* **2004**, *682*, 185.

(82) Wang, L.; Tao, X.; Yang, J.; Yu, W.; Ren, Y.; Xin, Q.; Liu, Z.; Jiang, M. *Journal of Solid State Chemistry* **2004**, *177*, 4293.

(83) Wang, L.; Tao, X.; Yang, J.; Xu, G.; Ren, Y.; Liu, Y.; Yan, Y.; Liu, Z.; Jiang, M. *Synthetic Metals* **2006**, *156*, 141.

(84) Stachelek, T. M.; Pazoha, T. A.; McClain, W. M.; Drucker, R. P. *The Journal of Chemical Physics* **1977**, *66*, 4540.

(85) Delysse, S.; Raimond, P.; Nunzi, J.-M. *Chemical Physics* **1997**, *219*, 341.

(86) Kennedy, S. M.; Lytle, F. E. *Analytical Chemistry* **1986**, *58*, 2643.

(87) Fisher, W. G.; Wachter, E. A.; Lytle, F. E.; Armas, M.; Seaton, C. *Applied Spectroscopy* **1998**, *52*, 536.

(88) Pond, S. J. K.; Rumi, M.; Levin, M. D.; Parker, T. C.; Beljonne, D.; Day, M. W.; Brédas, J. L.; Marder, S. R.; Perry, J. W. *The Journal of Physical Chemistry A* **2002**, *106*, 11470.

(89) Belfield, K. D.; Hagan, D. J.; Van Stryland, E. W.; Schafer, K.; Negres, R. A. *Organic Letters* **1999**, *1*, 1575.

(90) Chung, S.; Rumi, M.; Alain, V.; Barlow, S.; Perry, J. W.; Marder, S. *Journal of The American Chemical Society* **2005**, *127*, 10844.

(91) Lee, S.; Yang, W.; Choi, J.; Kim, C.; Jeon, S.; Cho, B. R. *Organic Letters* **2005**, *7*, 323.

(92) Zheng, S.; Beverina, L.; Barlow, S.; Zojer, E.; Fu, J.; Padilha, L.; Fink, C.; Kwon, O.; Yi, Y.; Shuai, Z.; Stryland, E.; Hagan, D. J.; Brédas, J.; Marder, S. *Chemical Communications* **2007**, 1372.

(93) Yoo, J.; Yang, S.; Jeong, M.; Ahn, H.; Jeon, S.; Cho, B. R. *Organic Letters* **2003**, *5*, 645.

(94) Bartholomew, G. P.; Rumi, M.; Pond, S. J. K.; Perry, J. W.; Tretiak, S.; Bazan, G. C. *Journal of The American Chemical Society* **2004**, *126*, 11529.

(95) Woo, H. Y.; Hong, J. W.; Liu, B.; Mikhailovsky, A.; Korystov, D.; Bazan, G. C. *Journal of The American Chemical Society* **2005**, *127*, 820.

(96) Zipfel, W.; Williams, R.; Webb, W. *Nature Biotechnology* **2003**, *21*, 1369.

(97) Helmchen, F.; Denk, W. *Nature Methods* **2005**, *2*, 932.

(98) Kierdaszuk, B.; Gryczynski, I.; Lakowicz, J. R. *Topics in Fluorescence Spectroscopy* **2005**, *5*, 187.

(99) Zipfel, W.; Williams, R.; Christie, R.; Nikitin, A.; Hyman, B.; Webb, W. *Proceedings of the National Academy of Sciences* **2003**, *100*, 7075.

(100) Xu, C.; Webb, W. W. *Journal of The Optical Society of America B* **1996**, 481.

(101) Drobizhev, M.; Tillo, S.; Makarov, N.; Hughes, T.; Rebane, A. *The Journal of Physical Chemistry B* **2009**, *113*, 855.

(102) Potter, S.; Wang, C.-M.; Garrity, P.; Fraser, S. *Gene* **1996**, *173*, 25.

(103) Drobizhev, M.; Makarov, N.; Hughes, T.; Rebane, A. *The Journal of Physical Chemistry B* **2007**, *111*, 14051.

(104) Tillo, S. E.; Hughes, T. E.; Makarov, N. S.; Rebane, A.; Drobizhev, M. *BMC Biotechnology* **2010**, *10*, 1.

(105) Kuba, K.; Nakayama, S. *Neuroscience Research* **1998**, *32*, 281.

(106) Wokosin, D.; Loughrey, C.; Smith, G. *Biophysical Journal* **2004**, *86*, 1726.

(107) Pond, S. J. K.; Tsutsumi, O.; Rumi, M.; Kwon, O.; Zojer, E.; Brédas, J.; Marder, S. R.; Perry, J. W. *Journal of The American Chemical Society* **2004**, *126*, 9291.

(108) Bozio, R.; Cecchetto, E.; Fabbrini, G.; Ferrante, C.; Maggini, M.; Menna, E.; Pedron, D.; Ricco, R.; Signorini, R.; Zerbetto, M. *The Journal of Physical Chemistry A* **2006**, *110*, 6459.

(109) Charier, S.; Ruel, O.; Baudin, J.; Alcor, D.; Allemand, J.; Meglio, A.; Jullien, L. *Angewandte Chemie International Edition* **2004**, *43*, 4785.

(110) Charier, S.; Ruel, O.; Baudin, J.; Alcor, D.; Allemand, J.; Meglio, A.; Jullien, L.; Valeur, B. *Chemistry - A European Journal* **2006**, *12*, 1097.

(111) Kim, J. S.; Kim, H. J.; Kim, H. M.; Kim, S. H.; Lee, J. T.; Kim, S. K.; Cho, B. R. *Journal of Organic Chemistry* **2006**, *71*, 8016.

(112) Kim, H.; Seo, M.; An, M.; Hong, J.; Tian, Y.; Choi, J.; Kwon, O.; Lee, K.; Cho, B. *Angewandte Chemie International Edition* **2008**, *47*, 5167.

(113) Kim, H. M.; Cho, B. R. *Accounts of Chemical Research* **2009**, *42*, 863.

(114) Bhaskar, A.; Ramakrishna, G.; Twieg, R.; Goodson, T. *The Journal of Physical Chemistry C* **2007**, *111*, 14607.

(115) Sumalekshmy, S.; Henary, M. M.; Siegel, N.; Lawson, P. V.; Wu, Y.; Schmidt, K.; Brédas, J. L.; Perry, J. W.; Fahrni, C. J. *Journal of The American Chemical Society* **2007**, *129*, 11888.

(116) Parson, W. W. *Modern Optical Spectroscopy*; Springer: New York, 2007.

(117) Lakowicz, J. R. *Principles of Fluorescence Spectroscopy*; Springer: Singapore, 2006.

(118) Berlman, I. B. *Handbook of Fluorescence Spectra of Aromatic Molecules*, 2nd ed.; Academic Press: New York, 1971.

(119) Crosby, G.; Demas, J. *The Journal of Physical Chemistry* **1971**, *75*, 991.

(120) Ahn, T.; Kim, K.; Kim, D.; Noh, S.; Aratani, N.; Ikeda, C.; Osuka, A.; Kim, D. *Journal of The American Chemical Society* **2006**, *128*, 1700.

(121) Frampton, M.; Akdas, H.; Cowley, A.; Rogers, J.; Slagle, J.; Fleitz, P.; Drobizhev, M.; Rebane, A.; Anderson, H. *Organic Letters* **2005**, *7*, 5365.

(122) Drobizhev, M.; Stepanenko, Y.; Dzenis, Y.; Karotki, A.; Rebane, A.; Taylor, P. N.; Anderson, H. L. *Journal of The American Chemical Society* **2004**, *126*, 15352.

(123) Drobizhev, M.; Stepanenko, Y.; Dzenis, Y.; Karotki, A.; Rebane, A.; Taylor, P. N.; Anderson, H. L. *The Journal of Physical Chemistry B* **2005**, *109*, 7223.

(124) Raymond, J. E.; Bhaskar, A.; Goodson, T.; Makiuchi, N.; Ogawa, K.; Kobuke, Y. *Journal of The American Chemical Society* **2008**, *130*, 17212.

(125) Williams-Harry, M.; Bhaskar, A.; Ramakrishna, G.; Goodson, T.; Imamura, M.; Mawatari, A.; Nakao, K.; Enozawa, H.; Nishinaga, T.; Iyoda, M. *Journal of The American Chemical Society* **2008**, *130*, 3252.

(126) Screen, T. E. O.; Thorne, J. R. G.; Denning, R. G.; Bucknall, D. G.; Anderson, H. L. *Journal of The American Chemical Society* **2002**, *124*, 9712.

(127) Drobizhev, M.; Stepanenko, Y.; Rebane, A.; Wilson, C. J.; Screen, T. E. O.; Anderson, H. L. *Journal of The American Chemical Society* **2006**, *128*, 12432.

(128) Derkowska, B.; Mulatier, J. C.; Fuks, I.; Sahraoui, B.; Phu, X. N.; Andraud, C. *Journal of The Optical Society of America B* **2001**, *18*, 610.

(129) Lee, W.; Lee, H.; Kim, J.; Choi, J.; Cho, M.; Jeon, S.; Cho, B. *Journal of The American Chemical Society* **2001**, *123*, 10658.

(130) Terenziani, F.; Katan, C.; Badaeva, E.; Tretiak, S.; Blanchard-Desce, M. *Advanced Materials* **2008**, *20*, 4641.

(131) Katan, C.; Terenziani, F.; Le Droumaguet, C.; Mongin, O. *Proceedings of SPIE* **2005**, *5935*, 593503.

(132) Yang, W.; Kim, C.; Jeong, M.; Lee, S.; Piao, M.; Jeon, S.; Cho, B. *Chemistry of Materials* **2004**, *16*, 2783.

(133) Kasha, M.; Rawls, H. R.; El-Bayoumi, M. A. *Pure and Applied Chemistry* **1965**, *11*, 371.

(134) Nguyen, P.; Yuan, Z.; Agocs, L.; Lesley, G.; Marder, T. *Inorganica Chimica Acta* **1994**, *220*, 289.

(135) Calvin, D. R.; William, F. S. *Progress in Physical Organic Chemistry* **1964**, *2*, 323.

(136) Lide, D. R., ed. *CRC Handbook of Chemistry and Physics, 89th edition (Internet Version 2009)*; CRC Press/Taylor and Francis: Boca Raton, FL, 2008.

(137) Ferguson, J. *Chemical Reviews* **1986**, *86*, 957.

(138) Herzberg, G. *Molecular Spectra and Molecular Structure*, 2 ed.; D. Van Nostrand Company, Inc.: New York, 1950; Vol. I. Spectra of Diatomic Molecules.

(139) Cornil, J.; Beljonne, D.; Shuia, Z.; Hagler, T.; Campbell, I.; Bradley, D.; Brédas, J. L.; Spangler, C.; Müllen, K. *Chemical Physics Letters* **1995**, *247*, 425.

(140) Strehmel, B.; Amthor, S.; Schelter, J.; Lambert, C. *ChemPhysChem* **2005**, *6*, 893.

(141) Valeur, B. *Topics in Fluorescence Spectroscopy* **1994**, *6*, 21.

(142) Valeur, B.; Leray, I. *Coordination Chemistry Reviews* **2000**, *205*, 3.

(143) Rurack, K. *Spectrochimica Acta Part A: Molecular and Biomolecular Spectroscopy* **2001**, *57*, 2161.

(144) Taki, M.; Wolford, J.; O'Halloran, T. *Journal of The American Chemical Society* **2004**, *126*, 712.

(145) Que, E.; Domaille, D.; Chang, C. *Chemical Reviews* **2008**, *108*, 1517.

(146) Carol, P.; Sreejith, S.; Ajayaghosh, A. *Chemistry - An Asian Journal* **2007**, *2*, 338.

(147) Grynkiewicz, G.; Poenie, M.; Tsien, R. *Journal of Biological Chemistry* **1985**, *260*, 3440.

(148) Takahashi, A.; Camacho, P.; Lechleiter, J.; Herman, B. *Physiological reviews* **1999**, *79*, 1089.

(149) Broder, J.; Majumder, A.; Porter, E.; Srinivasamoorthy, G.; Keith, C.; Lauderdale, J.; Sornborger, A. *Journal of the Optical Society of America A* **2007**, *24*, 2921.

(150) Sornborger, A.; Broder, J.; Majumder, A.; Srinivasamoorthy, G.; Porter, E.; Reagin, S.; Keith, C.; Lauderdale, J. *Journal of the Optical Society of America A* **2008**, *25*, 2185.

(151) Maruyama, S.; Kikuchi, K.; Hirano, T.; Urano, Y.; Nagano, T. *Journal of The American Chemical Society* **2002**, *124*, 10650.

(152) Zhang, Y.; Guo, X.; Si, W.; Jia, L.; Qian, X. *Organic Letters* **2008**, *10*, 473.

(153) Komatsu, K.; Urano, Y.; Kojima, H.; Nagano, T. *Journal of The American Chemical Society* **2007**, *129*, 13447.

(154) Kiyose, K.; Kojima, H.; Urano, Y.; Nagano, T. *Journal of The American Chemical Society* **2006**, *128*, 6548.

(155) Atilgan, S.; Ozdemir, T.; Akkaya, E. *Organic Letters* **2008**, *10*, 4065.

(156) Diwu, Z.; Chen, C.; Zhang, C.; Klaubert, D. H.; Haugland, R. P. *Chemistry & Biology* **1999**, *6*, 411.

(157) Keppler, A.; Pick, H.; Arrivoli, C.; Vogel, H.; Johnsson, K. *Proceedings of the National Academy of Sciences* **2004**, *101*, 9955.